KUNGL
TEKNISKA
HÖGSKOLAN

Remote Sensing and GIS: Applications for Groundwater Potential Assessment in Eritrea

Semere Solomon

April 2003

Environmental and Natural Resources Information Systems
Royal Institute of Technology
SE-100 44 Stockholm, Sweden

ISBN 91-7283-457-9

Doctoral Dissertation

To: Selam, Solomon and Kebedesh

Abstract

An integrated approach with remote sensing, Geographic Information Systems (GIS) and more traditional fieldwork techniques was adopted to assess the groundwater potential in the central highlands of Eritrea. Digitally enhanced color composites and panchromatic images of Landsat TM and Spot were interpreted to produce thematic maps such as lithology and lineaments. The potential of the Advanced Spaceborne Thermal Emission and Reflection Radiometer (ASTER) data for lithological and lineament mapping was evaluated. Topographic parameters such as surface curvature, slope and drainage systems were derived from digital elevation models and used to map landforms. Digital elevation models (DEM) derived from contours and acquired in the Shuttle Radar Topographic Mission (SRTM) were compared in relation to location, drainage networks and lineament extraction. Fracture patterns and spacing were measured in the field in different rock types and compared with lineaments. Selected springs and wells were visited to study their topographic and hydrogeological setting. Well logs, pumping tests, water table depth in dry and wet season as well as location of wells were collected. All thematic layers including hydrogeological data were integrated and analysed in a geographic information system. A groundwater potential map was generated and compared with yield data. Groundwater recharge was estimated based on water level fluctuations in large dug wells and chloride mass-balance method.

Principal component analysis for rock type mapping provided better results with ASTER than with Landsat TM data. DEM data permitted to create detailed landform maps useful tor groundwater potential assessment. DEM derived from SRTM data are better for detection of drainage systems and linear features than those derived from contours. Most of the fracture systems corresponding to lineaments are either extensional related to normal faults and dykes, or shear fractures related to strike-slip faults. N-S, NW-SE, WNW-ESE, NE-SW and ENE-WSW are dominant fracture orientations with often very dense spacing. High yielding wells and springs are often related to large lineaments and corresponding structural features such as dykes. Typically wells and springs in basaltic areas have higher yields mainly due to primary joints. Young alluvial sediments with high permeability and deeply weathered rock layers are important for water supply especially in hydraulic connection with fracture systems in crystalline bedrock. Groundwater potential zones demarcated through the model are in agreement with bore well yield data. The spatial distribution of groundwater potential zones shows regional patterns related to lithologies, lineaments, drainage systems and landforms. Recharge rates of 10 - 50 mm were estimated in this region. The results demonstrate that the integration of remote sensing, GIS, traditional fieldwork and models provide a powerful tool in the assessment and management of water resources and development of groundwater exploration plans.

Key words: Remote sensing, Geographic Information Systems, groundwater, geomorphology, Digital elevation model, lithology, hard rock, lineament, structures, hydrogeology, Eritrea

ACKNOWLEDGEMENTS

Greatest appreciation goes to my supervisor Prof. Dr. Friedrich Quiel for his invaluable assistance during my PhD studies. His continuous support, advice, discussions and suggestions guided me to become a self-reliant, critical researcher with in depth knowledge ready for professional activities, research and development. The social events shared with him and his wife deserves great thanks.

The financial support from the Swedish International Development Cooperation Agency (SIDA) was essential for my studies and merits great thanks. I extend my deep gratitude to the administrative staff of the International Science Program (ISP) of Uppsala University for providing support in all administrative matters pertaining to my studies, especially to Dr. S. Wiktelius, Prof. R. Tellgren, Åsa, Mona, Pravina and Solveig. I am grateful to my home institute, the University of Asmara (UoA) in Eritrea, for providing the opportunity to carry out this study and putting its resource at my disposal during field visits for data collection. Special thanks goes to the staff members at the Earth Science Department, Dr. Ghebreberhan, Dr. Baraki, Dr. Woldai and Dr. Mengist for their moral support as well as encouragements and discussions during the field study periods. The administrative staff of the UoA, Mr Awate, Mr. Solomon, Mr. Berhane, Mrs. Simret, Mrs. Tsega and Mrs. Lemelem was helpful in facilitating logistics and transportation for field studies. Thanks also go to many drivers for their genuine cooperation and dedication during fieldwork. In particular Mr. Bokre Ghebrezgabiher was helpful in showing villages, which I know only by name. The hospitality provided during the fieldwork by the residents of the village Adi Awhi Leallay merits great appreciation.

The staff members of the Water Resources Department (WRD) in the Ministry of Land, Water and Environment were highly cooperative in providing most of the data used for this study. Due thanks goes to Mr. Ghebremichael Hagos (Head of WRD), Mr. Michael Negash (Head of Groundwater Division), Mr. Tekle, Dr. Yemane, Mr. Semere, Mr. Yassin, Miss. Freweini, Mr. Asmelash, and all the other staff members of WRD. Special thanks goes to Dr. S. Drury for his kind cooperation in providing the Landsat TM data at the inception of this study. The German Aerospace Center (DLR) deserves great appreciations for providing the SRTM data. I want to thank Prof. C. Talbot and Prof. G. Jacks and all other teachers and researchers at Uppsala University and the Royal Institute of Technology who through rewarding discussions, suggestions and criticism furthered my studies.

Sincerest thanks are extended to the staff members Mr. Kidane Tsige, Mr. Solomon Foto and Mr. Misghina Gebreslassie in the Ministry of Local Government for their relentless assistance in data provision. My great thanks and appreciations go further to Mr. Teklay Zeray (Manager Universal Water Resources Consultant), Mr. Kibreab Tesfay (Manager Eritrean Core Drilling Comp.) as well as his colleagues Amanuel and Adiamseged, Mr. Estifanos Asrat from General Development Engineering and Construction Company (GEDECC) and Dr. Seife (Manager African Resources Comp.) for their cooperation in providing data. The field discussions I had and the material support I received from Mr. Teklay was very much appreciated.

My stay in Sweden has been made more comfortable due to the hospitality, generosity, encouragement and moral support provided by my relatives, colleagues and friends who live in Sweden as well as in other parts of the world. Special thanks go to my brother Indrias and his wife Hana. My colleagues at the Royal Institute of Technology Xie, Albert, Bereket, both Kebreabs, Petros, Estifanos, Fasil, Meseret, Aman, Henok, Daniel, Fitsum, Teclemariam, Samson and Abraham all deserve great appreciation. Many thanks are due to all colleagues at Uppsala University and, especially, Mehreteab for his continuous moral support. Special thanks also go to my friends Fissehaye, Taddese, Frezghi, Amanuel, Temesghen, Efrem, Yonas and Tsega.

Finally, deepest gratitude goes to my parents Solomon and Kebedesh for their continuous moral support, encouragements and care. Last but not least, my deepest gratitude goes to my wife Selam Tecle for her persistent moral support and encouragement during my study. Her tolerance and patience has contributed a lot towards a successful completion of my studies, which without her assistance would have been much more difficult. Once more I want to extend my heartfelt appreciations and thanks.

TABLE OF CONTENTS

1 INTRODUCTION

1.1 Objectives

Water is a scarce resource in Eritrea. The majority of water used for domestic purposes comes from groundwater sources. In almost all villages in Eritrea water supply comes mainly from dug-wells and to some extent from boreholes that are found along major streams and valleys. Studies of existing productive wells in relation to lithology and structures are absent. Selection of well sites for groundwater supply heavily relies on traditional field studies using existing water point sites as guidelines. In general a systematic approach to groundwater exploration is lacking. The overall aim of this study is to contribute towards systematic groundwater studies utilizing remote sensing, field studies, Digital Elevation Models (DEM) and Geographic Information Systems (GIS) in the assessment of groundwater resources, demonstrated in the central highlands of Eritrea. The specific objectives of the study are:

- To prepare thematic maps of the area such as lithology, lineaments, landforms and slopes from remotely sensed data and other data sources like DEM.
- To assess groundwater controlling features by combining remote sensing, field studies and DEM.
- To identify and delineate groundwater potential zones through integration of various thematic maps with GIS techniques.
- To evaluate the Advanced Spaceborne Thermal Emission and Reflection Radiometer (ASTER) data for lithology and lineament mapping.

- To compare digital elevation models, derived from contours and from radar interferometry in the Shuttle Radar Topographic Mission (SRTM) for geomorphologic and lineament mapping applications
- To make recommendations for future work and provide guidelines for groundwater prospection.

1.2 Methods of Study

The methodology employed is summarized in the flow chart in Figure 1.1. It involves digital image processing for the extraction of lithological and linear features, evaluation of digital elevation model (DEM) as well as field studies. The field studies are comprised of hydrogeological and structural investigations. The DEM was used to extract lineaments and to map drainage systems and landforms. All data were integrated in a Geographic Information System (GIS) and analyzed to assess the groundwater controlling features. Finally groundwater potential maps were prepared based on the GIS analysis.

The potential of ASTER data for lithology and lineament mapping were also assessed. Moreover comparisons of digital elevation models derived from contours and radar interferometry in the Shuttle Radar Topographic Mission (SRTM) were made in relation to location, extraction of drainage networks and linear features. The image processing software ENVI (Environment for Visualizing Images) version 3.5 was used for the remote sensing study. GRASS (Geographical Resources Analysis Support System) versions 4.3 and 5.0 were utilized for the GIS analysis. Structural field data were analyzed using the software package GeOrient version 8.0.

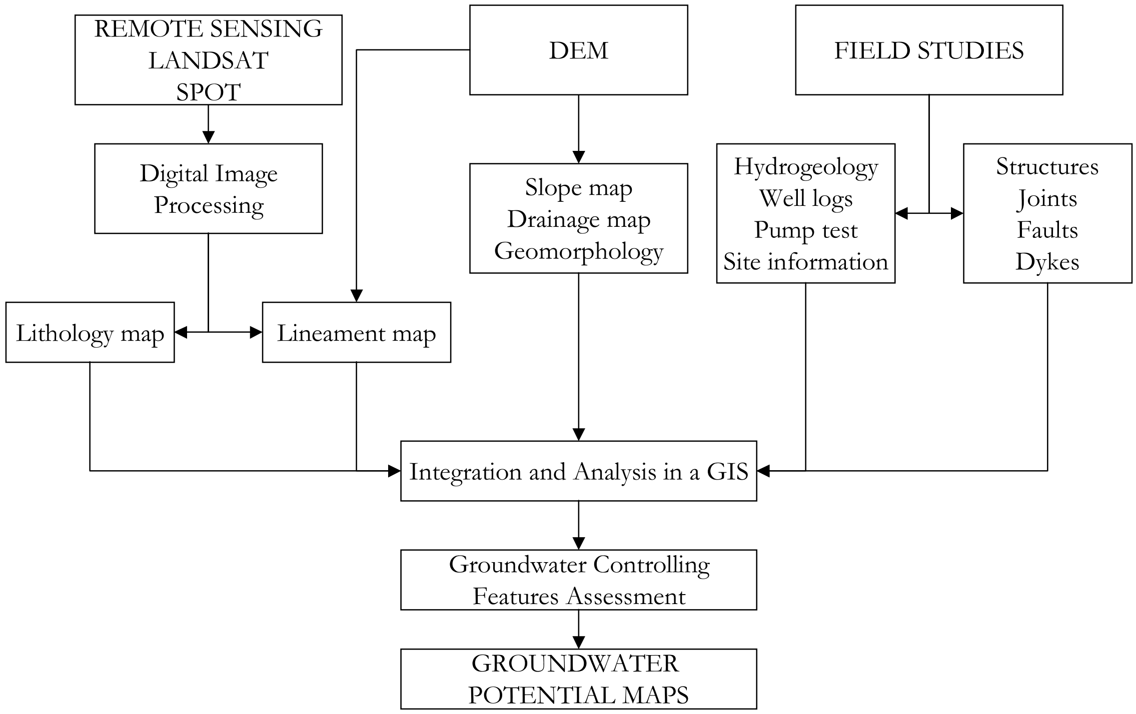

Figure 1.1. Flow chart showing data and methods employed for the study.

1.3 Thesis Layout

The thesis is organized into six chapters. After this brief introductory chapter, general background information of the study area is given in Chapter 2. This chapter describes the physiography, the regional geological setting and the geographical disposition of the area. Chapter 3 provides a literature review with an overview of related studies conducted in other parts of the world together with previous works in the area. The different data sets used and the methods utilized are described in Chapter 4. The data sets include digital data such as remote sensing images and digital elevation models as well as field observations such as lithological logs, pumping tests, and fracture orientation data. In addition to the field investigation techniques the methods used in the generation of the various thematic maps from remote sensing data as well as digital elevation models are described in detail. Methods to integrate and analyze the various thematic layers using a geographic information system (GIS) are given. Moreover the steps to generate groundwater potential zones using GIS are presented in detail.

The results obtained with the various methods are presented in Chapter 5. First the results from various digital image processing techniques for lithology and lineament mapping are discussed. The potential of ASTER data for rock type discrimination and lineament detection is demonstrated and the results compared with Landsat TM and SPOT data. This is followed by the results of field investigations of structures. Analysis of digital elevation model data including comparisons of results is presented under geomorphology in the same chapter. Assessment of groundwater controlling features through GIS analyses, field investigations, GIS modeling as well as estimation of groundwater recharge aspects is discussed in detail. Moreover hydrogeological implications of ASTER data are presented. Finally, the conclusions drawn together with recommendations are presented in Chapter 6.

2 BACKGROUND

2.1 Physiography and Climate

Eritrea is located in the horn of Africa (Figure 2.1). It is bounded by Ethiopia to the south, Sudan to the west and north, the Red Sea to the east and Djibouti to the southeast. Three physiographic regions characterize Eritrea. These are: the western lowlands with elevations 500 – 1500 m, central highlands with elevations 1500 – 2500 m and the eastern coastal lowlands with elevations 0 – 1500 m above sea level. The southern central highland is drained by the Mereb-Catchment and is seasonal.

The climate is arid to semi-arid with two rainy seasons locally known as 'Kiremti' (frequent and long rainy season during the summer, June to September), and 'Akeza' or spring rain (the short infrequent rainy season during March and April). The remaining months are dry. Rainfall is intense during the period mid-July to mid–August. Average annual precipitation ranges from 300 to 600 mm in the central highlands. Potential evapotranspiration is approximately 1700 mm/yr. Daily temperatures usually vary from 10^{o} to 30^{o} C. Natural vegetation cover is sparse and includes dominantly acacia trees and bushes occupying rocky steep slopes and lowlands. Dense vegetation cover is common along rivers and form limited woodland type of forest. Apart from these some man-made plantations dominated by eucalyptus trees are common in the highlands. Vegetation cover from small-scale irrigation schemes dominates along river courses and in the basaltic plateau.

2.2 Geological Setting

The country is part of the Arabian-Nubian Shield which extends from Saudi Arabia and Egypt in the north through Eritrea, Ethiopia and the Sudan to Somalia, Kenya and Uganda in the south. The Arabian-Nubian Shield consists dominantly of low-grade volcanosedimentary-ophiolite assemblage, granitoids and gneisses (Vail 1987). The Mozambique Belt (Holmes 1951) extends from Mozambique to Ethiopia and into Eritrea in a N-S trending zone of high grade gneisses and migmatites, with infolded schists, marbles and amphibolites intruded by granites. These two, the Arabian-Nubian Shield and the Mozambique Belt, form an important orogenic belt in Africa extending from Egypt to Mozambique and Madagascar. As both experienced a similar tectonic history since at least 1100 Ma, the term Pan-African has been applied for both orogenic belts (Berhe 1991).

The Precambrian terrain of Eritrea belongs to the least studied part of the Arabian-Nubian Shield. Several authors have described the Precambrian terrain of Eritrea (e.g. Drury et al. 1991, Drury and Berhe 1993, Ghebreab 1996). In general it is comprised of metamorphic and granitic rocks (Figure 2.1). A variety of felsic rocks with granitic-dioritic composition intrude the volcanosedimentary sequence. The granitoid rocks show variations from foliated gneissose granite merging into surrounding schists, porphyritic granite and granodiorite to fine grained microgranite, syenite and diorite with subordinate gabbro in places. The form of the intrusions varies between huge irregular or elongated complexes with schistose rocks preserved as roof pendants, and rounded circular masses of quite restricted dimensions (Hamrla 1978).

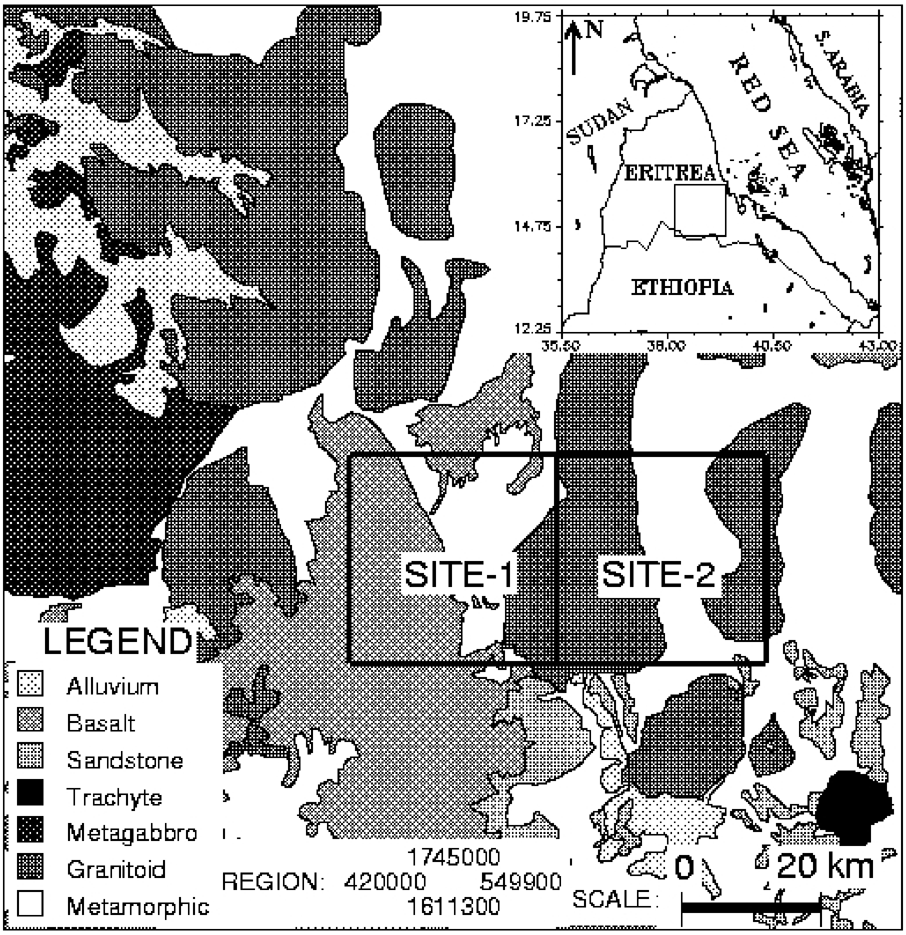

Figure 2.1. Location, regional geology and the study areas.

The dominant metavolcanic rocks are schistose metavolcanics with chlorite epidote muscovite quartz schists and massive metavolcanics, which are strongly epidotized and include metabasalts and metafelsites (rhyolites, tuffs and pyroclastic volcanics); in places intermediate volcanics (andesites and dacites) alternate. Metasedimentary units are comprised of slates, in places black colored, and turbiditic sediments of greywacke with minor interbeds of metavolcanic rocks (Teklay 1997). The metavolcanic and metasedimentary sequences show alterations of both primary (hydrothermal) and secondary (weathering) origin. Kaolinization, sericitisation, heamatitisation and silicification are among the most common types of hydrothermal alterations.

The Eritrean volcano-sedimentary sequence was metamorphosed to greenschist facies and locally to amphibolite facies at the end of the Precambrian (700-600 Ma) (Mohr 1979). Metamorphism is represented by chlorite-sericite-quartz association and occasionally tremolite-actinolite or epidote group. Occurrences of amphibolitic rock types are observed mainly near granitoid intrusions and their formation is perhaps caused by thermo-metamorphic process (GEOZAVOD 1982).

Mesozoic sandstone and Cenozoic volcanic rocks lie unconformably over the volcano-sedimentary rock units and the granitoids (Figure 2.1). The volcanic rocks are alkali-olivine basalt flows forming plateaus. The base of the basalt sequence is marked by a well developed lateritic paleosol. Remnants of the lateritic peneplains are commonly encountered in the region. The age of Eritrean lateritization is not well known, but throughout the Red Sea area, Tertiary flood basalts rest conformably on lateritic paleosols (Mohr 1970).

According to Mohr (1979), dips are steeply west over much of the Eritrean Highlands, in agreement with isoclinal folding. Fold axes are generally near horizontal, and gently plunging both to the north and south. The general trend of the metavolcano-sedimentary assemblage belt swings from NNE-SSW through N-S to NW-SE. Doleritic dyke swarms with orientations NNE-SSW and NNW-SSE intrude basaltic flows, the volcanosedimentary sequence and the granitoid complexes. The dyke swarms represent one of the major fracture systems in the region. Sets of WNW, EW, NE, NW-trending fractures, some with discernible displacements, are strongly expressed in the central Highlands, notably in the granitoids (Drury et al. 1994). In the study area most of the above rock units and structures are well exposed.

2.3 The Study Areas

The study areas are located in the southern central highlands of Eritrea (Figure 2.1) and are 30 by 30 km in size each. Site-1 covers part of the large Mereb catchment and is locally known as the Upper Mereb catchment. Mereb river is main stream draining the area and flows from northwest to southeast (Figure 2.2). In site-2 the southern part is drained by the tributaries of the Mereb River and the northern part it is drained by the Alla sub-catchment that flows east towards the Red Sea. The Alla catchment is fed by highland rains that flow down the escarpment (fig. 2.2).

Site-1 is dominated by basaltic and crystalline rocks and is characterized by a mainly flat topography with isolated basaltic hills. The elevation varies from 1500 to 2600 m above sea level. In contrast Site-2 is comprised of crystalline rocks mainly forming the highland plateau with a steep escarpment that parallels the Red Sea rift (fig. 2.2). Elevations vary from 1300 m down the escarpment to 2600 m on the plateau. The study areas, which are characteristic for the central highlands were selected based on the availability of hydrogeological data, digital elevation models (DEM) and their accessibilities for field investigations.

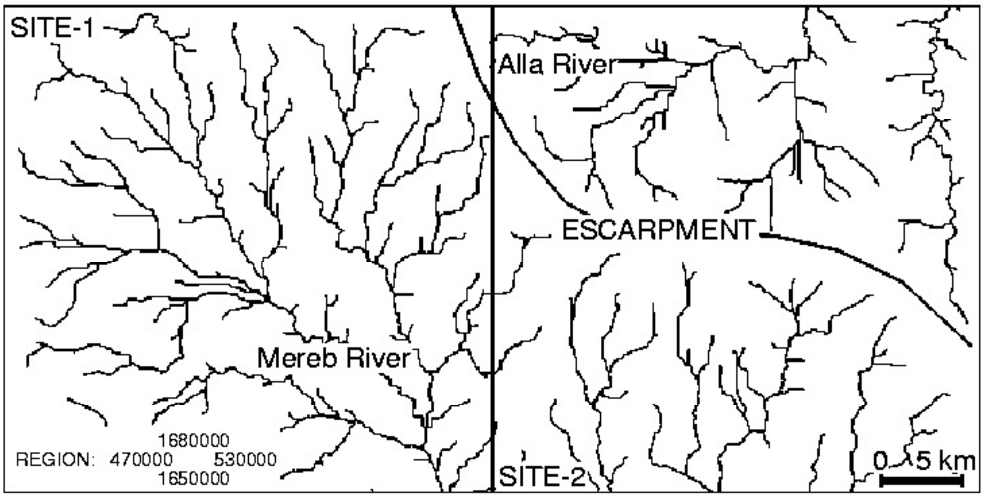

(a) (b)

Figure 2.2. Drainage maps of (a) Site-1 and (b) Site-2.

3 LITERATURE REVIEW

3.1 Remote Sensing Techniques

Groundwater availability in any terrain is largely controlled by the prevalence and orientation of primary and secondary porosity. Groundwater exploration entails delineation and mapping of different lithological, structural and geomorphological units. Satellite based remote sensing data facilitate the preparation of lithological, structural, and geomorphological maps, especially at a regional scale. These data show major rock groups, structural features, such as folds, faults, lineaments and fractures, and different landforms, due to their synoptic coverage and multispectral capability (Siegal and Gillespie 1980, Drury 1987). Visual interpretation of remote sensing images is achieved in an efficient and effective way using basic interpretation keys or elements (Sabins 1987). An interpretation key comprises combinations of characteristic features to identify objects in an image. Typical key features are size, shape, tone, texture, pattern and color. Similarly many procedures are available for image data manipulation (Jensen 1986, Lillesand and Kiefer 1994, Drury 1987, Hord 1982, Mather 1987, Schowengerdt 1983). Studies of the spectral reflectance of rock-forming minerals provide the physical basis for the remote determination of earth materials (e.g. Hunt and Salisbury 1970, Hunt 1977, Hunt 1979, Hunt and Ashley 1979, and Goetz et al. 1983). The use of spectral reflectance to improve understanding of the characteristics of rock formations in an image has been practiced in many studies (e.g. Kaufmann 1988, Amos and Greenbaum 1989, Abrams and Hook 1994, Nalbant and Alptekin 1995, Younis et al. 1997).

Lineament analysis of remote sensing data constitutes an important part of studies related to tectonics, engineering, geomorphology and in the exploration of natural resources such as groundwater, petroleum and minerals (e.g. Koopmans 1986, Kar 1994, and Philip 1996). Mapping of lineaments from various remote sensing imagery is a commonly used step in groundwater exploration in hard rock areas. The term hard rock commonly applies to hard and dense rocks that the main part of the groundwater exists and flows in secondary structures, mainly fractures. Crystalline rock types such as meta-volcano-sedimentary, gneiss, meta-igneous and igneous predominate but volcanic rocks are also included in the concept hard rock from a hydrogeological point of view (Olofsson et al. 2001). Lineaments were introduced in a groundwater context by Lattman (1958) and Lattman and Parizek (1964). Since then many workers followed their example and tried to quantify groundwater resources in hard rocks, based on linear features in various types of maps and remote sensing imagery (e.g. Greenbaum 1987 and 1992, Waters 1990, Mabee et al. 1994, Sander 1996, Koch and Mather 1997). The surface expression of geological structures such as fractures (faults, joints, dykes and veins), shear zones and foliations are often displayed or represented in the form of lineaments in aerial photographs or remote sensing data.

The routine procedure for geological lineament extraction from digital remote sensing data usually involves initial digital image enhancement followed by manual interpretation. There have been significant approaches for the evaluation and automatic detection of lineaments and curvilinear features from satellite images (Cross 1988, Cross and Wadge 1988, Taud and Parrot 1992, Karnieli et al. 1996), but the human expert is still an asset for lineament detection and interpretation with its subjective perception (Suzen and Toprak 1998). The availability of multi-spectral and multi-sensor data and image enhancement techniques provide an opportunity to prepare more reliable and comprehensive lineament maps. The extensive ground coverage and high resolution of satellite images enables regional and local lineament analysis.

3.2 Structures

A number of previous workers have identified fault systems, including normal faults, strike-slip faults as well as dykes, with several orientations, based on remote sensing interpretation and field studies. N-S/NNE-SSW, NW-SE, NNW-SSE and E-W to WNW-ESE trending linear features were identified using Landsat and large format camera images by Drury et al. 1994. The N-S, NW-SE and NNW-SSE trending fractures represent normal faults with variable dip to either side of the major strikes (Ghebreab 1998). Some of them with very large throws around 2.2 km gave rise to the Red Sea escarpment (Drury et al. 1994). N-S and NNW-SSE linear features show variations in strike and become parallel to the dominant strike in the basement (NNE-SSW) with sinistral strike-slip sense of movement (Drury et al. 1994). Ghebreab (1998) described that strike-slip faults dominantly have N-S orientations and concentrate along zones in the escarpment with dominantly left-lateral sense of displacement. The N-S, NNW-SSW/NNE-SSW and NW-SE oriented structures are described as Red Sea rift-related faults (Drury et al. 1994, Talbot and Ghebreab 1997, Ghebreab 1998). Drury et al. (1994) described the NW-SE trending lineaments as active strike-slip faults with dextral sense of movements and related them with neotectonic structures in the Red Sea. Linear features that trend E-W (between WNW-ESE and ENE-WSW) were considered as sets of post-Precambrian structures representing a regional N-S dilatation restricted to the main axis of Tertiary uplift and the western flanks of the Red Sea rift (Drury et al. 1994 and 2001). According to the same authors normal faults (e.g. WNW-ESE) parallel to this trend suggest that some structures are related in age to the Red Sea evolution.

Doleritic dyke swarms with orientations NNE-SSW, NNW-SSE, NW-SE and ENE-WSW were also mapped by many workers. The most revealing of the dykes are NNE-SSW trending swarms that parallel the steep, westerly dipping basement fabric and are formed late in the Tertiary tectonic evolution (Drury et al. 1994). Mohr (2001) called the same dyke swarms "Asmara dyke swarm" and claimed that the irruption took advantage of the regional structural grain of the basement schists/gneisses. NNW-SSE and NW-SE trending dykes were described as Red Sea rift-related structures (Drury et al. 1994, Talbot and Ghebreab 1997, Ghebreab 1998). Drury et al. (1994) stressed the idea that the main faults, which demonstrably participated in Red Sea rifting, parallel the dominant basement fabric and are reactivated Precambrian shear zones, as proposed by Berhe (1986). The same authors stated further the existence of major pre-Tertiary faults trending N-S roughly along the line of the escarpment foot and the main Tertiary extensional faults.

Ghebreab (1998) has mapped a few dykes about one kilometer long that trend ENE-WSW near the gentle foot of the escarpment and related them to Red Sea transform faults or to the ENE-WSW transverse structure along which the Red Sea spreading axis jumped westward as it propagated southwestward. Studies have shown increased seismic activity along the axis of the central Red Sea (Fairhead and Girdler 1970, Dixon et al. 1987). Earthquake fault plane solutions in this part of the Red Sea show strike-slip motion along N53°E striking vertical faults, perpendicular to the rift axis (Fairhead and Girdler 1970). Several authors have interpreted these structural features as transform faults, which dissect the rift into numerous northerly to northeasterly-trending segments (Bäcker et al. 1975, Dixon et al. 1987).

The age relationship of all the structures, namely, the dykes, normal faults and strike-slip faults for each set are not known from the previous studies. However, Ghebreab (1998) stated that alternate episodes of faulting and dyking are likely and a single set of faults and dykes appear to occur contemporaneously. Moreover, he described that some of the normal faults are along highly strained, altered and rotated dykes indicating perhaps that the faults exploited the weak surfaces along which the vertical dykes were emplaced though dykes along other faults are fresh. He mentioned also that strike-slip tectonism is at least younger than the oldest set of normal faults and dykes.

3.3 Geomorphology

Geomorphological investigations include the delineation and mapping of various landform and drainage characteristics that could have a direct control on the occurrence and flow of groundwater. The mapping activities significantly contribute in deciphering areas of groundwater recharge and their potential for groundwater development (Singhal and Gupta 1999). Nowadays the use of digital elevation models (DEM) for landform classification, identification of landform types, extraction of landform components and modeling of landform associations are common practice in the field of geomorphology. A systematic parameterization of a DEM was suggested and used by Evans (1972, 1979, 1980, 1984). He suggested that a unifying framework is provided by taking the first and second derivatives of altitude, e.g. slope, aspect, profile convexity and plan convexity (see appendix i for details). Parameterization of a surface model has been defined as "the numerical description of continuous surface forms" (Pike 1993). More geomorphologically, it has been described as "a set of measurements that describe topographic form well enough to distinguish topographically disparate landscapes" (Pike 1988).

The attraction of a simple matrix of elevation values (amenable to processing with procedural computer languages) was one of the reasons for its uptake in the early 1970s as a model suitable for landscape analysis (e.g. Evans 1972). More recently, its continued widespread use as a model of surface form may be attributed to its easy integration within a GIS environment (Weibel and Heller 1990 and 1991, Wood 1996). Several workers have used DEM data for purposes such as delineating the drainage networks (Zhang et al. 1990), deriving hydrogeomorphological units (Hodgson 1999) and for landscape description and classification (Brabyn 1996 and Swati 2002).

3.4 Hydrogeology

In Eritrea the majority of water used for domestic purposes comes from groundwater sources. A large portion of the country is underlain by hard rock. In such rocks the success rate of drilling is low and a reliable water supply consequently is difficult to accomplish (Sander 1996). This research was initiated to study the groundwater conditions in the hard rock areas in the central highlands of Eritrea and aimed at understanding the groundwater systems by utilizing more systematic methods.

Several groundwater related studies have been conducted mainly on a regional scale in Eritrea since its independence in 1991. In 1998 the Euroconsulant group has undertaken groundwater resources assessment under the auspices of "Sector Study on National Water Resources and Irrigation Potential". The Japan International Cooperation Agency (JICA) conducted in 1997/98 a study on groundwater development and water supply for seven towns in the southern central highland of Eritrea. The two studies mainly focus on compilation of existing data with some newly drilled boreholes that are used also in this study. Results of the investigations were presented in reports and are available at the Water Resources Department in the Ministry of Land, Water and Environment in Eritrea. Asgedom (1998) made in his M.Sc. thesis an assessment of groundwater in the southern central highlands of Eritrea using Landsat Thematic Mapper images. Drury et al. (2001) carried out a regional systematic study about the hydrogeological potential of the major fractures in Eritrea. According to the authors the major fracture zones and associated aquifers constitute lineaments with N-S, WNW-ESE and NNE-SSW to NE-SW trends.

Zerai (1996) summarizes variations in chemical quality of well waters in Eritrea. For the central highlands, electrical conductivity and chemical data from sparsely sampled wells suggests that this area has good groundwater quality, except where sewage contamination around Asmara produces high nitrate concentrations in some wells. Problems with chemical quality might exist in this region, due to lithologies penetrated by some wells (Andrews in press). Water wells sited in lateritic paleaosoles can have high salinity and sulphate contents owing to lateritization (release of chloride, fluoride and sulphate ions). Due to this villagers have abandoned some wells in favor of water trucked in from better quality sources (Drury et al. 2001).

Studies about groundwater development categorization carried out by Viswanatham (2002) in Eritrea show that some areas are under critical overdraft conditions. A typical example of over exploitation is the Alla valley with decreasing of water levels, dry wells, reduced yields and sometimes deterioration of water quality. Assessment of the catchment of 1465 km^2 area based on rainfall for Alla has shown that the total groundwater recharge is 6.43×10^6 m^3 while the total annual groundwater draft is 1.062×10^7 m^3 leaving a negative balance of – 4.19×10^6 m^3 (The calculations ignored drinking water component). The above figure indicates groundwater mining. Therefore Alla valley is a classic case of an overexploited area, which can be termed as critical area.

Groundwater recharge estimations in hard rock areas are commonly associated with large uncertainties. Detailed investigations such as drilling and pumping tests are thus necessary for a complete understanding of groundwater systems in hard rocks. Previous studies carried out by FAO (1994) in the basaltic rocks using water-table fluctuation method assume 22 – 44 mm per annum of groundwater recharge. The Euro Consultant group (1998) in their sector study of the whole country assumed the same estimated figures of groundwater recharge for both the basaltic and alluvial aquifers. For basement rocks (intrusive igneous and metamorphic rocks) the recharge was estimated in analogy with similar hydrogeological conditions in the order of 1 % of annual rainfall (550 mm). Haile (pers. com. 2002) estimated the groundwater recharge in the central highlands of Eritrea using the chloride-mass balance method. From rainwater analysis, he obtained a mean chloride content of 2 mg/l and a recharge rate of 38.5 mm/yr. This value is about 6 to 7 % of the annual rainfall (550 mm). Recharge rates of 11 – 17 mm have been recorded in continental parts of Africa with about 500-600 mm rainfall (Bromley et al 1997, Nkotagu 1996). In arid regions of different parts of the world, the groundwater recharge in basaltic terrains is reported to be about 10 % of the annual rainfall (UNESCO 1975). Estimates of recharge from the crystalline rock terrains in semi-arid areas of Australia show variation in recharge depending upon local geology and climatic conditions but in most cases the recharge is less than 1 % of annual rainfall (Lloyd 1999).

3.5 Geographic Information Systems

The full potential of remote sensing and GIS can be utilized when an integrated approach is adopted. Integration of the two technologies has proven to be an efficient tool in groundwater studies (Krishnamurthy et. al 1996, Sander 1996, Kamaraju et. al 1996, Saraf and Choudhury 1998). For effective groundwater exploration and exploitation it is important to study the different parameters in an integrated approach. The integration of multiple data sets, with various indications of groundwater availability, can decrease the uncertainty and lead to 'safer' decisions (Sander 1996). The Geographic information system offers spatial data management and analysis tools that can assist users in organizing, storing, editing, analyzing, and displaying positional and attribute information about geographical data (Burrough 1986). Remote sensing data provide accurate spatial information and can be economically utilized over conventional methods of hydrogeological surveys. Digital enhancement of satellite data results in extraction of maximum information and an increased interpretability. GIS techniques facilitate integration and analysis of large volumes of data. Whereas field studies help to validate results further. Integrating all these approaches can offer a better understanding of groundwater controlling features in hard rock aquifers.

4 DATA AND METHODS

4.1 Remote Sensing

Data

Three types of remote sensing data were utilized (see Table 4.1):

- Landsat Thematic Mapper (TM) 4 data (28.5 m resolution) path/row (169/050) acquired September, 1987
- SPOT-4 Multispectral data (20 m resolution) row/column (135-320 and 136-320) acquired April 6, 1996
- Advanced Spaceborne Thermal Emission and Reflection Radiometer (ASTER) data with scene center at 39.09° E longitude and 14.98° N latitude acquired December 15, 2001.

ASTER covers a wide spectral region with 14 bands from the visible to the thermal infrared with high spatial, spectral and radiometric resolution. An additional backward looking near-infrared band provides stereo coverage. The spatial resolution varies with wavelength: 15 m in the visible and near-infrared (VNIR), 30 m in the short wave infrared (SWIR), and 90 m in the thermal infrared (TIR).

The Landsat-TM and SPOT image data were geometrically corrected using well-distributed ground control points (GCPs) in the images. Ground control points are features with known ground coordinates that can be accurately located in the digital images. The selected GCPs consist mainly of stream intersections and bends. About 12 to 15 GCPs were selected to carry out the geometric transformations. The coordinate system used in the map is the Universal

Transverse Marcator (UTM). The Landsat TM 28.5 m and SPOT 20 m resolution were resampled to 30 m and 20 m resolutions, respectively, using the nearest neighbor resampling technique. The mean square error in each transformation corresponds to 1 to 1.5 pixels in size (30 to 45 m in Landsat and 20 to 30 m in SPOT). The base map used for geometric transformations has a small scale (1:250,000) and was prepared from four topographic sheets. Therefore, ground check of the coordinates was made by collecting GCP's using Global Positioning System (GPS) in the field and the coordinates were further corrected to account for geometric errors attributed to the mosaicing. Sub-scenes of 900 Km^2 each were created for all data sets to cover the area of the two sites (Figure 4.1).

ASTER data are provided as two types of Level-1 data: Level-1A and Level-1B. ASTER L1A data are reconstructed and unprocessed instrument data at full resolution. The ASTER Level-1B data are L1A data with radiometric and geometric coefficients applied. Level-1B data type was ordered from Japan Ground Data System (GDS). The L1B data product is generated in UTM projection in swath orientation with Cubic Convolution resampling technique applied (Abrams et al. 2002). To make the data sets the same size as the SWIR image, geometric transformations were carried out using ground control points and all bands were registered to 30 m ground resolution applying cubic convolution resampling. The TIR bands were converted from unsigned integer to byte data type in order to avoid statistical bias during the principal component transformations. Furthermore the digital number (DN) values from the VNIR and SWIR bands of ASTER data were scaled by a factor of two to facilitate comparisons of image spectra of geological materials in all wavelength regions. Color composites created from the three wavelength regions of ASTER data for the study site-2 are presented in Figure 4.2.

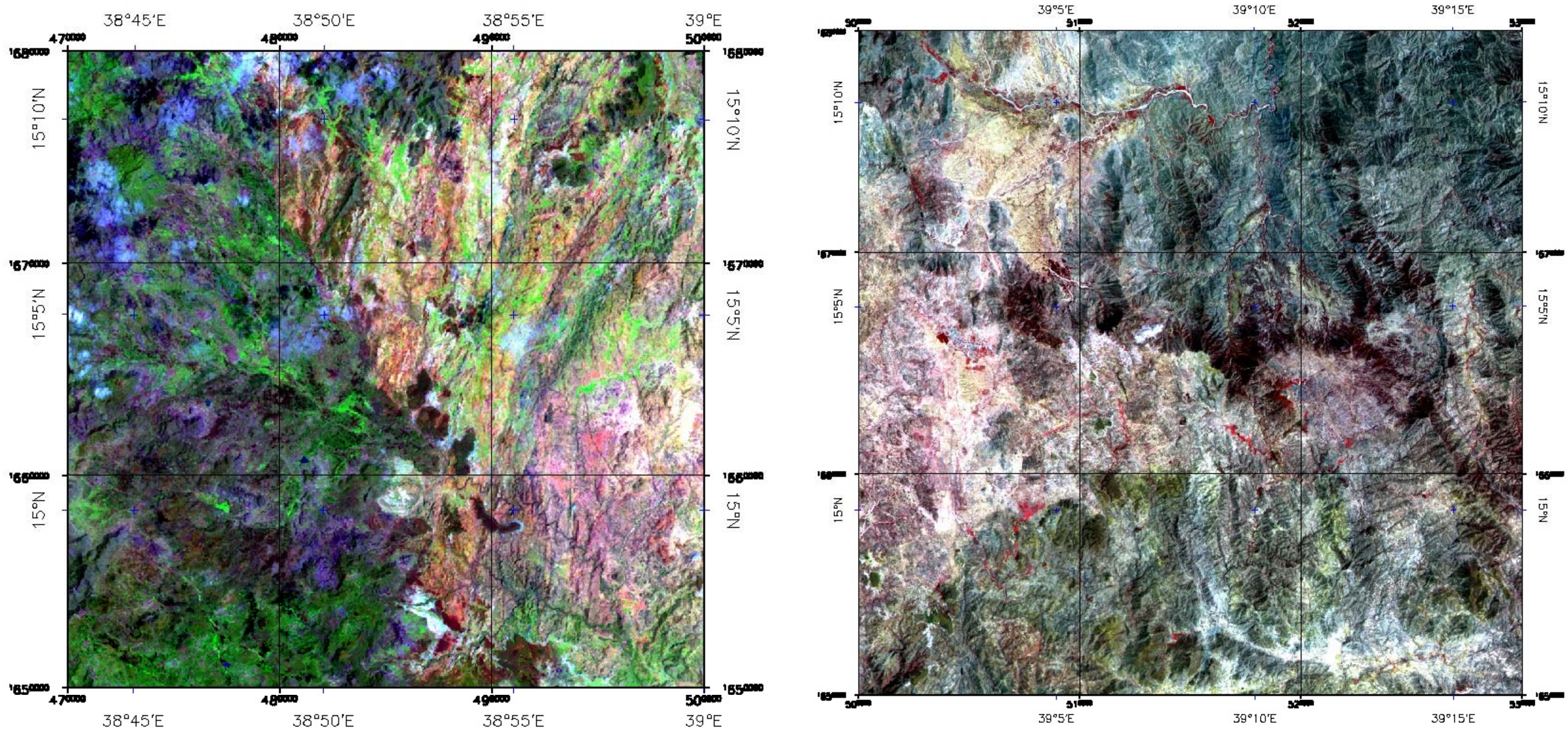

(a) (b)

Figure 4.1. Color composites of (a) Landsat TM bands 7, 4, 1 for site-1 and (b) SPOT bands 3, 2, 1 for site-2, both in red, green and blue colors.

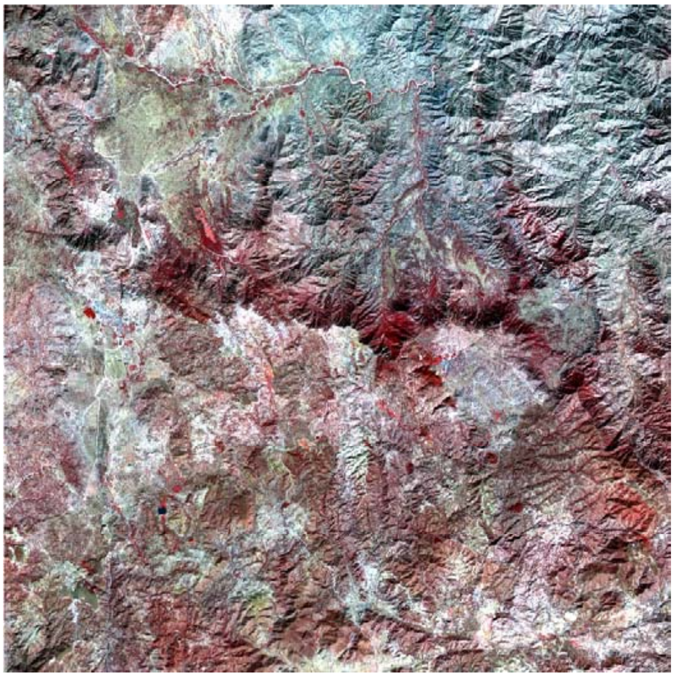

(a)

(b)

(c)

Figure 4.2. Color composites from ASTER data (a) VNIR bands 3, 2, 1 (b) SWIR bands 4, 6, 9 and (c) TIR bands 13, 12, 10. All in RGB order with ground resolutions of 15, 30 and 90 m, respectively. Image size 30 x 30 km.

Table 4.1. Remote Sensing data used in the study.

Sensor	Band	Wavelength (μm)	Spatial Resolution (m)
LANDSAT TM	1	0.45 – 0.52	
	2	0.52 – 0.60	
	3	0.63 – 0.69	30
	4	0.76 – 0.90	
	5	1.55 – 1.75	
	7	2.08 – 2.35	
SPOT	1	0.50 – 0.59	
	2	0.61 – 0.68	20
	3	0.79 – 0.89	
ASTER	1	0.52-0.60	
	2	0.63-0.69	15 (VNIR)
	3	0.78-0.86	
	4	1.60-1.70	
	5	2.145-2.185	
	6	2.185-2.225	
	7	2.235-2.285	30 (SWIR)
	8	2.295-2.365	
	9	2.360-2.430	
	10	8.125-8.475	
	11	8.475-8.825	
	12	8.925-9.275	90 (TIR)
	13	10.25-10.95	
	14	10.95-11.65	

All image data have been made available for input in a format that is suitable to ENVI (the Environment for Visualizing Images) software package (V. 3.5). The image processing was done on a PC based system. Table 4.1 lists the spectral bands of the TM, SPOT and ASTER data utilized in this study.

The spectral information in multispectral satellite images enables the identification of different vegetation types, bedrock and soils, based on their spectral signature in different wavelength bands. For example, as seen in Figure 4.3, ASTER data will allow a better discrimination of rock types than Landsat TM and the TM data better lithological discrimination than SPOT multi-spectral data as there are more bands covering a wider part of the electromagnetic spectrum with significant information.

In this study remote sensing methods were applied to identify major lithologies and lineaments. The main goal in using remote sensing techniques for groundwater exploration is to identify and isolate regional and subregional factors of significance to groundwater occurrence in a cost-effective and rapid manner (Greenbaum 1992). In the following sections the different digital image processing methods used to extract lithology and lineaments are described in more detail.

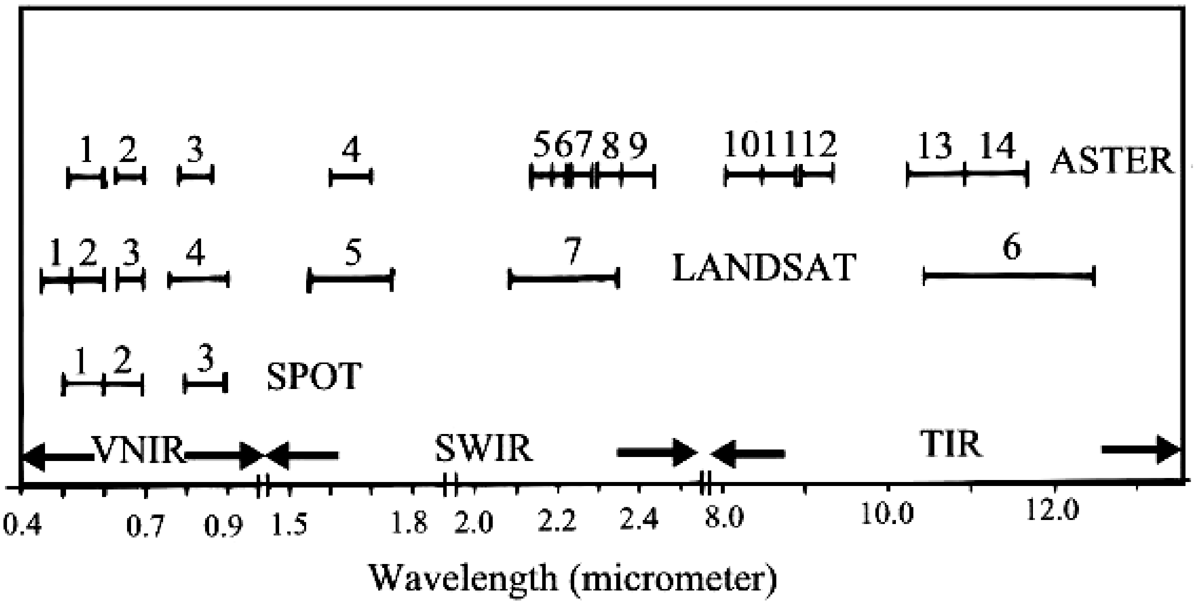

Figure 4.3. Sketch of the spectral bands in ASTER, LANDSAT and SPOT showing wavelength regions together with the number of bands in each sensor. VNIR=visible near-infrared, SWIR=shortwave infrared and TIR=thermal infrared wavelength regions.

4.1.1 Band Selection for Color Composites

Because the human eye uses only three primary colors, and Thematic Mapper returns seven bands of data, one problem that inevitably arises is that of selecting the most effective three-band color composite images. If we consider the 6-reflective bands (three visible and three infrared) of the seven Landsat TM imagery data (excluding the thermal band, band-6), three bands can be selected from these six bands in 20 ways. Also any band can be assigned any color and this gives a total of 180 different possible color presentations of three-band TM images.

For geological mapping purposes different combinations of three bands are recommended. Pontual (1988) recommends composites based on TM bands 7, 5, and 4 or 7, 4 and 2 in red, green and blue, respectively. TM band 7, 4 and 1 combination has been designated as a kind of standard product for geological mapping (e.g. Kaufmann 1988, Davis and Berlin 1989).

In this study a procedure adopted by Sheffield (1985) was employed. The procedure takes full account of any correlations that exist between different bands and provides a single preferred choice, determined by the statistics of a scene or subscene. The method entails the calculation of the 6 by 6 variance-covariance matrix for a scene or subscene, ignoring the TM thermal band. Then the determinants of 3 by 3 submatrixes from the 6 by 6 matrix are calculated. The band triplets are ranked from highest (best band triplet) to lowest (worst band triplet) determinant.

4.1.2 Principal Component Analysis

A challenge encountered with Landsat TM data is to map as much information as possible into a reduced subset of bands for digital analysis and/or color compositing, e.g. three images for compositing (Chavez and Kwarteng 1989). Principal components analysis (PCA) is a widely used digital image processing technique by which a multi-spectral data set is transformed into a new decorrelated coordinate system (e.g. Gillespie et al. 1986). It is a mathematical transformation that generates new images, referred to as components or axes, which are linear combinations of the original bands. Most of the total variance is mapped to the first component, with decreasing variance in each of the subsequent components. Thus the first principal component contains most of the information and is usually a high quality image on its own, especially for structural interpretation, and is well suited to edge enhancement (Sander 1996). Experience from groundwater projects in Ghana and India (Minor et al. 1994 and Krishnamurthy et al. 1992) showed that PC images, both single band PC1 and color composite of the three first principal components, can be very useful in feature discrimination and are often superior to other images. PCA is often used to reduce dimensionality of the data. Problems are encountered with both the loss of information of interest that is mapped to lower components not used and difficulty in interpreting a color composite made from standard PCA results (Chavez and Kwarteng 1989). To overcome the high correlation between bands, PCA was carried out on the six reflective TM bands.

In order to assess the potential of ASTER data for geological mapping applications, PCA was performed on the 14 wavelength bands that cover the visible near-infrared (VNIR), short wave infrared (SWIR) and thermal infrared (TIR) regions (Table 4.1). To evaluate better the spectral information contained in the ASTER VNIR, SWIR and TIR bands, image spectra on selected rocks were determined and used to interpret the color composites from the principal component analysis. Color composites created from the PC images of ASTER and Landsat TM data were also compared. The potential of the ASTER data for lineament mapping was investigated in relation to SPOT and Landsat TM data.

4.1.3 Intensity-Hue-Saturation Transformation

Intensity, hue and saturation (IHS) transformation is a digital color enhancement technique widely used in geological mapping (e.g. Grasso 1993, Nalbant and Alptekin 1995, Kenea 1997). The IHS-transformation can only be used with three input bands. Intensity is the measure of the total light energy reflected from an object, regardless of wavelength. Intensity is also a function of albedo (Gillespie et al. 1986). Hue is the average wavelength of light reflected from an object and represents the wavelength of the dominant color. Saturation is the width around the average wavelength of the spectral region in which a significant amount of light is reflected from an object. Saturation, therefore, represents the purity of color. Intermediate values of saturation represent pastel shades and high values represent purer and more intense colors (Sabins 1987, Nalbant and Alptekin 1995). Two notable virtues of the IHS transformation are:

(1) Its ability to effectively separate intensity and spectral information from a standard image, and
(2) The possibility to convert IHS elements back to RGB display components (Grasso 1993).

By stretching the Saturation and Intensity images independently and then retransforming the images to the original color coordinate system for display, enhanced color pictures are created. These are easier to interpret, as the hues are substantially unchanged. Consequently, this is also one type of decorrelation stretching. For interpretation of geological lineaments high-pass filtering of the intensity image is recommended (Wester 1992).

4.1.4 Decorrelation Stretch

Decorrelation stretch (DS) is a technique whereby the color information in red, green and blue color composite images is accentuated, thus facilitating visual discrimination of color differences (Rothery and Hunt 1990). It is used to remove the high correlation commonly found in multispectral data sets and to produce a more colorful composite image. This technique again requires only three input bands. For most interpretation purposes a decorrelation stretched image is very similar to one produced by stretching saturation in the intensity-hue-saturation (IHS) space followed by an inverse transformation back to red, green and blue space, as discussed by Gillespie et al. (1986). This process introduces little distortion in hue and thereby makes interpretation of the enhanced images straightforward. DS can be easily conducted if the PC images are stretched and retransformed back to the original color-space using the inverse of the original eigenvector (Rothery and Hunt 1990). Several studies have shown the potential of using this technique (Kahle and Goetz 1983, Gillespie et al. 1986 and 1987, Abrams 1984).

4.1.5 Spatial Enhancement for Lineament Mapping

In this study the objective of the lineament mapping and analysis is to investigate the role of the mapped lineaments in controlling groundwater availability in hard rock aquifers. Lineament interpretation is based on visual interpretation of various digitally enhanced single band (black and white) and multiband (color) composites that involve standard band combinations, principal component images, IHS-transformed and decorrelated and stretched images (Figure 4.4). Also spatial domain filtering was employed using digital filters for different directions as well as Laplacian filter. A kernel of 3x3 pixel size was selected and employed along directions N (0°), NW (45°), NE (45°) and E (90°) to highlight linear features in their respective directions. The lineaments were identified by visual inspection and interactively digitized in the images. A lineament map was constructed based on the total knowledge compiled from the digital enhancement of individual single band and multiband images (Figure 4.4), together with ground truth data. An attempt was made to avoid linear features that do not correspond to geological structures e.g. artifacts introduced by the digital filters. This includes man-made linear features such as roads and crop-field boundaries. Lineament mapping was done separately for each of the data sets, that is Landsat TM, SPOT and DEM images. Figure 4.4 illustrates the steps followed during the study.

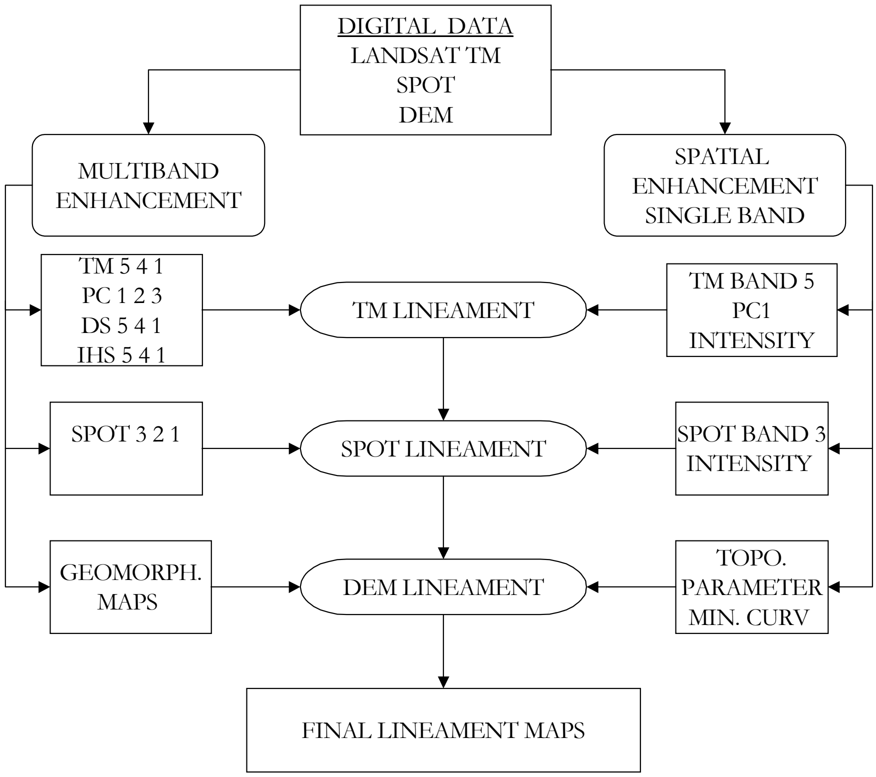

Figure 4.4. Flow chart depicting methodology of lineament mapping.

4.1.6 Image Interpretation

The visual interpretation of the remote sensing data was carried out by interactively digitizing the specific features of interest such as lithology and lineaments. The feature identifications were based on the recognition of boundaries between different assemblages of tone/color, texture, various shapes and patterns as well as interrelationships between features that may have geological significance in the imagery. These include, 1) Shapes (igneous intrusives and extrusives) and distribution of layering and/or layer parallel fabrics (foliation) and 2) Recognition of lineaments expressed by geomorphological features and tonal differences. In addition to previous knowledge of the study area and field excursions, different geological maps were utilized in the process of feature identification and classification. These include, at the scales of:

- 1:2,500,000 (Geological map of Eritrea, 1998)
- 1:250,000 (Geological map of Adi Grat Sheet, Ethiopia 1977)
- 1:250,000 (Geological map of Masswa sheet, Ghebreab 1998).
- 1:75,000 (Geological sketch map of the Asmara – Axum area, Hamrla 1978)

4.2 Structures

It is generally recognized that lineament or "fracture trace" analysis, used in conjunction with groundwater investigations of fractured hard rock aquifers, are not credible without field verification. For regional scale studies field checking of each lineament is impossible because of the significant cost and time involved (Mabee et al. 1994). However, systematic checking is possible and is necessary to decipher the nature of lineaments. Confidence estimates can be derived from a combination of suitable field observations together with supporting 'evidence' from other data sources (e.g. Sander et al. 1996 and 1997, Mabee et al. 1994).

The field data include observation and measurement of structural features. The major structures encountered in the study areas are joints, dykes and faults. The field investigations for site-1 and site-2 are discussed together. Location maps of the structures observed in the study area are presented in Chapter 5. Field data include orientation measurements, estimated spacing of joints as well as other field evidences presented in the form of figures and sketches.

Fracture orientations were obtained by measuring the dip and dip direction using a compass. The spacing was estimated on randomly selected outcrops. The data collection was confined to areas where the bedrock lithology is fresh, thus the observations were made along major streams and road cuts. After checking the data were grouped according to rock type and proximity of sampling points to take into account the geographic locations of observation points.

In order to understand the structural-geological significance of fracture arrays, it is common practice to subdivide the fracture system into separate sets on the basis of orientation. Rose diagrams were used to reveal the orientations of steeply dipping joints and dykes. Orientations of all measured fractures have also been presented as poles on the lower-hemisphere equal area projection. The measurements of joints and dykes were analyzed with Geo-orient version 8.0.

4.3 Geomorphology

Two types of digital elevation model data were available for this study. The first is a DEM with 50 m spacing derived from contours with 40 m equidistance. The histogram of the elevation data clearly shows frequency peaks at regular intervals of 40 m (Figure 4.5). Russian topographic map at a scale of 1:100,000 were used to derive the DEM. The digital elevation model are presented in Figure 4.6 and were used for derivation of topographic parameters such as slope as well as geomorphological mapping.

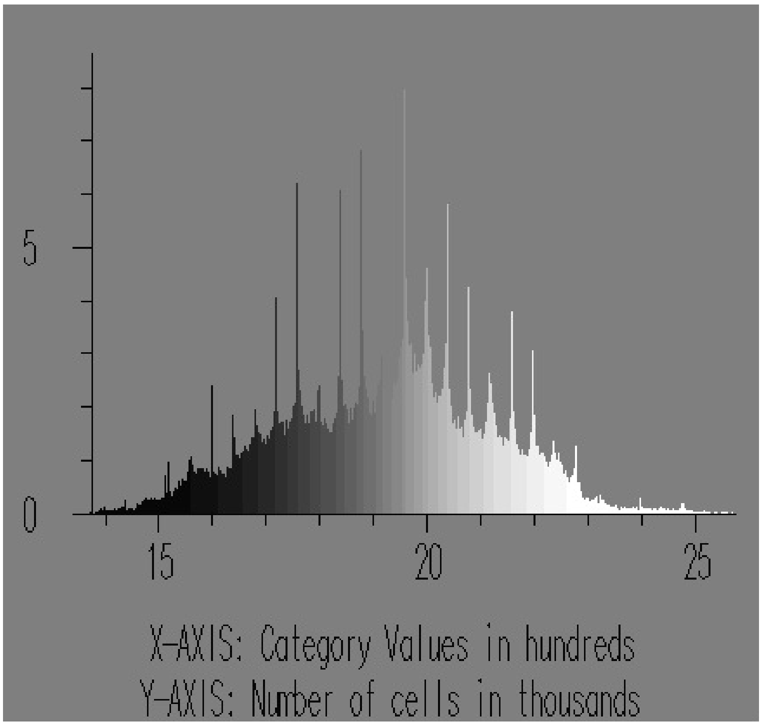

Figure 4.5. Frequency distribution of the contour derived DEM for site-2.

Data to derive the second digital elevation model were acquired during the Shuttle Radar Topographic Mission (SRTM) that was launched on February 11, 2000. The Shuttle Radar Topography Mission (SRTM) is an international project spearheaded by the National Imagery and Mapping Agency (NIMA) and National Aeronautics and Space Administration (NASA) in cooperation with the German Aerospace Center (DLR). The main objective of the SRTM mission is to obtain elevation data on a near-global scale and generate the most complete high-resolution digital topographic database of the Earth. SRTM was launched into an orbit with an inclination of 57 degrees. This allowed to cover the Earth's land surface between 60 degrees north and 56 degrees south latitude corresponding to 80 percent of the Earth's landmass. Using the Spaceborne Imaging Radar-C and X-Band Synthetic Aperture Radar (SIR-C and X-SAR) hardware, SRTM collects data that are used to generate a digital elevation model with data points spaced every 1 arcsecond of latitude and longitude (approximately 30 meters at the equator). The absolute horizontal and vertical accuracy is better than 20 meters and 16 meters, respectively.

SRTM uses radar interferometry. In radar interferometry, two radar images are taken from slightly different locations. This is realized in the SRTM system by one sending and receiving antenna in the shuttle cargo bay, and another receiving antenna at the tip of a 60 m long beam. Phase differences between these images allow for the calculation of surface elevation. For details in the techniques of radar interferometry see e.g. Jet Propulsion Laboratory (JPL) website (http://www.jpl.nasa.gov). With radar inteferometry the elevation of the top for instance buildings or vegetation cover is measured. In bare areas the elevation represents ground surface. Analysis of SRTM data by Koch (2002) indicates accuracy in height of about ± 3-4 m in open areas and the accuracy depend on land cover in particular in forests, settlements and water bodies. He also suggested the existence of some other systematic error (see Koch, 2002 for details). The SRTM data are compared with the contour derived DEM in terms of information content for geomorphologic and lineament mapping applications. The data have been smoothed using a 5 by 5 window low pass filter to reduce noise.

Topographic model parameters were calculated from the digital elevation model in figure 4.6 and used for geomorphological analysis. The theoretical background and the definitions of topographic model parameters are taken from Wood (1996) and are presented in appendix i. The topographic model parameters slope, longitudinal curvature, cross-sectional curvature, plan convexity and minimum curvature were calculated using a 5x5 kernel (Figure 4.7). They are used as input bands for landform feature classifications. Different combinations of 2 or 3 input bands are used to characterize the different feature types. Unlike the supervised classification, that involves a training step followed by the classification step, the unsupervised classification aggregates the data into a number of classes based on the natural groupings, or clusters, present in the data.

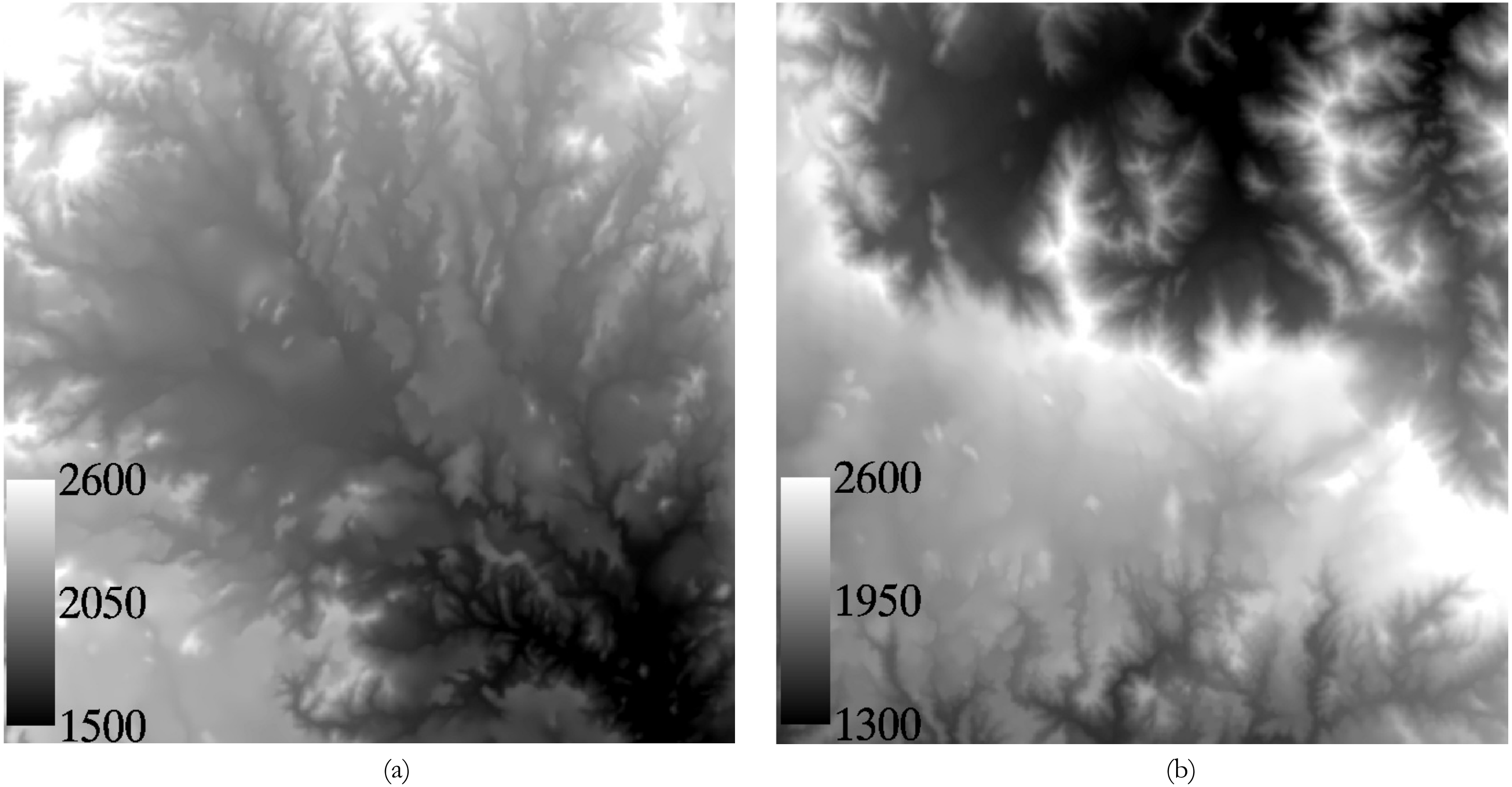

Figure 4.6. Digital elevation model (50 m) resolution data (a) site-1 and (b) site-2. White high elevation values and black low elevation values.

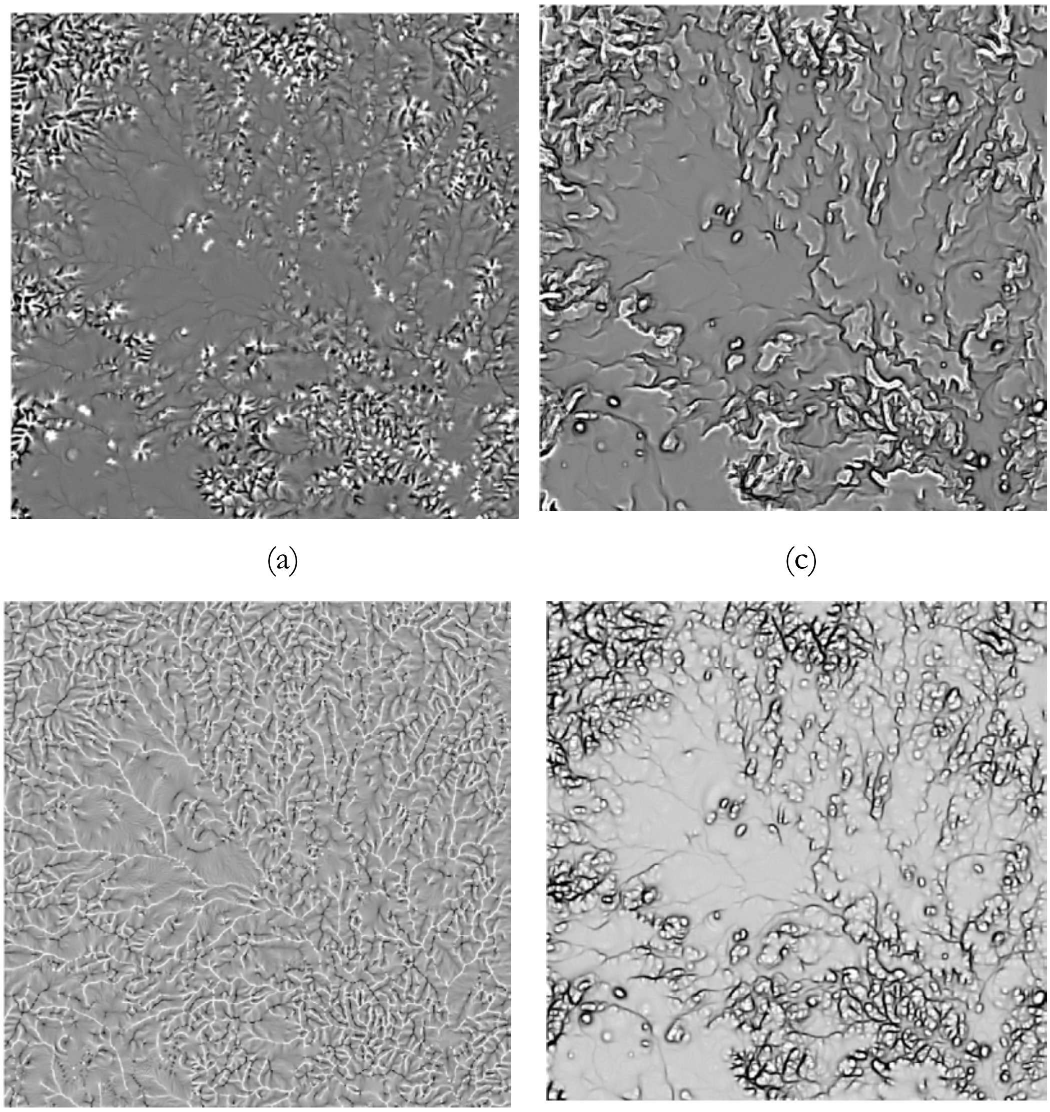

(a) (c)

(b) (d)

Figure 4.7. Topographic model parameter outputs derived from a DEM for site-1 (a) cross-sectional curvature showing partly the drainage networks, planes and ridges (b) plan convexity showing dominantly the drainage networks (c) longitudinal curvature showing the morphology of planes, terraces, and scarps (d) minimum curvature showing partly the surface curvatures, drainage networks and linear features.

The K-means clustering algorithm is used to determine natural groupings. It requires the number of clusters present in the data as input. The algorithm then arbitrarily defines that number of cluster centers in the multidimensional measurement space. Each pixel in the image is then assigned to the nearest cluster. After all pixels have been classified in this manner, new mean vectors for each cluster are computed. The revised means are then used to reclassify the image. The procedure continues until there is no significant change in assignment of pixels to clusters between successive iterations of the algorithm. Once this point is reached, the analyst has to determine the landform type of each class. In each classification stage the number of classes were set from 10 to 15 and the number of maximum iterations was set to 10. Clustering was performed using the original data for most of the inputs but for the slope the data were standardized (the slope values were divided by 10). Clusters representing similar landform types are combined to produce the geomorphological maps.

4.4 Hydrogeology

Data

Most hydrogeological data were provided by the Ministry of Land, Water and Environment, Department of Water Resources (WRD). The hydrogeological data obtained from the WRD consist mainly of water point database. The database was continuously updated during the fieldwork in August 1999 and January 2001. Additional hydrogeological data were collected from governmental and private organizations. These include the Ministry of Local Government (MLG), Eritrean Core Drilling Company (ECDC), General Development Engineering and Construction Company (GEDECC) and Universal Water Resource Consultants (UWRC). The hydrogeological data collected during the last two phases of the fieldwork include mainly well yield data on old and new boreholes, pumping tests and geological logging. All these data were collected from reports prepared by the different companies and entered into a common database.

The water point database is comprised of dugwell and borehole information. A total of 1867 water point data were obtained of which 96 percent in Excel file format and the remaining 4 percent were extracted from reports compiled by various organizations. The database includes borehole/dugwell identifier, site name, altitude, latitude, longitude, UTM X and Y coordinates, electrical conductance, approximate yield, depth to static water level, water point depth, pumping tests, geological logging, population size and other parameters such as pump system, water chemistry, and water point diameter. All the data do not include all the parameters mentioned and this required editing of the data set. From a total of 1867 records, about 75% of the data were excluded because of the following deficiencies:

1. Lack of location and/or coordinates
2. Duplicate observation points
3. Important parameters, such as, yield, depth, etc. missing
4. Obvious error in data entry

The remaining 25% or 470 records do not contain all the above parameters. About 69 percent (324 records) represent dugwell information and about 31 % (146 records) represent borehole data with estimated yield values. From the borehole data about 14 records include pumping test data. Thus, only 14 records contain most of the above mentioned parameters. The data set containing estimated yield values is based on 14 records from pumping tests and estimates based on observations made from hand pumps and bucket draws. The hydrogeological database used for this study is summarized in Figure 4.8. The frequency distribution for both the well yield (Fig. 4.8a) and depth to static water level (Fig. 4.8b) show a lack of symmetry, indicating a skewed distribution. However, the histograms of the log-transformed data in both variables show near symmetrical lognormal distribution. In contrast the frequency distributions of the well depth (Fig. 4.8c) and surface elevations (Fig. 4.8d) show near normal distribution. The data presented in figure 4.8 include all records, which contain the parameters used in this study. From the 14 pumping test records, only 4 data were used because the remaining lie outside of the study areas.

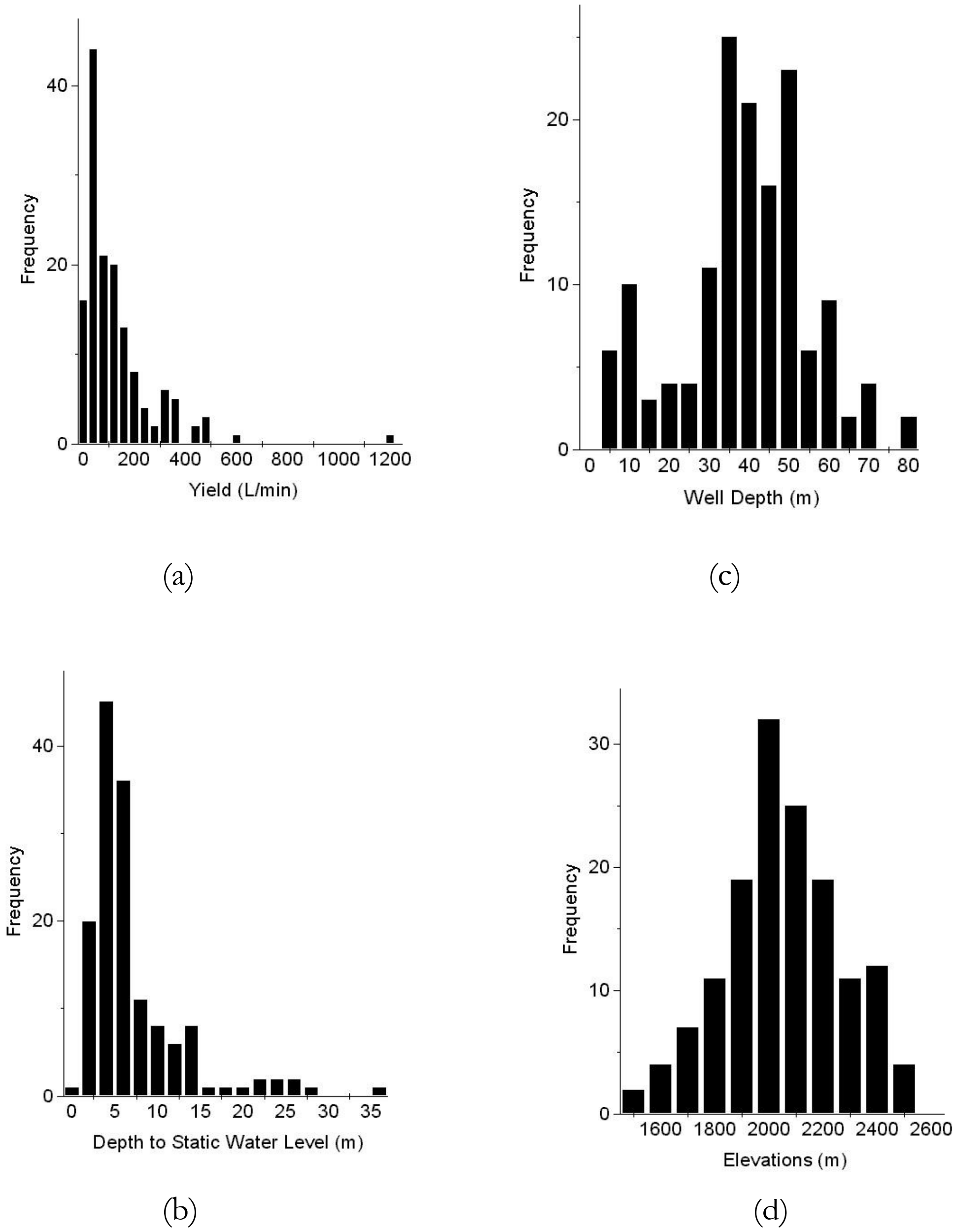

Figure 4.8. Summary of the hydrogeological data using the frequency distribution of (a) well yield data (b) depth to static water level (c) well depth and (d) surface elevations of wells. Number of observation is 146.

4.4.1 GIS Analysis

The hydrogeological data were entered into a GIS as an ASCII file. The GIS software utilized was GRASS versions 4.3 and 5.0 for a Linux based PC. Data sets were entered as site maps and many site maps were created that include the different parameters. The site maps were then converted into raster format. The raster files created within the GIS include water point yield, depth to static water level, well depth and elevations. The relationship of water point yields with lithology, lineament, topography and geomorphology was then assessed using GIS.

Water point locations were selected using a "MASK" layer and statistics was calculated for different map layers such as yield, static water level depth (SWLD), well depth, lithology, geomorphology and elevation. Furthermore, in order to investigate the relationship between well yield and local topography, the median elevation was calculated from the DEM map layer using a 5 by 5 pixel window and these estimated values were subtracted from the original elevation to compare well yield to variation in topography. If the median elevation is lower than the spot elevation then the difference will be positive indicating a topographic high and otherwise negative a depression. Thus the correlation of local topography with well yield can be easily portrayed. It is important to note that in assessing the relationship of water point yields with lithology, lineament and topography data values over a larger geographic region than Sites-1 and –2 were used in order to have more data for the statistical calculation.

Lineament interpretations of the study area were correlated with existing borehole data. The correlation studies were carried out using first the location values from the records and then GPS (Global Positioning System)-positioned or surveyed boreholes in the study area. The well yields were examined in relation to the mapped lineaments. Buffer zones with 20 m distance interval were created around the lineaments and then relationship between borehole yields and proximity to lineaments was assessed.

4.4.2 Field Investigations

Field investigations were conducted to assess the hydrogeological conditions of selected boreholes, dugwells and springs. Existing well sites were investigated with regard to location, relation to rock type, siting, topography and structure. Lithological log data at selected water points were constructed and correlated to establish the stratigraphy and unravel the subsurface hydrogeological controlling features. Pumping test data were used in conjunction with the lithological log to understand the nature of the aquifer systems in the study area. During the field investigations, static water level measurements were taken in open dugwells. Since the fieldwork was conducted during the peak dry season the measurements represent the lowest level of the water table.

4.4.3 GIS Modelling

All thematic maps were integrated into a raster based GIS. The modeling involves delineation of groundwater potential zones based on four thematic maps:

(i) Lithology
(ii) Lineaments
(iii) Geomorphology
(iv) Slope.

Every class in the thematic layers was placed into one of the following categories viz. (i) Very Good (ii) Good (iii) Moderate (iv) Low and (v) Poor depending on their groundwater potential level. Considering their behavior with respect to groundwater control, the different classes were given suitable values, according to their importance to other classes in the same thematic layer. The values assigned

to different classes for all thematic layers are given in table 4.2. The values were assigned in terms of their importance with respect to groundwater occurrences.
The values assigned to the lithology layer take into account the hydrogeological significance of the rock types. The characteristics considered for lithology are: rock type, type and thickness of weathering, fracture density, dykes etc. For instance, a maximum value of 80 was given for alluvium and basalt due to their favorable characters for groundwater accumulation owing to their primary porosities and permeabilities. The granitoid and schistose metamorphic rocks were assumed to have better groundwater accumulation than other rock types due to primary structures owing to joints and secondary structures owing to foliations, respectively. Furthermore, overall lineament density was also considered in assigning values for the lithology. For example, visual inspection of the lineament map showed high lineament density in the granitoid rocks compared to other rock types due to sparse soil cover.

In general, lineaments act as conduits for groundwater flow, and hence are hydrogeologically significant. The values given for lineaments were based primarily on the relation of well yields to proximity of lineaments. Accordingly five classes were defined based on distance from lineaments:

(i) Class 1 (0-50 m)
(ii) Class 2 (50-100 m)
(iii) Class 3 (100-150 m)
(iv) Class 4 (15-200 m)
(v) Class 5 (200-250 m).

Values assigned to the various classes in the lineaments decrease as the distance of buffer zones around the lineaments increase. This implies that the closer the buffer zones are to lineaments the better are the chances for groundwater targeting.

Table 4.2. Values assigned for different groundwater control parameters (modified after Krishnamurthy et al. 1996).

Parameter		Value	Parameter		Value
Lithology			*Geomorphology*		
Alluvium	(VG)	80	Channels	(VG)	80
Basalt	(VG)	80	Planes	(G)	70
Foliated met.	(G)	70	Terraces	(G)	60
Metasediments	(G)	70	Pediment	(M)	50
Granite (syntectonic)	(M)	60	Scarps	(P)	10
Granite (posttectonic)	(M)	60	Ridges	(P)	10
Nonfoliated met.	(M)	50	Peaks	(P)	10
Gneiss	(L)	40			
Laterite	(L)	40			
Kaolinized Granite	(P)	10			
Lineament (buffer zones)			*Slope*		
0 -50 m	(VG)	80	0 -3°	(VG)	80
50 –100 m	(G)	70	4 -7°	(G)	70
100 -150 m	(M)	60	8 -11°	(M)	60
150 -200 m	(L)	40	12 -15°	(L)	40
200 -250 m	(P)	10	> 15°	(P)	10

VG=*Very Good* G=*Good* M=*Moderate* L=*Low* P=*Poor*

The landforms of the study areas were classified into seven classes and values assigned according to the landform type. For instance, channels and planes were considered best targets of groundwater occurrence and thus labeled with 80 and 70, respectively. In contrast, scarps, ridges and peaks are labeled 10 as poor candidates for groundwater. The DEM (figure 4.6) was used to produce slope maps.

The following slope classes were defined:

(i) Class 1 (0-3^{o})
(ii) Class 2 (4-7^{o})
(iii) Class 3 (8-11^{o})
(v) Class 4 (12-15^{o})
(vi) Class 5 (>15^{o})

It can also be seen from table 4.2 that the value given for the parameter slope decreases as the slope increases. This implies that the flatter the topography is the better are the chances for groundwater accumulation. The values for each thematic layer were added and then grouped into different groundwater potential zones. The final groundwater potential zone map was generated and compared with the yield data to ascertain the validity of the developed model.

4.4.4 Groundwater Recharge Estimation

Estimation of recharge is of high importance for the assessment of groundwater resources of an area. Two dominant mechanisms occur: direct recharge, whereby water enters the saturated zone of the aquifer directly from precipitation infiltrating through the unsaturated zone, and indirect recharge, whereby recharge enters the saturated zone indirectly through some form of runoff infiltration (Lloyd 1999). Various methods to estimate groundwater recharge are available. In this study the groundwater recharge is estimated based on the water table fluctuation and chloride mass-balance methods and the estimates are compared with previous studies. The estimation of groundwater recharge in crystalline and other hard rocks is faced with greater problems than in sedimentary rock aquifers, on account of their heterogeneity (Singhal and Gupta 1999).

Water-table Fluctuation Method

Observations of the seasonal fluctuation of groundwater table are used to estimate groundwater recharge in the various rock units encountered in the study area. High groundwater levels were determined from encrustations on the sides of open wells as well as by enquiring local people about the level to which the groundwater rises during the peak rainy seasons. Measurements of low groundwater levels were made immediately before the start of the wet season. The main assumption is that if the rainfall reaches the water table, the amount of rise is mainly a function of the effective porosity (specific yield) of the strata, which become saturated. If the actual fluctuation in groundwater level is Δs (mm), and the effective porosity of the strata is ϕ, the recharge (mm) can be calculated as $\phi\Delta s$ (mm). The major drawback of this method is that average rise in water table over the extent of the aquifer is difficult to estimate accurately and large errors in the estimation occur due to unrepresentative values of the effective porosity. Effective porosity is difficult to measure without long duration pumping tests with observation boreholes. Nonetheless such measurements are useful as a check on other methods.

Chloride Mass-Balance Method (CMB)

The chloride mass-balance (CMB) technique has been suggested as suitable tool in estimating groundwater recharge in arid regions where measurement of hydrological parameters are not reliable because influx and outflux are very small and difficult to determine (Simmers 1988). Input of chloride to groundwater comes mainly from rainfall and dry fallout and it can be either oceanic or terrestrial in origin. Chloride is selected due to its conservative nature and its availability in large quantities for measurements with reliability and ease. Chloride has been used for estimating regional recharge based on its concentration in the saturated zone by Eriksson and Khunakasem (1969) as well as in estimating localized recharge by considering its concentration in the unsaturated zone (Allison and Hughes 1978). Nkotagu (1996) has applied the CMB method in a semi-arid environment in the fractured crystalline basement area of Dodoma, Tanzania. The main assumptions behind the technique can be summarized as follows:

1. Flux rates have reached a steady state over time and thus the concentration is accurately represented by the mean concentration measured from available rainfall samples.
2. No addition of chloride from other external sources (e.g. fertilizers, animals and/or human faeces waste),
3. There is no net change of chloride due to storage or loss by water-rock interaction.
4. Water movement from the surface to the saturated zone is through the matrix, no bypass or preferential flow.

Application of the method requires that the only source of chloride in groundwater be from precipitation. That is, chloride concentrations in the aquifer reflect the degree to which the chloride in rainwater has been concentrated by evaporation. Thus knowing the amount of annual precipitation, and the chloride concentration in both groundwater and precipitation, it is possible to calculate the recharge flux using:

$$Q = \frac{PCl_{wap}}{Cl_{gw}}$$

Where Q = groundwater recharge flux (mm/yr); Cl_{gw} = chloride concentration in groundwater (mg/l); P = precipitation (mm/yr); and Cl_{wap} = weighted average chloride concentration (wet and dry) in precipitation (mg/l).

5 RESULTS

5.1 Remote Sensing

5.1.1 Band combinations

The selection procedure using the statistical techniques was applied for a subscene of Thematic Mapper data that covers the most prominent rock types in site-1, the basalt and the crystalline rocks (igneous intrusive and metamorphic rocks). The band combination 1 4 5 is the triplet with the highest determinant (appendix ii). Figure 5.1a shows TM band 5, 4 and 1 combination in red, blue and green (RGB) order for site-1. The basaltic rocks appear in dark gray to dark green in color. The greenish color in this unit is attributed to vegetation. The lateritized crystalline rocks are characterized by dark brown to pinkish to reddish color. Highly altered foliated metamorphic unit appear in yellowish color with shades of white color attributed to kaolinization. Similarly, kaolinized igneous intrusive rocks, which are in contact with the basaltic rocks, appear in white color. Non-foliated metamorphic rocks appear gray to dark gray and are in contact with the granitic intrusive of light brown to pinkish in color. The quaternary sediments within the intrusive rocks appear in white color. Other features such as geologic contacts for most of the lithologic units encountered in the area as well as lineaments of N-S orientations and dyke swarms of NW-SE trends are conspicuous within the granitic intrusive bodies (Fig. 5.1a).

The same color composite image for site-2 proved to be less informative (Figure 5.2a). Site-1 consists of rocks of contrasting mineralogy such as basalts and crystalline rocks and this is reflected by contrasting colors on the image (Figure 5.1a). In contrast, in site-2 crystalline igneous intrusive and metamorphic rocks dominate with more or less similar mineralogy and thus less contrast as manifested in the color composite image. The statistical technique for color composite selection was also applied in this site which covers the crystalline rocks only and again the band triplet 1 4 5 has the highest determinant (appendix ii). Determinant values for band triplet 1 4 5 are about 67 times higher for site-1 than for site-2 (see appendix ii). The very low determinant value for site-2 is attributed to the low information content in the scene as a consequence of little mineralogical contrast in the crystalline rocks. The band triplets associated with the determinants are ranked in order of decreasing overall information content (Sheffield 1985).

It is important to note that although band triplet 1 4 5 has the highest determinant and is used for the purpose of this study, a quick visual inspection of band triplet 1 4 7, ranked second in site-1 provides similar results. Triplets that rank high always include either band 5 or band 7. This emphasizes the great importance of bands 5 and 7 on general information-bearing grounds (Sheffield 1985). In contrast the natural color combination 1 2 3 and the color infrared 2 3 4 combination are ranked very low in both sites. This is probably a consequence of the high correlation between the first four bands because the determinant analysis is based on selection of band triplets with least correlation.

5.1.2 Principal Component Analysis

Principal component analysis (PCA) was performed with the six reflective bands of TM and a number of different three-band PC color composite combinations were created and analyzed for their content. After transformation the data were subjected to histogram equalization to enhance spectral differences in the terrestrial materials. Several color combinations of PC images were assessed. The most informative PC color composite for site-1 is that of PC 1, 2 and 3 in RGB order (Figure 5.1b).

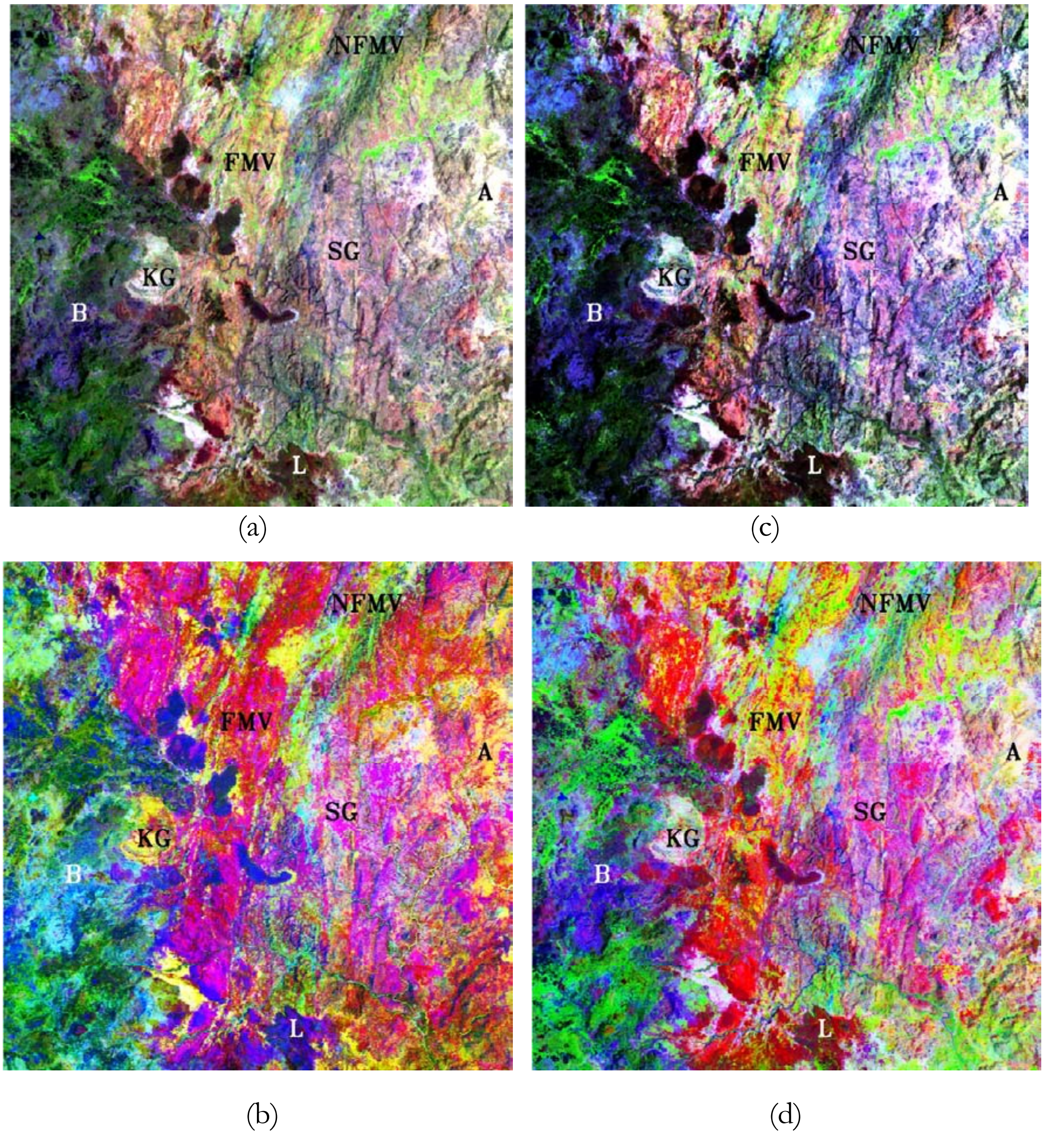

Figure 5.1. Processed Landsat TM images for Site-1. Image size 20 x 20 km covering the southeast corner of figure 5.3a; (a) Color composite bands 5 4 1 (b) Color composite of PC 1 2 3 (c) IHS-enhanced composite of bands 5 4 1 and (d) DS composite bands 5 4 1, all in RGB orders, respectively. A=alluvium, B=basalt, L=laterite, KG=kaolinized granite, SG=syn-tectonic granite, NFMV=non-foliated metavolcanic and FMV=foliated metavolcanics.

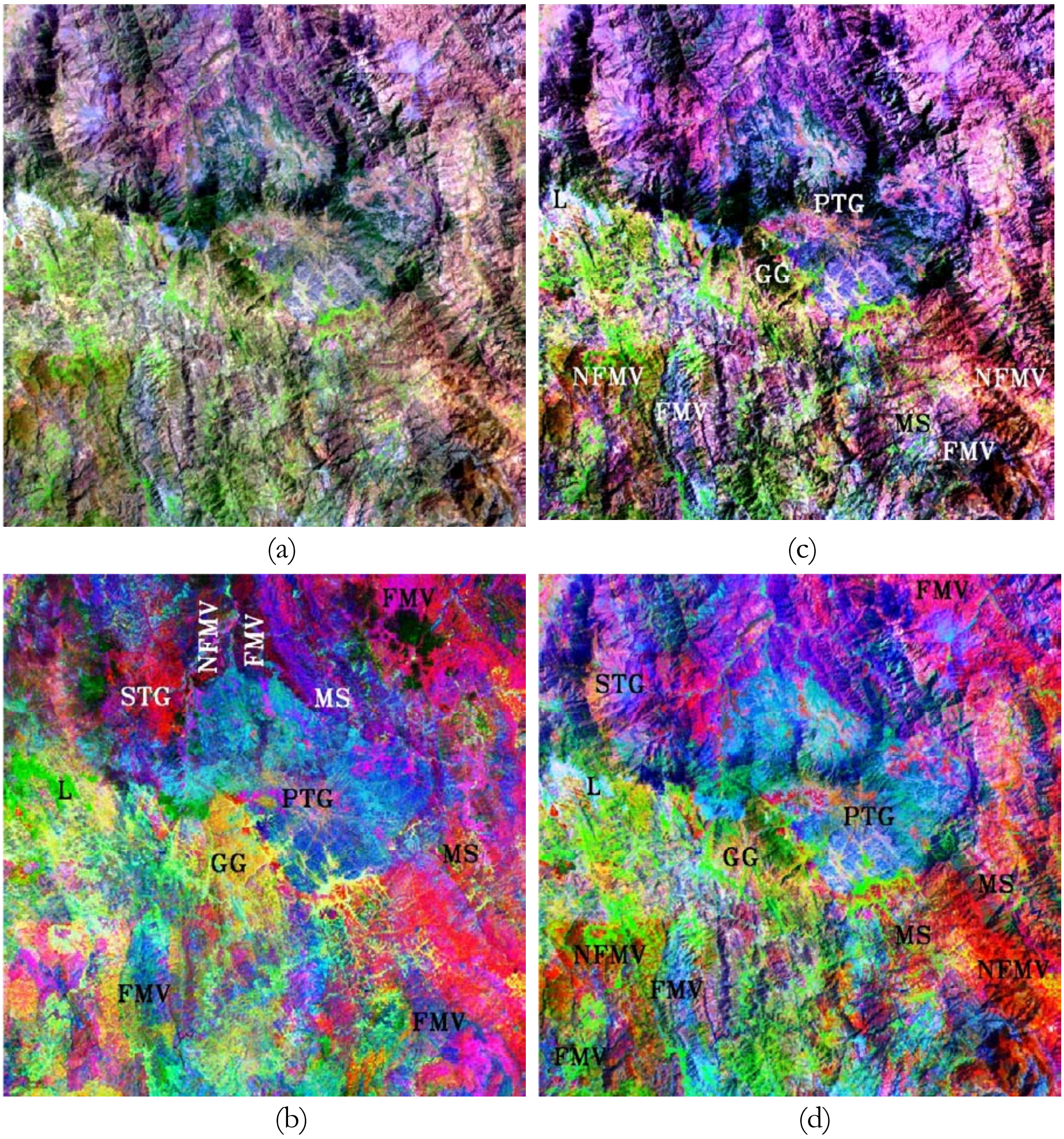

Figure 5.2. Processed Landsat TM images for Site-2. Image size 20 x 20 Km covering the southeast corner of figure 5.3b; (a) Color composite bands 5 4 1 (b) Color composite of PC 3 2 4 (c) IHS-enhanced composite of bands 5 4 1 and (d) DS composite bands 5 4 1, all in RGB orders, respectively. L=laterite, STG= syntectonic granite, PTG=post-tectonic granite, MS=metasediment, FMV= foliated metavolcanic, NFMV=non-foliated metavolcanic and GG=granite gneiss.

Although most of the geologic contacts are obvious in this image, certain lithologic units share similar colors. For instance the foliated metamorphic rocks and part of the intrusive igneous rocks both appear in magenta and dark red colors. Similarly basalt and laterite exhibit blue color. A disadvantage of the PCA approach is the difficulty in interpreting a color composite made from PC (Chavez and Kwarteng 1989, Kaufmann 1988). This diminishes the interpretability of data. Other features such as geologic contacts for most of the lithologic units encountered in the area as well as lineaments of N-S orientations and dyke swarms of NW-SE trends are conspicuous within the granitic intrusive bodies (Fig. 5.1b). Lineaments with orientations of N-S, NNE-SSW and NW-SE trends appear to be more enhanced. The enhancement of the lineaments in the PC image is due to the inclusion of PC1 in the color composite which contains mainly brightness information enhancing the topography.

In site-2 PC 3, 2, 4 in RGB order (fig. 5.2b) proved to be more effective in discriminating the geologic contacts among the metamorphic rocks, e.g. foliated metavolcanics and metasedimentary rocks (e.g. top of Figure 5.2b). Moreover the post-tectonic granitic intrusion with oval shape, which appear in blue, and the granitic gneiss that exhibit yellow color, are more enhanced in the PC image (Figure 5.2b) than in the standard color composite (Figure 5.2a). Linear features are not obvious on the PC image due to the exclusion of PC1 that resulted in lack of contrast.

5.1.3 Intensity-Hue-Saturation Transformation

An intensity, hue and saturation (IHS) - transformation was applied to TM bands 5, 4 and 1, and is presented in Figures 5.1c and 5.2c, respectively, for site-1 and site-2. The different lithologic units have similar colors as in the standard color composites (Figures 5.1a and 5.2a) but the IHS images obtained from the transformed data gave an image with higher color saturation. In general geologic contacts (e.g. between foliated and nonfoliated metavolcanic units in site-2, Figure

5.2c) and structural features (e.g. NW-SE trending dykes in site-1, Figure 5.1c) are better enhanced when compared with the standard color composites. The advantage with the IHS enhanced image (Fig. 5.1c and 5.2c) is that since the transformation effectively separates intensity and spectral information from a standard image such as in fig. 5.1a, better color saturation allows to differentiate major lithologies. The diagnostic features are discernible mostly by distinct hues. The enhancement of the structural features is presumed to be due to enhancement of the topographic features in the intensity image.

5.1.4 Decorrelation Stretch

The decorrelation stretch (DS) conducted on TM bands 5, 4 and 1 is shown in Figures 5.1d and 5.2d. In site-1 (Fig. 5.1d) better lithological contrast was obtained when compared, for instance, with the standard band combination (Fig. 5.1a), PC (Fig. 5.1b) and IHS-transformed images (Fig. 5.1c). The distinction between non-foliated (deep red color) and foliated metavolcanic (blue and magenta color) rock units was possible using this technique in site-2 (Fig. 5.2d). Moreover most of the lithologic units in the site are discernible in the image. In general, decorrelation stretch proved to be the most effective in accentuating colors, thus facilitating visual discrimination of various lithologies in both sites. This is because the technique removes the high correlation commonly found in multispectral data sets and thus produces more colorful composite images.

5.1.5 Lithological Interpretation

In site-1 all digital image-processing outputs gave good results that enable to map the major lithologic units. Other features such as geologic contacts for most of the lithologic units encountered in the area as well as lineaments of N-S orientations and dyke swarms of NW-SE trends are conspicuous in all digitally processed images (Fig. 5.1). In this site, lithological interpretation is principally based on the standard color composite of TM bands 5, 4, 1 in RGB order (Fig.

5.1a) and the DS image (Fig. 5.1d) is used to refine the geologic contacts. Seven lithologic units were mapped and could be distinguished one from the other by distinct colors in the processed images. These are: alluvium, basalt, laterite, kaolinized granite, foliated metavolcanics, nonfoliated metavolcanic and syn-tectonic granites. Figure 5.3a shows the obtained interpretation map of site-1.

Unlike in site-1, lithological interpretation in site-2 was difficult because of the complexity of the geology. In this site several color composites were used for the lithological interpretation because certain features are more enhanced in certain outputs than others. Due to little contrast in mineralogy certain lithologic units could not be identified distinctly in the processed images (Figure 5.2). Typical examples include the syn-tectonic granites and various units in the metamorphic rocks. The meta-sedimentary unit is comprised of pelitic to phyllitic rocks and the foliated metavolcanic unit is dominantly chloritic schists, however, inter-layering of these two units is common. Moreover, carbonaceous rocks such as marble and siliceous rocks such as quartzite are locally found interbedded within these rock units. The resemblance in color in most of the rock units is thus probably attributed to composition. Figure 5.3b is the lithological interpretation map of site-2 constructed from the input of all digitally processed images. Ground truth data was used to supplement the interpretation and refine geologic contacts. Several lithologic units were mapped: alluvium, laterites, post-tectonic granite, syn-tectonic granite, granitic gneiss, metasediments, foliated metavolcanics and nonfoliated metavolcanic rock units.

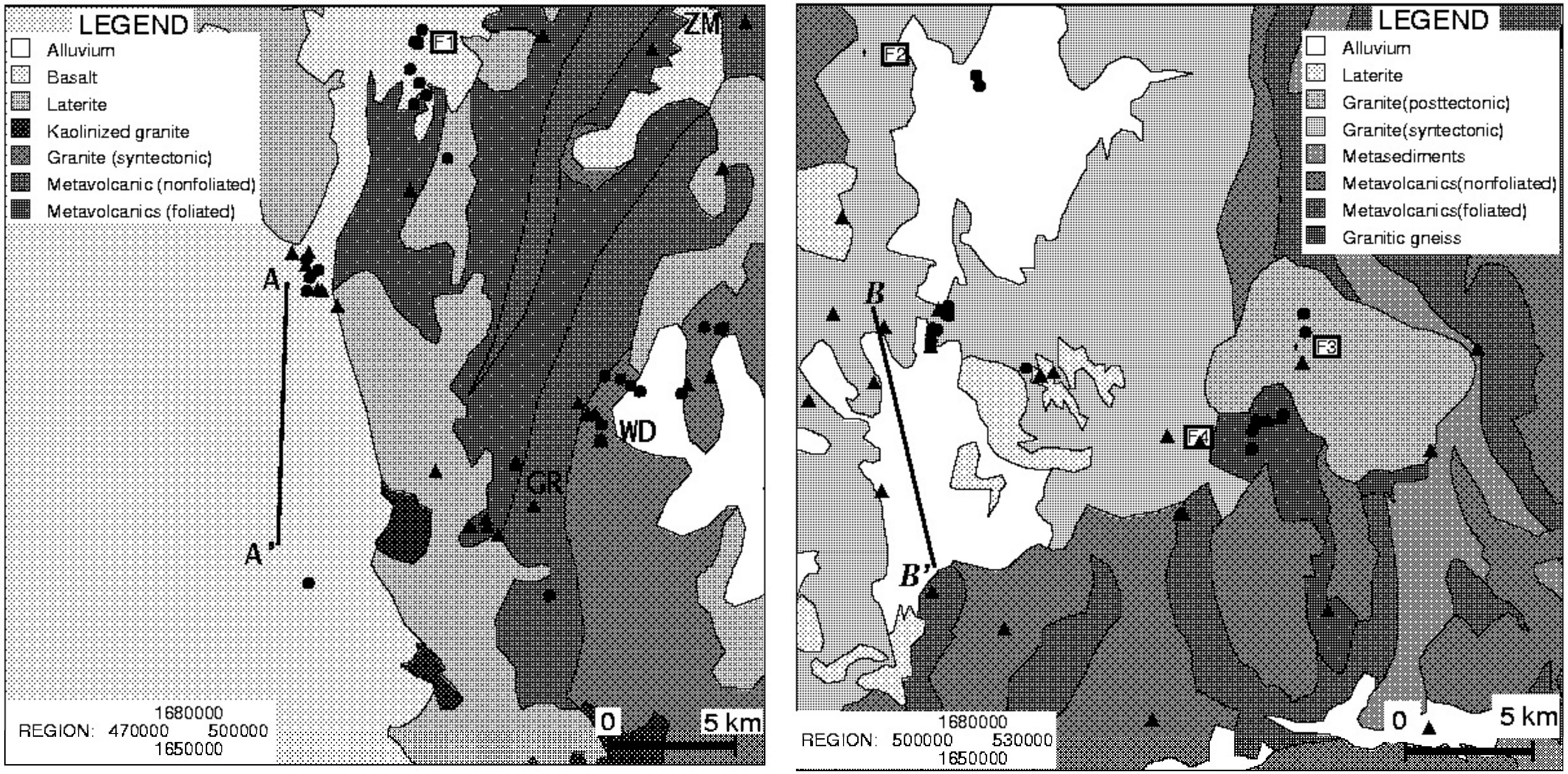

(a) (b)

Figure 5.3. Lithological interpretation of (a) site-1 (b) site-2. Locations of joint measurements (triangles), dykes (circles) and faults (alphanumeric). Localities ZM=Ziban Mengeb, GR=Gergera and WD=West Dekemhare. The profiles along A-A' and B-B' are discussed in Section 5.4.2.

5.1.6 Spatial Enhancement for Lineament Mapping

Lineaments are clearly discernible in almost all the digitally processed color composites (Fig. 5.1 and 5.2). Most of the linear features are enhanced due to color contrast with some of them representing geologic contacts. The absence of visible lineaments in the basaltic rocks in the color composites might be due to lack of contrast. Directional filtering was applied to single band images outlined in Section 4.1.5 along N-S, NW-SE, NE-SW and E-W directions. The results show good enhancements of linear features along most of the directions except E-W. This is probably due to the absence of lineaments in this direction or use of a too small kernel size. The output of directional filtering of Landsat TM band 5 (Fig. 5.4a) along the N-S direction is presented in figure 5.4b for site-1. The application of the directional filter strongly highlighted lineaments along the filtering direction. Moreover, it also emphasized NNE-SSW, NNW-SSE, NW-SE and NE-SW trending linear features, because these trends are oblique to the direction of filter. Although major lineaments can be detected from the raw image data, most of the finer details are more clearly recognizable in the filtered image. Most of the lineaments detected from the directional filtering lie in the crystalline rocks and almost no lineaments are visible in the basaltic rocks (Fig. 5.4b). Lineaments with NW-SE orientation (northeast in fig. 5.4a and 5.4b) represent a pair of dyke swarms.

A Laplacian (non-directional) filter applied to the minimum curvature image, a topographic model output from the DEM, is shown in figure 5.4c. In this image most of the lineaments are associated to geomorphological features mainly drainage channels. The most conspicuous ones are lineaments with N-S trends defined by aligned drainage channels. Lineaments with NE-SW and ENE-WSW trends are less obvious and NNE-SSW trending ones are absent on this image. However, lineaments in the basaltic rock units are well identified in this image when compared with the directionally filtered output of the TM image (Fig. 5.4b).

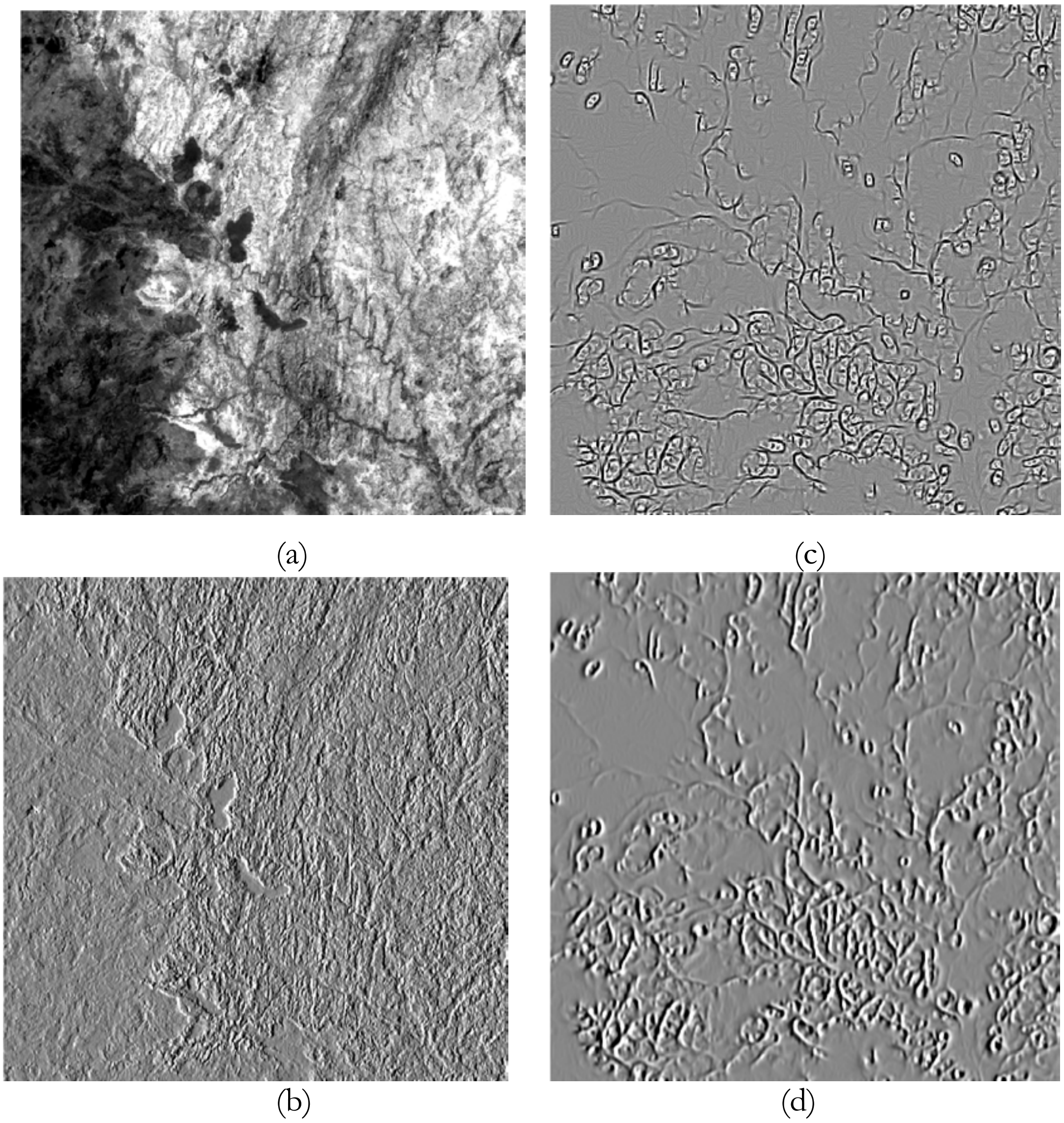

Figure 5.4. Edge enhanced images in Site-1 (a) Landsat TM band 5 raw image (b) directional filtering applied along N-S direction on TM band 5 (c) Laplacian filtering applied on topographic model output (minimum curvature) image and (d) directional filtering applied along N-S direction on the minimum curvature image. Image size 20 x 20 Km each and represent the same locality as figure 5.1.

The dyke swarms visible on both the raw TM band 5 and filtered images are not visible on the minimum curvature images (Figs. 5.4c and 5.4d). Application of directional filtering on the minimum curvature image (Fig. 5.4d) proved to be less useful.

Application of directional filtering along a N-S direction on PC1 image is shown in figure 5.5a for site-2. The filtered image exhibits obvious lineaments with orientations of N-S, NNW-SSE, NW-SE and NE-SW. Directional filtering applied along NE-SW direction on the Landsat TM intensity image is given in figure 5.5b. This figure appears more or less similar to the N-S directionally filtered PC1 image (figure 5.5a). Lineaments oriented oblique to the direction of filtering (NE-SW) such as the N-S and NNW-SSE are equally enhanced. In contrast the NW-SE lineaments appear to be subdued because they parallel the filter direction. On the other hand, NE-SW trending lineaments are slightly more enhanced than in figure 5.5a. These variations are due to the filtering direction. Figure 5.5c is the raw Spot band 3 image and the output of filtered image along the N-S direction is given in figure 5.5d. Already in the raw image linear features are conspicuous, for instance, N-S, NNW-SSE, NW-SE and NE-SW trending lineaments. In the filtered image all these linear features are enhanced but some lineaments still appear better defined in the raw image than the filtered ones possibly due to lithologic variations. A typical example is the N-S lineament, which lies top center of figure 5.5c. Comparison of the N-S filtered images, for instance, from PC1 (fig. 5.5a) and Spot band 3 (fig. 5.5d) images shows that linear features are better enhanced in the former despite high resolution in the later. This is probably due to lack of brightness in Spot band 3 image. Similar explanations may be provided for the difference in highlighting the NE-SW trending lineaments between the filtered image of Spot (fig. 5.5d) and the TM intensity image (fig. 5.5b) though the direction of filtering is different.

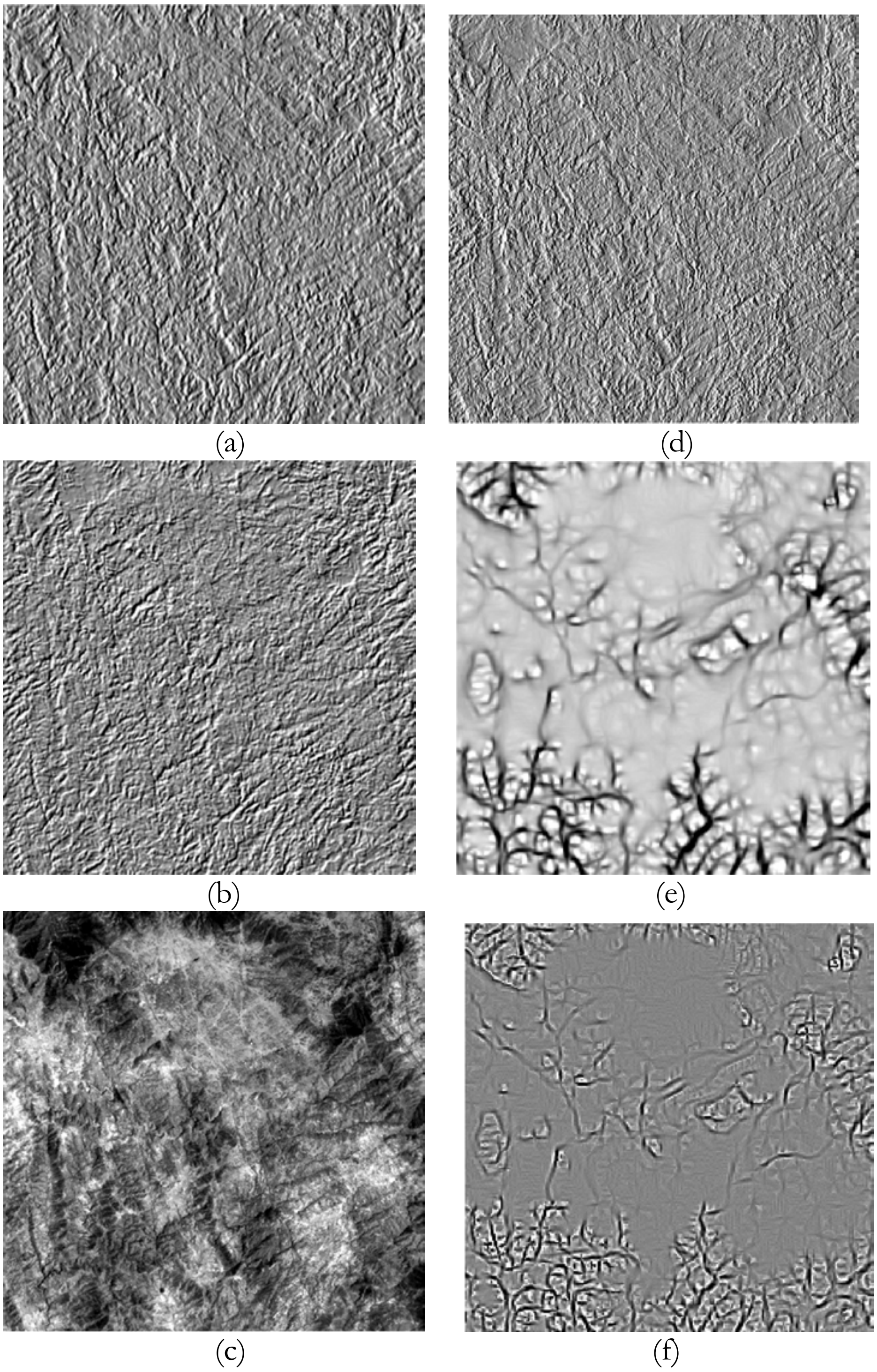

Figure 5.5. Edge enhanced images in Site-2 (a) directional filtering applied along N-S direction on PC1 image (b) directional filtering applied along NE-SW direction on TM intensity image (c) Spot band 3 raw image (d) directional filtering applied along N-S direction on Spot band 3 image (e) Topographic model output (minimum curvature) image and (f) Laplacian filtering applied on minimum curvature image. Image size 12 x 12 Km each.

The minimum curvature image, an output from the DEM is presented in figure 5.5e. Figure 5.5f show non-directional filtering applied at the same image. In both of these images lineaments that are mainly expressed by topographic features appear well identified and enhanced. However, lineaments from the non-filtered minimum curvature image are more conspicuous than the filtered ones. Lineaments trending N-S, NNW-SSE, and NW-SE appear more conspicuous than NE-SW trending ones. Major lineaments are better enhanced in the minimum curvature images (figs. 5.5e and 5.5f) than other images (figs. 5.5a-5.5d). An example is the N-S trending lineaments that lie at the center and bottom of the images in figures 5.5e and 5.5f. This is due to containment of topographic information in the digital elevation model data. However, not all major lineaments of N-S orientation are also visible in the minimum curvature images. For instance the N-S lineament, which lies center top of figs. 5.5a-5.5d, is not visible in figures 5.5e and 5.5f. This shows that major lineaments are partly expressed by lithologic variations, which cannot be seen in the DEM data. NE-SW trending lineaments are better enhanced in images other than the minimum curvature images. Although most of the major linear features are obvious in the DEM data, the density of lineaments is less when compared with the lineaments observed in the Landsat TM and Spot images. These differences are attributable to lack in spectral information in the DEM data as well as its low resolution (50 m) in comparison to the improved resolutions of TM (30 m) and Spot (20 m) data.

5.1.7 Lineament Interpretation

Lineament maps produced from Landsat TM, SPOT and DEM digital data were used as an input for the preparation of the final lineament maps. Figures 5.6a and 5.6b are the final lineament maps created by combining the three interpretations and editing the duplications in each of the file records for sites-1 and site–2, respectively. Rose diagrams for DEM, SPOT, TM and total lineaments, are also given for both sites in Figures 5.7 and 5.8. Length and trends of lineaments are displayed in the rose diagrams. The azimuth sector size is 5 degrees and length is cumulative for all lineaments within each sector. The number of lineaments in the diagram (n) is noted. Lineament trends are strongest at N-S (NNW-SSE), NW-SE, NE-SW and ENE-WSW. All the major linear features are detected in all the imagery groups. However, certain trends appear to be masked by the frequency of other trends, for instance, the N-S trending lineaments derived from the SPOT images (Figures 5.7b and 5.8b). The number of lineaments mapped from SPOT data is the highest in both sites possibly due to the improved resolution when compared with the other digital data. NE-SW trending lineaments were not detected from the DEM data in site-2 (Fig. 5.8a). As discussed earlier this is probably due to the low resolution of the DEM data, because lineaments with the same trends are detected in both the SPOT and TM data (Figures 5.8b and 5.8c). WNW-ESE trending lineaments are also represented by minor peaks in both sites. The existence of this trend is more obvious in the rose diagram produced over 60 by 60 km area from the TM data that includes both sites (figure 5.9).

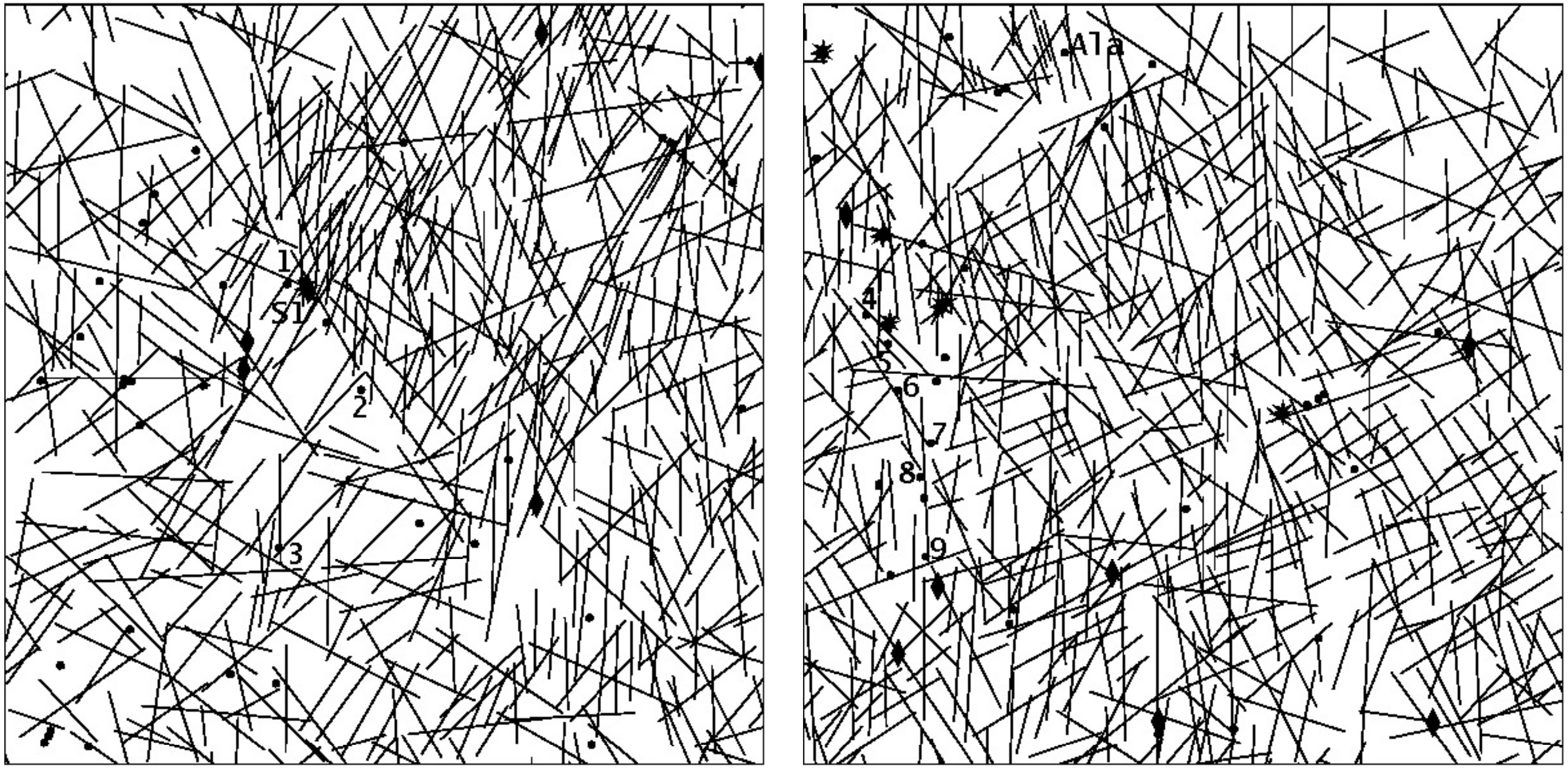

(a) (b)

Figure 5.6. Lineament interpretation maps of (a) site-1 (b) site-2. Locations of wells (circles), springs (stars) and groundwater outcrops (diamond). S1=location of spring, Ala=locality in site-2, and numbered boreholes used to construct cross-sections along A-A' (fig. 5.3a) and B-B' (fig. 5.3b).

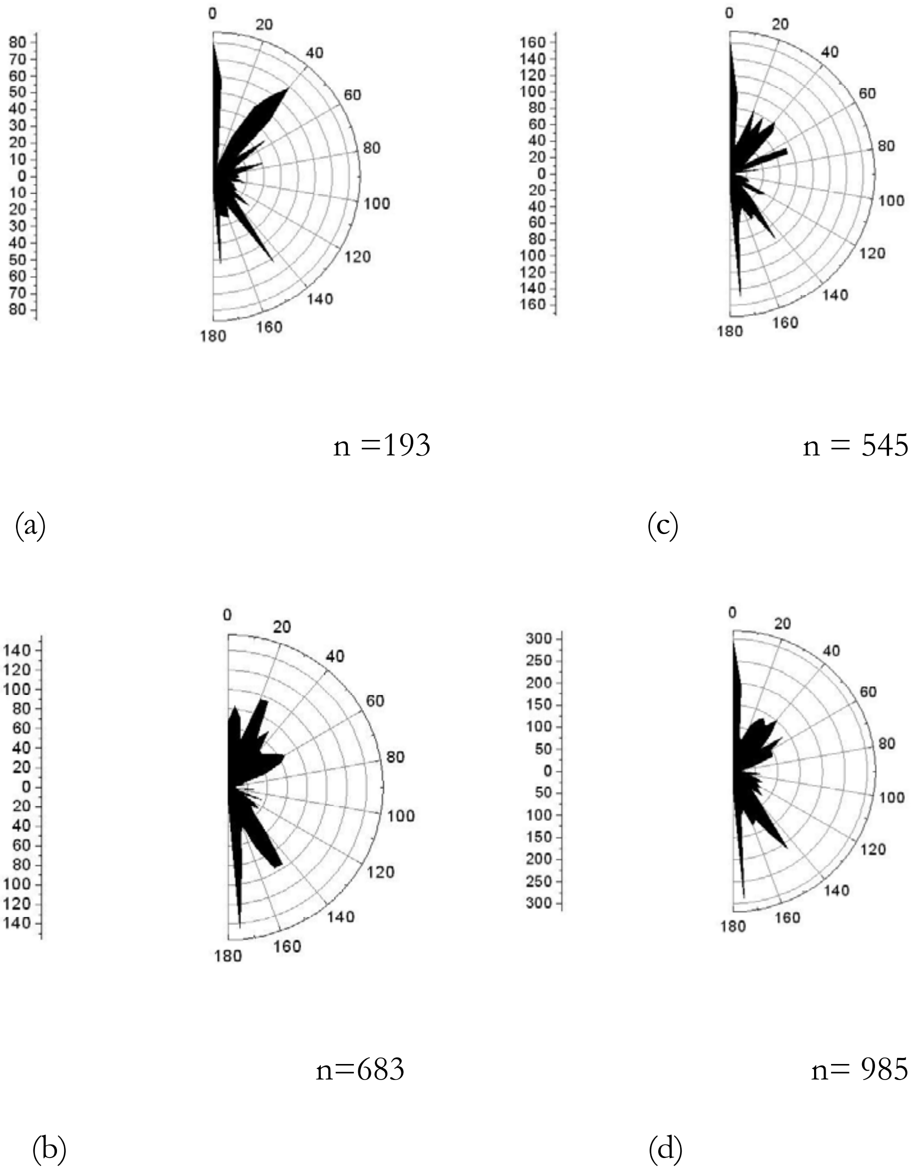

Figure 5.7 Length weighted rose diagrams of lineaments in site-1 (a) DEM (b) SPOT (c) Landsat TM and (d) total lineaments. Vertical scale cumulative lengths in kilometers.

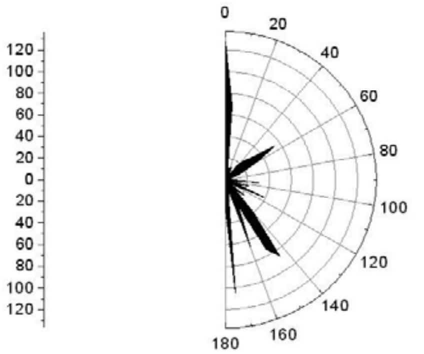

n = 218

(a)

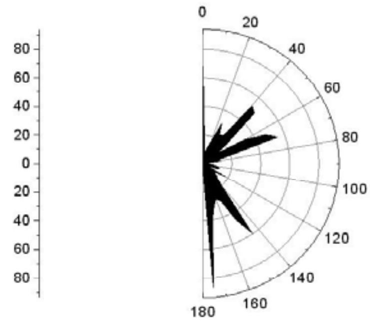

n = 288

(c)

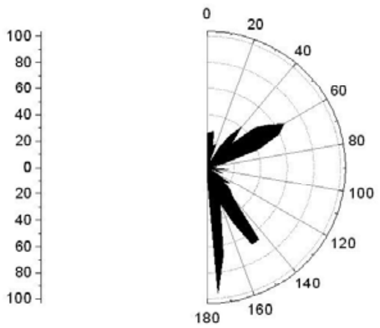

n = 413

(b)

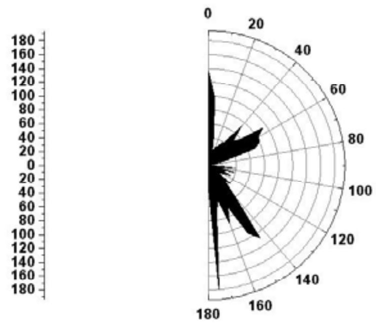

n = 546

(d)

Figure 5.8 Length weighted rose diagrams of lineaments in site-2 (a) DEM (b) SPOT (c) Landsat TM and (d) total lineaments. Vertical scale cumulative lengths in kilometers.

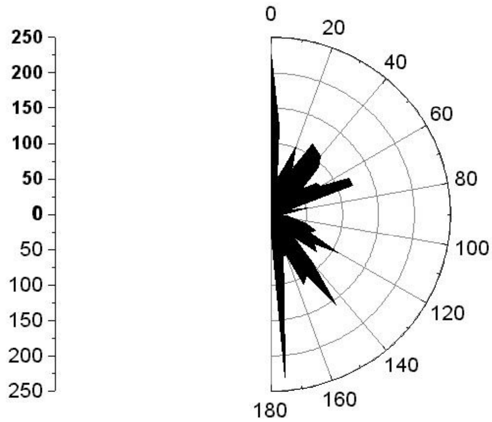

n = 891

Figure 5.9. Length weighted rose diagram of regional lineaments from TM. Vertical scale cumulative lengths in kilometers.

5.1.8 Evaluation of ASTER Data for Lithology and Lineament Mapping

In order to assess the potential of ASTER data for rock type discrimination, principal component transformation was performed on the data that covers study site-2. Results of the PC transformation of the 14 ASTER bands were first evaluated one by one and then different sets of color composites were created to assess their potential for rock type mapping. The first principal component image (PC1) is dominated by topography and brightness attributed from the TIR bands. The image is acquired at about 10:30 local time in the morning and this is not the optimum hour to see radiant temperature differences that could exist between earth surface materials. The brightness difference is due to shadows from topographic features and slope orientation effects. The second and third PC images (PC2 and PC3) show morphology, drainage, infrastructures and land use patterns. PC4 to PC9 contain information on rock types and their variations due to weathering. The higher order principal components (PC10-14) are dominated by noise.

A color composite of the first three principal component images (PC 1, 2 and 3 in RGB order) is presented in Figure 5.10a. The regional geology including local variations in geologic materials are apparent on this image. The metamorphic rocks to the south (bottom of fig. 5.10a) appear in magenta and red colors. Yellow to light green to cyan colors immediately south of the escarpment represent the granitoid rocks. The metamorphic and granitoid rocks also persist down the escarpment to the north with more or less similar colors in the PC 1, 2, 3 image. The alluvial materials exhibit yellow color (south of the escarpment) and red color (north of the escarpment). On the escarpment and south of it the shadow effect appears in green to cyan color. Lateritized crystalline rocks (metamorphic and granitoids) appear in white with shades of yellow colors. Despite similarity in the composition of the rocks to the south and north of the escarpment, variations in color is conspicuous on the color composite created from PC 4, 5 and 6 (Figure 5.10b) in RGB order. Rocks on the north side of the escarpment (down) show dominantly blue color whereas rocks on the south side of the escarpment (up) show dominantly magenta, cyan and green colors.

A post-tectonic granite unit was not mapped earlier (west in figure 5.3b) because it appears less obvious on the Landsat TM principal component images. It is more conspicuous on the PC 4, 5 and 6 (west in fig. 5.10b) derived from ASTER data. Moreover the regional color variations observed up and down of the escarpment are not obvious in the Landsat TM principal component color composites. A detail of the geology taken down the escarpment is presented in the color composite of PC 7, 8 and 9 in RGB order (Figure 5.11a) derived from the ASTER data. The geological contacts between the various types of metamorphic rocks are clearly apparent in the PC images derived from ASTER data. Comparisons of the same area with a color composite created from Landsat PC 3, 2 and 4 in RGB order (Figure 5.11b) show less detail.

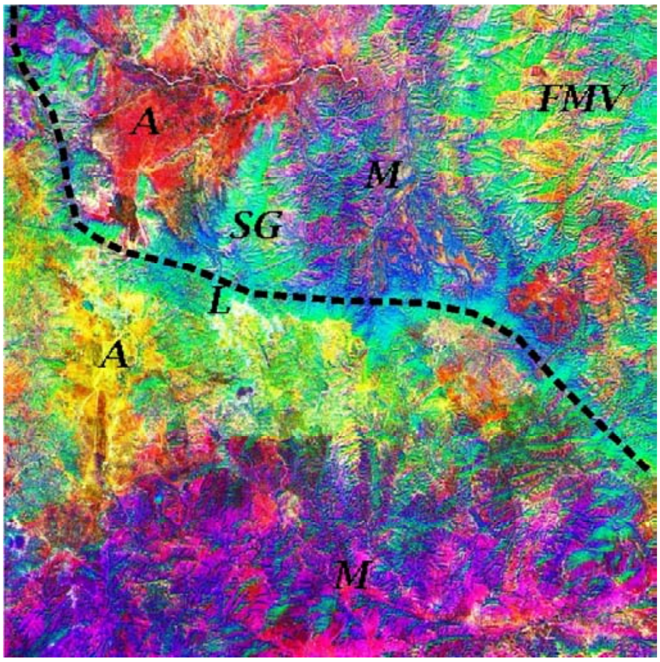

(a)

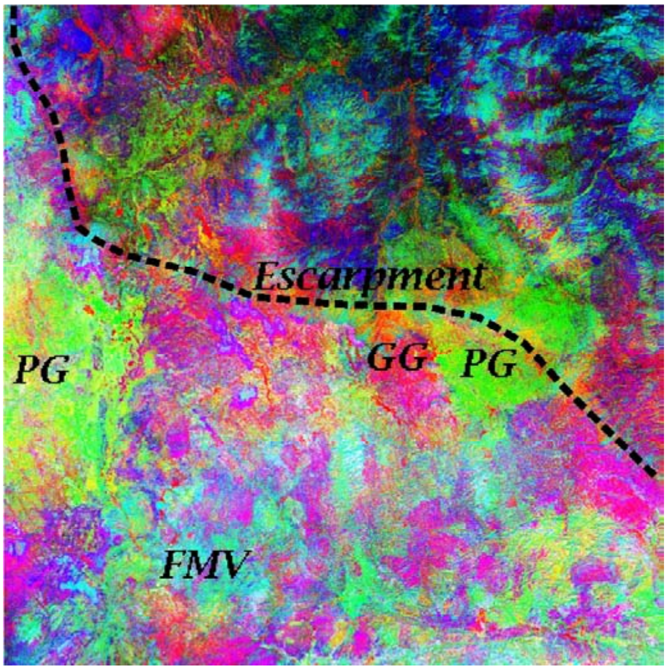

(b)

Figure 5.10. Principal component color composite images from ASTER data for site-2 (a) PC 1, 2, 3 (b) PC 4, 5, 6 both in RGB order. Escarpment shown by dash line, A=alluvium, PG=post-tectonic granite, GG=granite gneiss, FMV=foliated metavolcanics, SG=syntectonic granite, M=metamorphic and L=laterite. Image size 30 by 30 km and north (top).

(a)

(b)

Figure 5.11. Comparisons of principal component images in site-2 north of the escarpment in the metamorphic rocks (a) PC 7, 8, 9 derived from ASTER and (b) PC 3, 2, 4 derived from Landsat TM, both in RGB order. A=non-foliated metavolcanics, B=foliated metavolcanics and C=metasediments. Image size 10 x 10 km and north (top).

The various units in the metamorphic rocks are hardly differentiated in the PC image derived from the Landsat TM data. This shows the level of detail that can be extracted from the ASTER data for lithological mapping purposes even from the higher order principal component images. This supremacy is a consequence of the high spectral resolution of the ASTER data that covers a wide range of wavelength regions capable of discriminating geological materials.

The potential of ASTER data for lineament mapping was evaluated using the VNIR bands with 15 m spatial resolution. An area of 6 by 6 km that is covered by the ASTER, SPOT and Landsat image data was selected and the images evaluated visually (Figure 5.12). Dyke swarms with dominantly NNE-SSW orientations are clearly visible in the VNIR color composite with IHS-transformation applied on the bands 3, 2 and 1 and presented in RGB order (Figure 5.12a). The dyke swarms are less obvious on the IHS-transformed SPOT bands 3, 2 and 1 color composite RGB order, 20 m resolution, (Figure 5.12b). Color infrared bands 4, 3 and 2 from the Landsat data were selected in order to suit the spectral resolution in each sensor and subjected to IHS-transformation (Figure 5.12c). In the Landsat TM data the same dyke swarms are hardly recognizable because of the relative low resolution (30 m). Vegetation cover appears in red color in all the images in figure 5.12. Variations in vegetation cover are clearly visible in all images and this effect is due to seasonal differences. In addition to variations in the resolution among the digital data, the differences in vegetation cover have adversely affected also visibility of linear features. This investigation shows the potential of ASTER data for lineament mapping as a result of the improved resolution of 15 m. It further demonstrates importance of the date of remote sensing data acquisition in image interpretation.

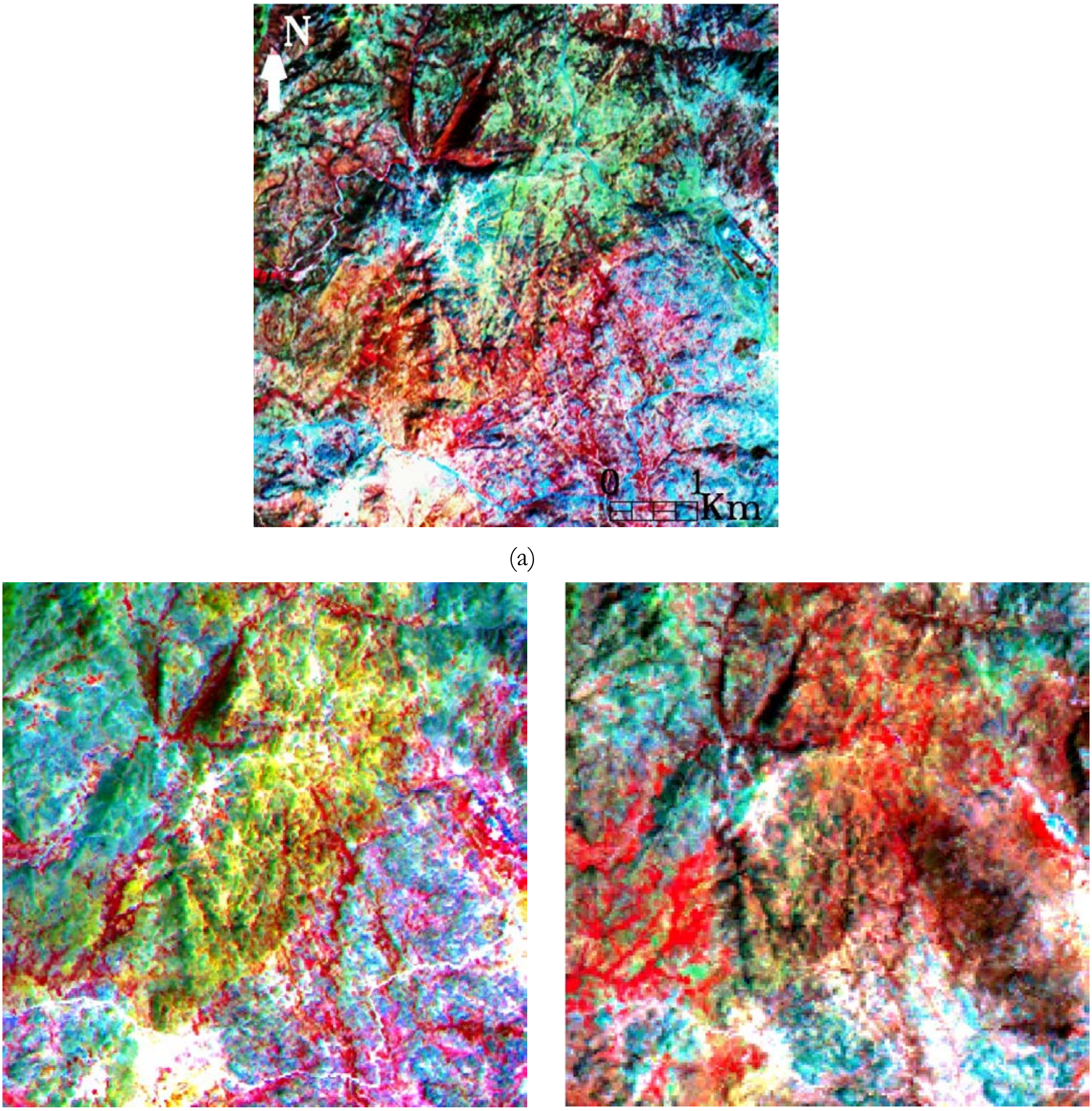

(a)

(b) (c)

Figure 5.12. IHS-transformed color composites in RGB order (a) from ASTER VNIR bands 3, 2, 1; 15 m resolution (b) SPOT bands 3, 2, 1; 20 m resolution and (c) Color infrared TM bands 4, 3, 2; 30 m resolution. Dyke swarms mainly located center of image in (a). Vegetation cover appears in red color. Image size 6 x 6 km.

To better evaluate the spectral information contained in ASTER's three wavelength regions, single pixel image spectra of selected rock types were extracted and examined in relation to the color variations in the PC color composite images. Image spectra collected from the rocks up and down the escarpment are given in Figure 5.13. The spectra collected from rocks on the down side of the escarpment are marked with squares and those on the up side of the escarpment marked with asterisk. In the metamorphic and granitoid rocks, the spectral profiles collected down side of the escarpment generally show higher reflectance and/or emissivity in all wavelength regions than the ones collected on the upper side of the escarpment (e.g. Figs. 5.13a and 5.13b). These spectral variations are clearly visible on the PC 4,5,6 (Fig. 5.10b) and are reflecting the degree of weathering of the rocks involved. This observation is further supported by the ease in discriminating lithological units in the metamorphic rocks down the escarpment because of less alteration and absence of thick soil cover. Thick soil development derived from chemical weathering and dense natural vegetation cover caused difficulty in lithological discrimination south of the escarpment. Figure 5.13c shows image spectra taken from the post-tectonic granites (east and west in fig. 5.10b). Agreements in the spectral profiles from the two suggest similarity in minerals that make up the rocks and this is conspicuous in the PC 4, 5, 6 color image which appears in green. The spectral profile obtained from the alluvial materials is given in Figure 5.13d. Difference in colors in the PC 1, 2, 3 image (fig. 5.10a) is also shown in the image spectra. Variations in color in the PC 1, 2, 3 image in alluvial materials are thus probably attributed to differences in temperature from PC1. Variations in surface temperatures are due to difference in elevation on both sides of the escarpment. A general pattern is noted from the image spectra presented in Figure 5.13. Improved ASTER data product with reflectance and emittance values will make the image spectra interpretation better. However, general inferences can be made from the data. Difference in the VNIR bands reflect the degree of weathering of iron-bearing minerals, for instance, chlorite, actinolite and hornblende in the non-foliated metavolcanic rocks on both sides of the escarpment (Fig. 5.13a). The cause of the variations in the VNIR bands in the post-tectonic granites and alluvium is similar to non-foliated metavolcanic rocks. A continuous decline in the reflectance curves in the SWIR bands in all spectral profiles suggests presence of clay minerals derived from chemical weathering of crystalline rocks. No significant variations in the emissivity of minerals from the less altered (down escarpment) and highly altered (up escarpment) metamorphic rocks are observed in the TIR wavelength region (Fig. 5.13a). This is probably due to fewer amounts of silica-bearing minerals in the metamorphic rocks when compared to the granitoid rocks, which show variations in the emissivity in the TIR bands.

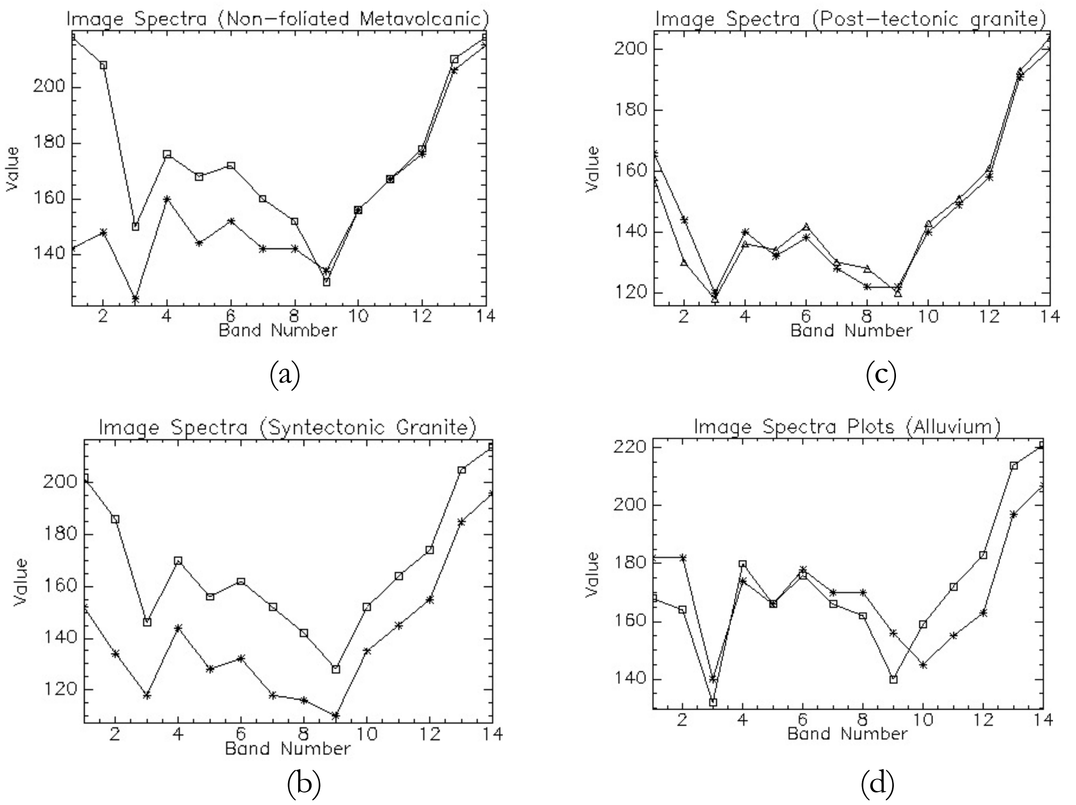

Figure 5.13. Image spectra collected from selected rocks (a) non-foliated metavolcanic rocks (b) syntectonic granites (c) post-tectonic granites and (d) alluvium. In figures (a), (b) and (d) spectra with square points represent down the escarpment and asterisk points from up-side of the escarpment. In figure (c) both spectra are from the up side of the escarpment with the asterisk from east and triangle from west post-tectonic granite rocks (see location in fig. 5.10).

5.2 Structures

Joints

Seven joint systems are observed in the study area including the subhorizontal to gently dipping (20° - 50°) joint sets that are characteristic to almost all rock units (Appendix iii). The orientations of the six steeply dipping (60°-90°) joint sets including the number of observations are presented using rose diagrams for the total joint systems in figure 5.14a. The major orientations are: NW-SE, N-S, NE-SW, ENE-WSW, NNE-SSW and WNW-ESE. The least frequent joint sets with NNE-SSW trends are only characteristic of the foliated metavolcanic rocks (Figure 5.14b). These joint sets are parallel to the foliation planes and are not observed in the non-foliated metavolcanic (Figure 5.14c), syn-tectonic granites (Figure 5.14d) and post-tectonic granites (Figure 5.14e). The second least frequent joint set with WNW-ESE trend (Fig. 5.14a) is more conspicuous in the foliated metavolcanic unit (Fig. 5.14b) than on the other rock units (e.g. figs 5.14c and 5.14d). The main reason is that joint sets perpendicular to the foliation planes share the same trend and are ubiquitous in the foliated rocks.

All other joint sets are characteristic of all other rocks, except in the post- tectonic granites (Figure 5.14e) where the nearly perpendicular, NW-SE to NNW-SSE and ENE-WSW trending joints represent primary joints. Certain joint sets are not observed in some rock units. For instance the WNW-ESE and NE-SW trending joint sets are missing in the post-tectonic granites (Fig. 5.14e). Both sets of joint systems are perhaps older than the rock. ENE-WSW trending joint sets are not discernible in the foliated metavolcanic rocks (Fig. 5.14b). This is probably due to local variations. Local variations exist between different rock units as well as within a single unit (fig. 5.15b-5.15d). A minimum of three joint sets is characteristic for most outcrops. The major structures observed in the basaltic rocks are dominantly primary jointing. These include sub-vertical columnar joints as well as sub-horizontal sheet joints, which are formed as a result of cooling (Fig.

5.15a). The basaltic rocks also show, at places, vesicles being filled with secondary minerals such as zeolites.

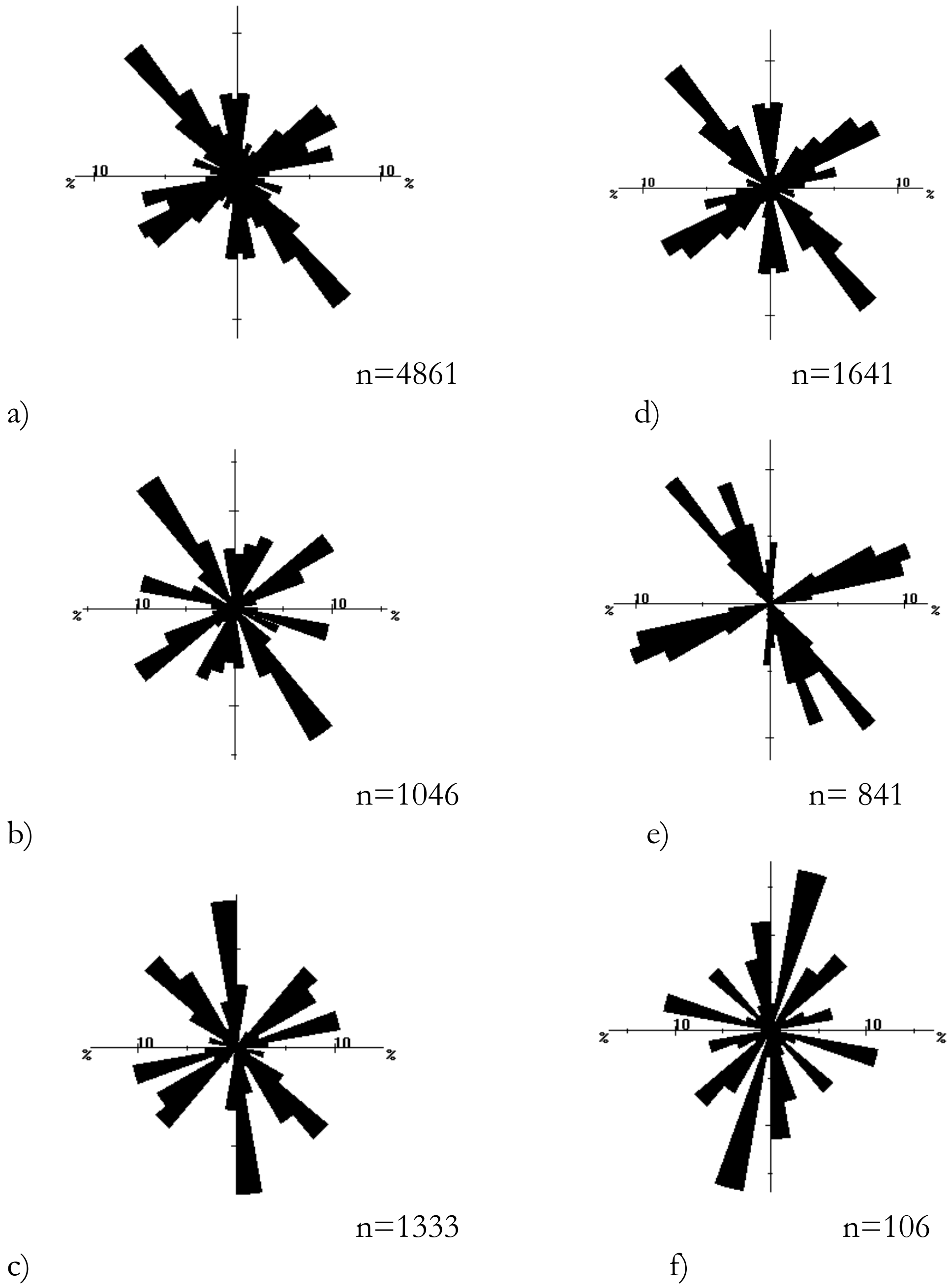

Figure 5.14. Rose diagram of joint sets (a) total joint sets (b) in the foliated metavolcanic unit (c) in the non-foliated metavolcanic unit (d) in the syn-tectonic granites e) in the post-tectonic granites and (f) total dykes.

The spacing of joint sets varies within a single rock unit as well as among different rock units from locality to locality. Even at the same locality within a single unit, the spacing of one joint set shows variation. For example figures 5.15b and 5.15c represent sketch maps of joint sets from the non-foliated metavolcanic rocks at Ziban Mengeb and Gergera, respectively (see Fig. 5.3a for locality). Spacing of N-S trending joint set show variations in both sketches. Note that the ENE-WSW trending joint sets are locally absent at Gergera (Fig. 5.15c). Compare also the spacing of joint sets of the same trend in the syn-tectonic granites west of Dekemhare (Fig. 5.15d, see fig. 5.3b for locality). In general, however, closest spacing is observed in the NNE-SSW trending joint sets that are parallel to the foliation. Spacing of steeply dipping joint sets is given in Table 5.1. The subhorizontal to gently dipping joint systems have spacings between 0.5 to 2 m. Apart from the primary joints in the post-tectonic granites, most of the joint systems cross-cut each other suggesting that they are well connected in a three-dimensional network. Moreover the joint sets are devoid of any mineral infillings, except the subhorizontal to gently dipping fracture sets where mineral infillings of quartz are common.

Dykes

There are six sets of dyke swarms in the area studied (Figure 5.14f). The most prominent set trends NNE-SSW. The other sets have trends N-S/NNW-SSE, NW-SE, WNW-ESE, NE-SW and ENE-WSW. Most of them are sub-vertically dipping, but a few have gentle to sub-horizontal dips and can be categorized rather as sills. The dyke swarms exhibit variations in lengths, widths and spacings. The widths in all of the sets vary from a few tens of centimeters up to 10 to 15 m. The strike lengths can be traced from a few meters to hundreds of meters and the spacings from a few centimeters to a few tenths to hundreds of meters. The dykes are dominantly basaltic to doleritic in composition, and some aplitic dykes are characteristics of the granitoid rocks. All sets of dyke swarms cut the granites, lateritized basement and the overlying Tertiary basalts.

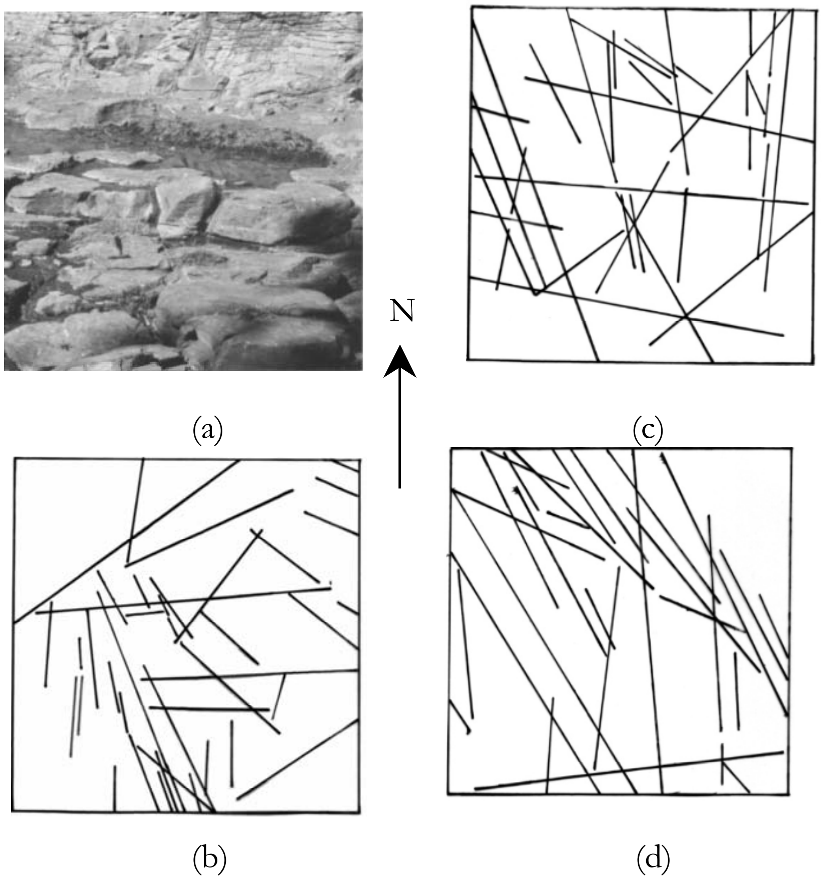

Figure 5.15. Joint patterns in (a) basaltic rocks sheet and columnar joints (scale 1:300) (b) non-foliated metavolcanics at Ziban Mengeb (scale 1:300) (c) non-foliated metavolcanics at Gergera (scale 1: 200), and (d) syn-tectonic granite West of Dekemhare (scale 1:300).

Dyke parallel fractures are well developed adjacent to most dyke swarms. Again closest fracture spacing was observed along the NNE-SSW trending dyke swarms. Fracture spacing adjacent to the remaining sets of dyke swarms correspond to that of joint spacing described above.

The WNW-ESE trending dyke swarms cut through the NNE-SSW trending dykes (Fig. 5.16a). ENE-WSW trending dykes also cut through N-S/NNW-SSE oriented dykes. Also NE-SW trending dykes are observed to be cutting through N-S trending dykes northwest of the study area in the vicinity of Barentu (personal communication Zerai 2001). There is no indication regarding the age relationship of the ENE-WSW and NE-SW trending dyke sets. The relative age of the dykes are inferred thus based on the observations made during field studies and from inferences of the previous studies done in the region. The oldest dyke swarms are the ones with NNE-SSW trends, because these dykes are formed late in the Tertiary tectonic evolution (Drury et al. 1994). It appears that the orientation of the dykes is influenced more by the inherited Pan-African shear zones. The fact that they are being cut by the WNW-ESE dykes may suggest that they are pre-Red Sea rift in age. All the N-S (NNW-SSE), NW-SE and WNW-ESE trending dykes are considered to have the same age and are formed by lateral extension. The extension direction can be related to the generally accepted NE-SW to ENE-WSW directions. The variation in strikes may reflect the inhomogeneous nature of the state of the stress during the Red Sea rift formation. NE-SW and ENE-WSE striking dykes are younger than the Red Sea rift-related dykes (e.g. N-S trending) as evidenced from the crosscutting relationships. Their origin is probably associated to the Red Sea rift-related transform faults.

Faults

Two types of faults, namely strike-slip and normal, dominate the study area. The strike-slip faults are oriented generally N-S, WNW-ESE, NE-SW and ENE-WSW. They are generally steeply dipping. The N-S faults have a sinistral sense of movement, which is marked by well-developed sub-horizontal fault striations (slickenlines) on the metavolcanic rocks (Figure 5.16b). The second set is oriented WNW-ESE and offsets NNE-SSW trending dykes dextrally (Figure 5.16a). Both of them appear to represent conjugate shear fractures and fit well into the current tectonic setting of the region. The NE-SW and ENE-WSW striking ones have sinistral and dextral sense of movement, respectively, and both offset WNW-ESE trending dykes (Figure 5.16a). Again both of them represent a second set of conjugate shear fractures presumed to have links to the Red Sea-related transform faults.

The normal faults have a number of sets with N-S/NNW-SSE, NW-SE, NE-SW to ENE-WSW strikes (Figures 5.16c and 5.16d) that are variable in size and direction and amount of displacement. Prominent strain markers include Precambrian aplitic dykes/sills and Tertiary basaltic flows and display normal displacements that vary from cm to hundreds of meters. Fault breccias/gouge with associated slickenlines are usually well developed.

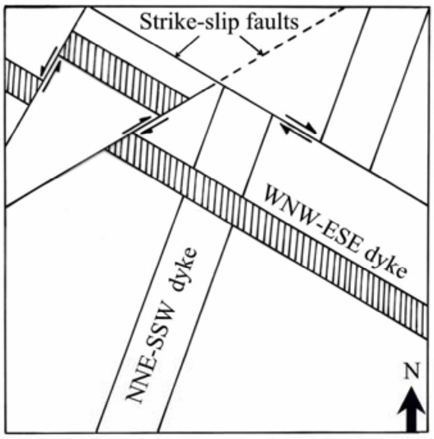

(a)

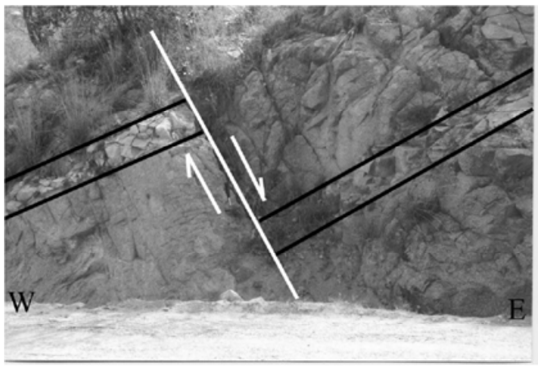

(c)

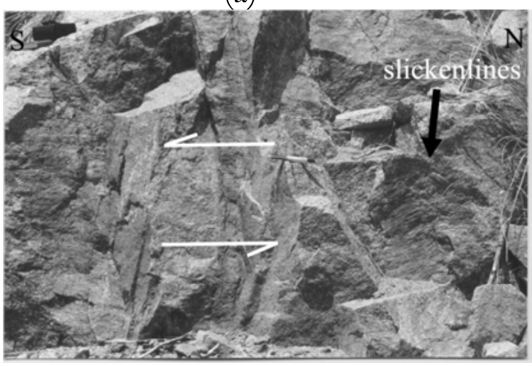

(b)

(d)

Figure 5.16. Field structures (a) a sketch map showing cross-cutting of WNW-ESE and NNE-SSW trending dykes as well as strike-slip faults (b) N-S oriented subhorizontal structural slickenlines showing sinistral sense of movement (c) N-S oriented normal fault and (d) ENE-WSW trending steeply dipping normal fault.

The relative age of the strike-slip faults can be inferred indirectly from the age relationship of the crosscutting dykes. The first set of conjugate strike-slip faults (the N-S/NNW-SSE trending with sinistral sense of movements and the WNW-ESE trending with dextral sense of movements) is older than the second set of conjugate strike-slip faults (NE-SW trending with sinistral sense of movement and ENE-WSW trending with dextral sense of movement). Dykes that have orientations similar to the second set of conjugate shear fractures cut through the older dykes with N-S orientations. Similarly strike-slip faults that have orientations similar to the second set of conjugate shear fractures cut through the older dykes with WNW-ESE orientations (Fig. 5.16a). The occurrence of dyke parallel fractures adjacent to the dykes coupled with presence of normal faults indicates that most of the fracture sets were generated as extensional. The strike-slip faults responsible for the formation of the shear fractures might have been generated from the reactivation of the dilatational fractures. Thus the strike-slip faults are the youngest structures. No evidence is available regarding the age relationship of the dykes and the normal faults that are both older than the strike-slip faults. The assumption is that both of them might be of the same age.

Description of Fractures

In this section the types of fractures and their relationship with the lineament are presented. The general term fracture is used to describe all the structures. For example, N-S trending fracture sets apply to all structures, that is, joints, dykes and faults. Fracture types are mentioned explicitly where deemed necessary.

NNE-SSW trending fracture sets are parallel to the foliation in the region. Dyke parallel joints are common in areas where this set of dykes cut through the granitic rocks and Tertiary basaltic flows. Although these fracture sets share the strike of Precambrian tectonic fabric (foliation), the presence of dyke parallel joints hints dilatational nature. Assuming that the direction of dykes corresponds to planes of deformation (parallel to the major trend of the dykes), the fractures are considered tensile (extensional) fractures. Some of the fracture sets with this trend were filled with magma and formed dykes. The presence of N-S oriented sinistral strike-slip fault in the study area suggests that some of the N-S striking fracture sets are shear fractures. Whereas presence of normal faults with similar trends show partly tensile nature with some of them filled with magma to form the dykes. Thus the N-S fracture sets are both shear and tensile fractures in type. Similarly, NE-SW and ENE-WSW trending fracture sets represent both shear as well as tensile fracture types. The shear fractures are inherited from the strike-slip faults whereas the tensile fractures are related to the normal faults. Again some of the fractures are filled with magma to form dykes in their respective orientations. The NW-SE normal faults indicate that NW-SE trending fracture sets are tensile fractures with some of them filled with magma to form the dykes.

Comparisons of the rose diagrams of total joints (fig. 5.14a), dykes (fig. 5.14f) and regional lineaments (figs. 5.7d and 5.8d) show a good correlation of the orientations of most of the major structures in the study area. In general, the good correlations in orientation of all structural features suggest that most of the lineaments mapped in the areas correspond to fractures. The fractures can be related to either tensile or shear or both. Most of the fracture sets are also filled with magma to form the dykes. Summary of all fracture systems in relation to the tectonic setting in the Red Sea is described in a sketch diagram (Figure 5.17).

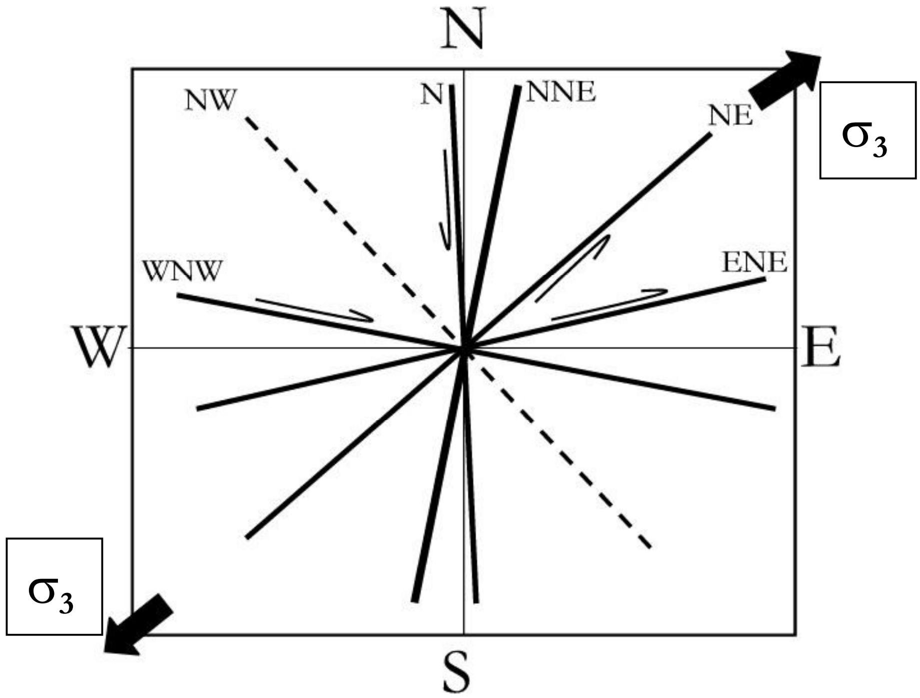

Figure 5.17. Sketch diagram showing the fracture systems in the study area in relation to the current tectonic set-up of the Red Sea. NNE=Late Tertiary (oldest); N, NW and WNW= Red Sea rift-related; NE and ENE=Red Sea rift-related transform faults (youngest). N-S (sinistral) and WNW-ESE (dextral) represent Red Sea rift-related old conjugate shear fractures. NE-SW (sinistral) and ENE-WNW (dextral) represent Red Sea rift-related (transform faults) young conjugate shear fractures. σ_3 shows direction of maximum extension along NE-SW, in agreement with the tectonic setup of the Red Sea region.

Table 5.1. Comparisons of spacing of joints and lineaments.

Joint/Lineament Sets	Spacing	
	Joints (m)	Lineament (m)
NNE-SSW	0.05 – 0.15	130 – 640
N-S	0.5 – 6	180 – 1500
NW-SE	0.3 – 6	180 – 1500
WNW-ESE	1.5 – 4.5	270 – 3200
NE-SW	0.8 – 5.5	360 – 2500
ENE-WSW	0.2 – 1.2	280 – 2200

A close visual inspection of the lineaments mapped from remote sensing data (fig. 5.6) display variations in spacing within a set of lineaments as well as among different sets. Table 5.1 shows comparisons of the spacing of fractures derived from remote sensing data and spacings observed on outcrops. Comparisons of joint and lineament spacing for the NNE-SSW, N-S, NW-SE and WNW-ESE show generally good correlation. The closest spacing was observed in the NNE-SSW trending fractures that parallel the foliation. Generally NE-SW and WNW-ESE fractures show wider spacing. The minimum lineament spacing of NE-SW and ENE-WSW trends are generally wider despite closer spacing of the corresponding joint sets. This is due to the fact that some of the lineaments could not be resolved at the scales involved. Field observations show close spacing of joints in most of the cases and this may imply that a single lineament mapped could represent sets of fractures or fracture zones.

5.3 Geomorphology

The classification results for landforms were assessed for many combinations. The best results were obtained for three input parameters with standardized slope, longitudinal curvature and plan convexity and for two input parameters with standardized slope and longitudinal curvature. Drainage channels (green to dark green color) are well defined in the classification results from three bands (Figure 5.18a). Features other than drainage channels are best defined in the two bands classification (Figure 5.18b). For example terraces (yellow and blue colors) are well identified in the two parameters case and are missing from the three parameters output. Similarly, the drainage channels are missing from the two parameters output but are well identified in the three parameters output. Also certain drainage channels appear to be discontinued due to lack of detail from the DEM as a result of wide contour spacing. It is worth mentioning that although peaks represent maximum curvature values also locally low curvatures, which are slightly higher than the surrounding areas are classified as peaks. Moreover local depressions that may not necessarily be related to the drainage channel are also

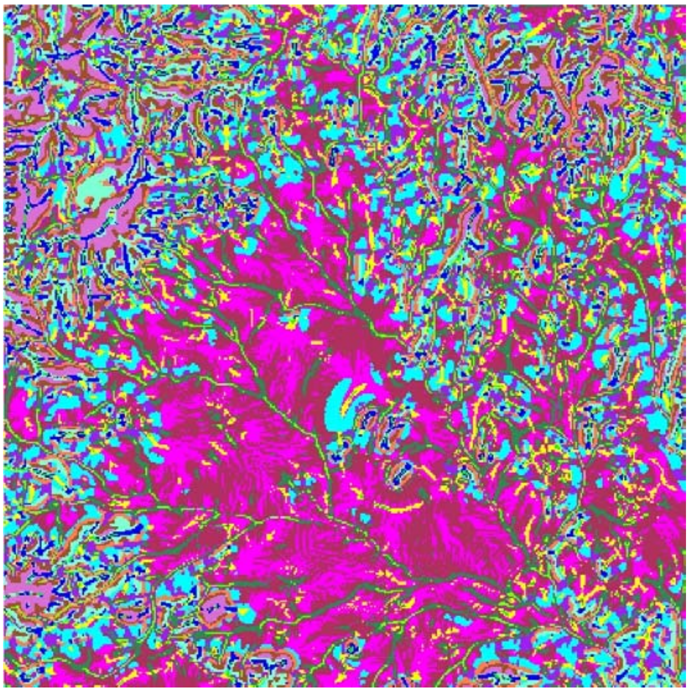

(a)

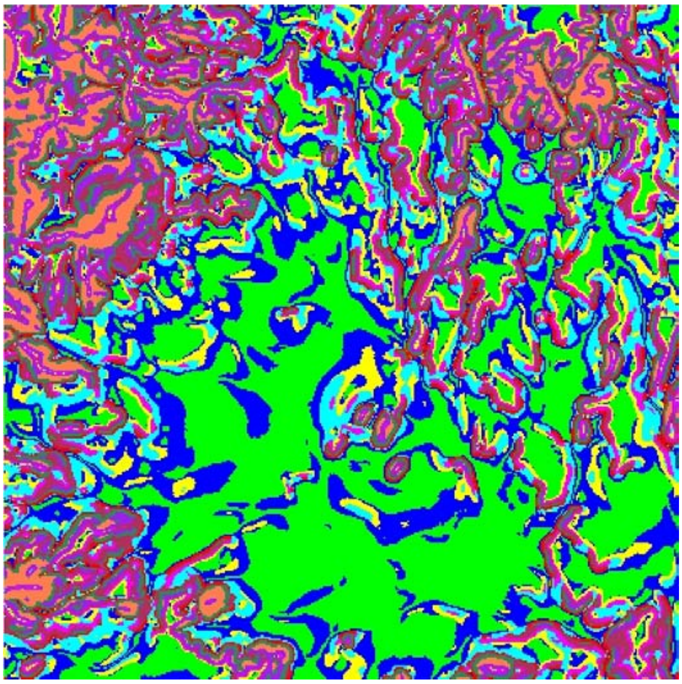

(b)

Figure 5.18. Examples of output of classification results in site-1 (a) three parameter classification (standardized slope, plan convexity and longitudinal curvature) and (b) two parameter classification (standardized slope and longitudinal curvature).

classified as channels. The effects of these local variations may be reduced by using a larger kernel size when creating the topographic model parameters but then there is a risk of loosing important topographic details. In general, however, maximum information is available from the DEM data for geomorphological feature identification.

Both classification results were visually evaluated and a combination of the two outputs were reclassified to generate the geomorphological maps (Figures 5.19a and 5.19b). The interpretation of landform features was based on local knowledge of the landform types in the study areas. A description of the different landform types is presented in figure 5.20. The classification results were grouped into seven major geomorphological features: peaks, ridges, scarps, pediments, terraces, plains and channels.

Description of Landform Types

The ridges form isolated and chain mountains in basalts and crystalline rocks with peaks at the crests. The scarps generally represent steep slopes formed adjacent to deeply incised V-shaped gullies. Some of the scarps are associated with tectonic activity and represent fault surfaces. The pediments are moderately inclined erosion surfaces that slope away from mountain fronts (ridges) and are typically formed by running water. The bedrocks in the pediments may be exposed or thinly covered with alluvium and soils. Terraces in the basaltic rocks mark successive lava flow layers. In the alluvium they represent different flood plains with alluvial deposits. The plains are flat to gently sloping topographic features. Where located in the basaltic rocks they represent plateaus and mark the top of individual lava flow surface. In the crystalline rocks the plains represent the peneplains or flood plains.

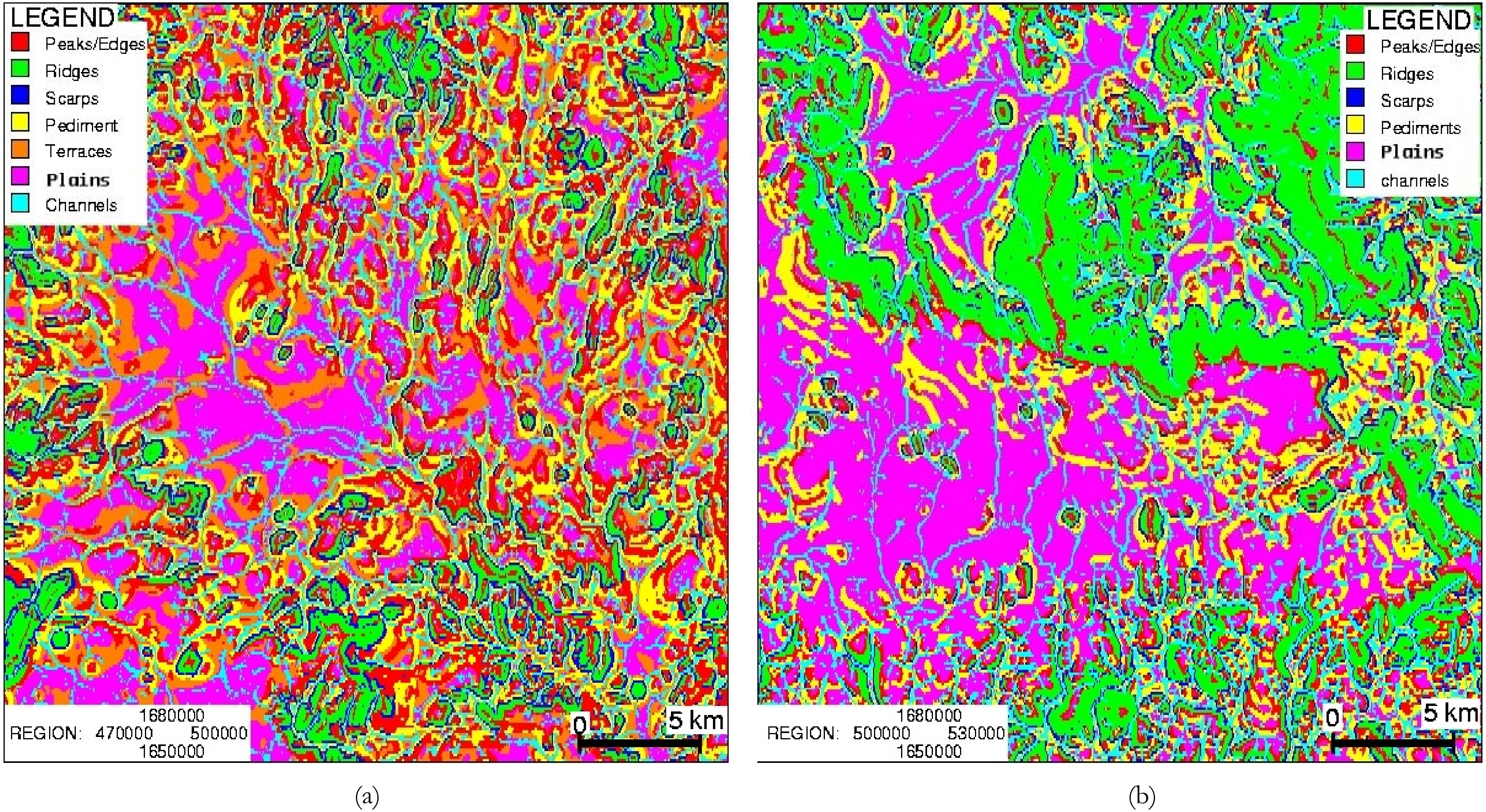

Figure 5.19. Geomorphological maps of (a) site-1 and (b) site-2.

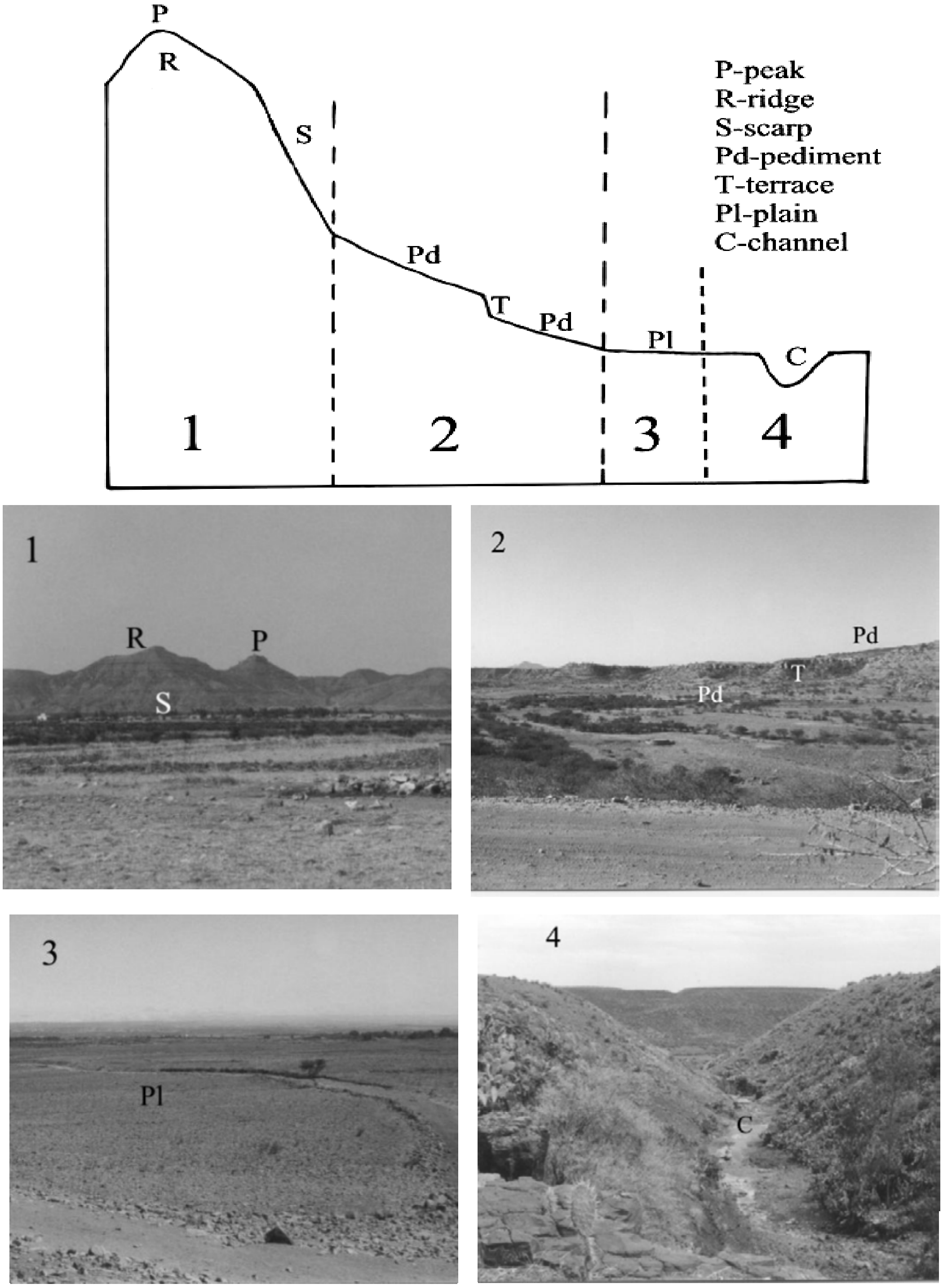

Figure 5.20.Description of geomorphological feature types.

The peneplains are remnants of older erosional surfaces indicative of landscape features that are reduced through long and continued mass wasting, stream erosion and sheet wash (peneplanation). Deep weathering of crystalline bedrock formations produced the laterites during periods of tectonic quiescence. Tectonic uplift resulted in terminations of the deep weathering and initiated a cycle of stripping. The periods of tectonic uplift and cycles of stripping are not known in Eritrea, however, remnants of the peneplanation surfaces are well preserved in the field. The age of Eritrean lateritization is not well known, but throughout the Red Sea area, Tertiary flood basalts rest conformably on lateritic paleosols (Mohr, 1970). Some of the lateritic peneplains form isolated patches at the top of the ridges in the crystalline rocks. Valleys and gullies form the drainage channels and dissect all topographic features. Most of the drainage channels are straight and aligned with dendritic to rectangular patterns suggesting structural control. Valley fill deposits are clearly visible in Spot and TM data and constitute colluvial and/or alluvial materials.

Comparison of DEM's from Contours and SRTM

In order to assess the potential of the SRTM DEM for geomorphologic and lineament mapping, a comparison with the contour derived DEM was made in a test area about 15 by 15 km in size. The comparisons were made in relation to location and information contained with regard to drainage and linear features. The frequency distribution of the difference between the two digital elevation model data is given in figure 5.21. The histogram shows near normal distribution of the differences in elevations ranging from about –200 to +200 m. The mean elevation difference is about 40 to 50 m and indicates existence of systematic shift between the two digital elevation model data. The extreme positive difference is noted on higher grounds such as ridges and peaks or crests. In contrast the extreme negative difference are related to narrow valleys and along sloping surfaces. In general the elevation difference in flat areas are small.

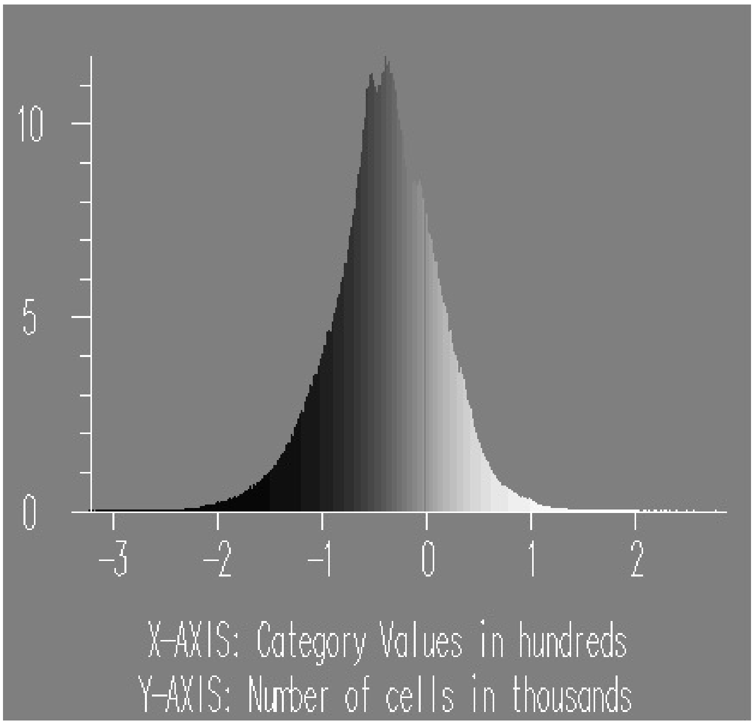

Figure 5.21. Histogram of elevation difference between the SRTM and contour derived digital elevation model data (SRTM minus contour).

Figure 5.22 shows elevation profile along section A-A'. The profile from the contour derived DEM (Fig. 5.22a) generally smoothens the topography. Overall picture looks good but lacks details of drainage systems. In the SRTM DEM the elevation varies over short distances (Fig. 5.22b). This shows the level of detail available from the radar derived digital elevation model. The wide range in elevation differences is thus attributed to variations in details in the two DEM's. Note that the peaks and depressions in the difference profile (Fig. 5.22c) coincide with the profile from the SRTM (Fig. 5.22b).

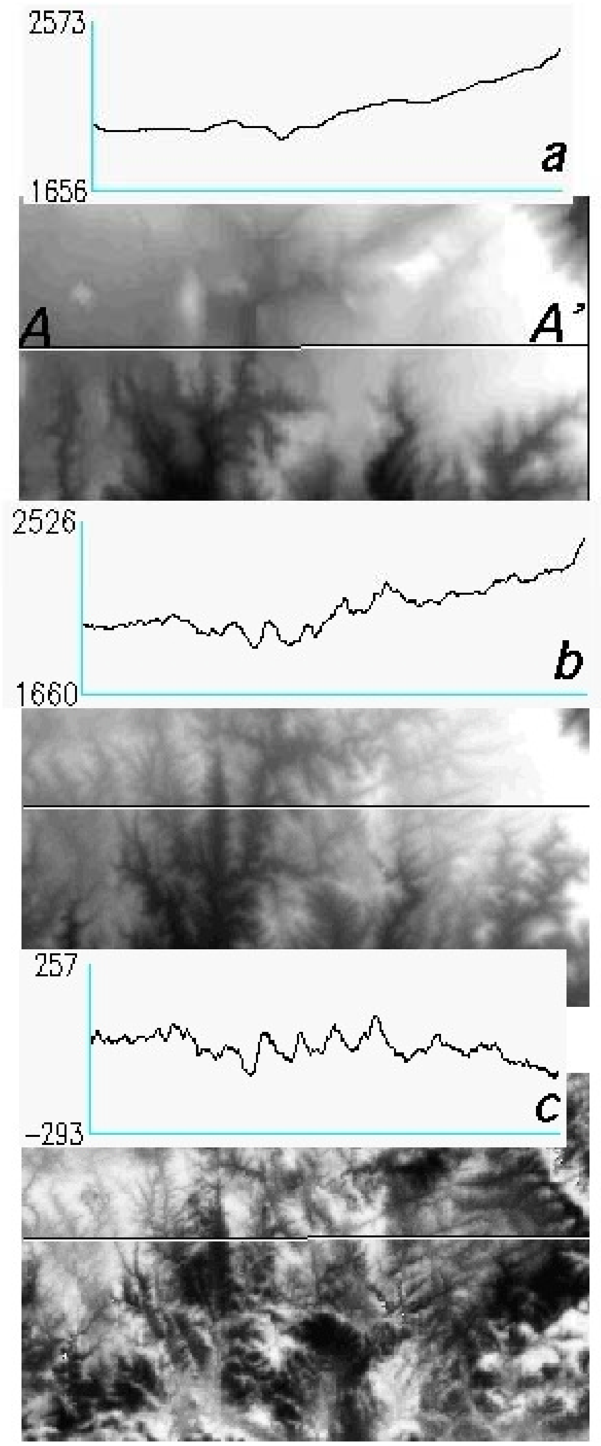

Figure 5.22. DEM and elevation profiles along A-A' (a) contour (b) SRTM and (c) difference of SRTM and contour DEM.

The general patterns of the drainage network derived from the two digital elevation models are similar (Figure 5.23). Major high order tributaries are apparent in both DEM's, while low order drainage channels are better delineated in the SRTM data. Moreover several drainage channels that are extracted from the SRTM DEM are not detected from the contour DEM due to lack in continuity in the data set. The existence of systematic locational shift between the two data sets is clearly visible from the overlays of the drainage systems. Moreover, overlays of the drainage networks over SPOT band 3 image shows additional shift. Since the SPOT data were not height corrected this is sufficient to cause the additional systematic error. Moreover errors in geometric transformation of all data sets could contribute to the overall location shift.

The minimum curvature images derived from both digital elevation models (figure 5.24) show linear features mostly expressed by alignment of drainage channels. The most conspicuous trends are N-S, NW-SE and NE-SW to ENE-WSW. The NE-SW/ENE-WSW is not obvious from the contour DEM. Other trends though discernible in the contour DEM generally are less numerous when compared with the SRTM data. The comparison between the two digital elevation models demonstrates that the SRTM digital elevation model is better for detection of drainage systems and linear features than the contour DEM. This superiority is mainly due to greater amount of detail in the SRTM data as a result of continuous data and its improved resolution. Vegetation covers in the study area are dominantly bushes and acacia trees with heights of about 2 to 5 m. The vegetation cover is sparse and thus has insignificant effects on the accuracy in height.

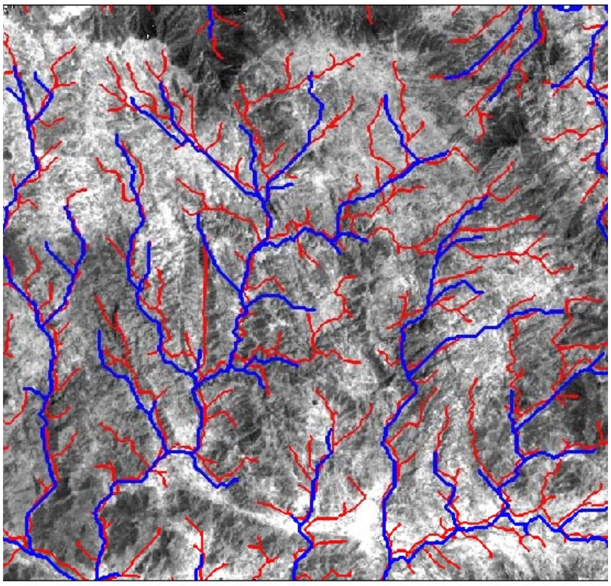

Figure 5.23. Drainage networks derived from the contour DEM (blue) and the SRTM DEM (red) overlain on SPOT band 3 image.

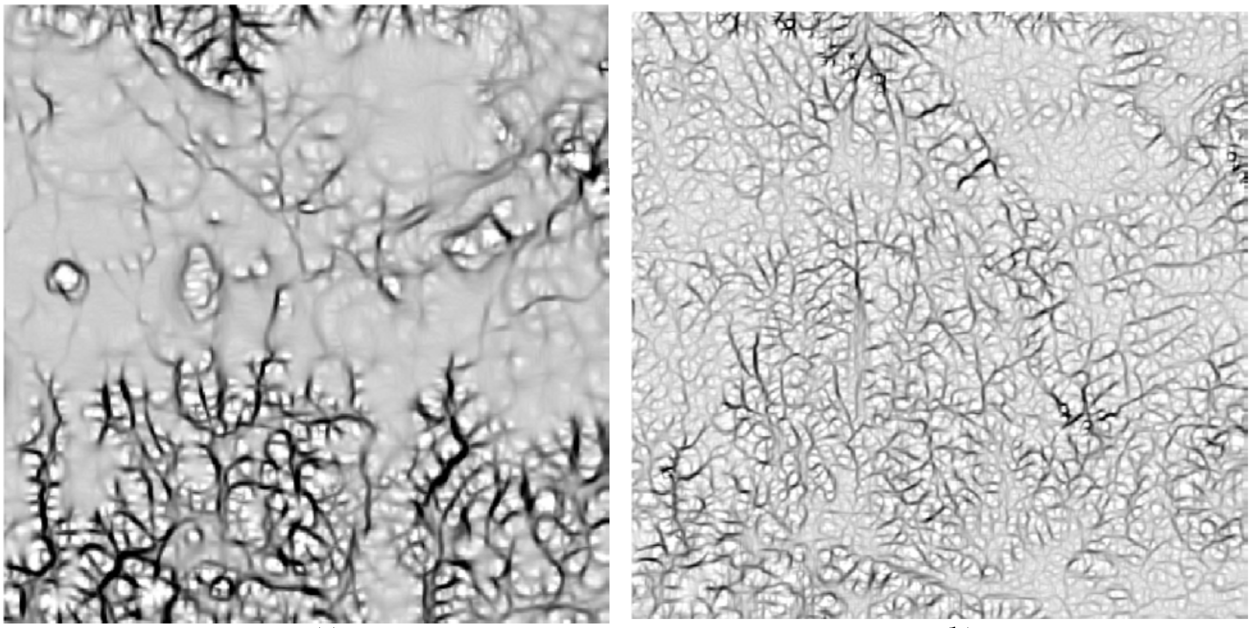

(a) (b)

Figure 5.24. Minimum curvature images derived from the digital elevations (a) contour (b) SRTM

5.4 Hydrogeology

5.4.1 GIS Analysis

Lithology and Yield

Table 5.2 summarizes combination of hydrogeological and lithological data in the GIS. The log mean well yield within the different rock types is highest in the basalts 105 L/min followed by foliated metamorphic rocks with 81.5, alluvium 75, granitoids 70, and lowest in the non-foliated metamorphic rocks 32. The high yield in the basalts is due to primary porosity that is the columnar and sheet jointing as well as vesicles. Comparison of the metamorphic rocks shows that the foliated varieties are more permeable than the nonfoliated ones due to foliation planes, which enhance permeability. The well depth in the alluvium extends up to 60 m and thus some of the wells reach the bedrocks. In spite of high porosity and permeability in alluvium the average yield is low. This is due to the fact that some wells, which tap crystalline rock aquifers with low yields are included here and thus lowered the mean values. The hydrogeology of the alluvium in relation to the bedrock is described in detail in Section 5.4.2. The static water level is deep in alluvium and this is an influence of decline in water table in wells from Alla area. The variations of the yield values within one rock type for instance in basalts from 6 L/min to as high as 1200 L/min and between different rock types is associated to the inhomogeneous nature of hard rock aquifers. It is important to note that yield values are dependant on the capacity of pumps and thus may not represent the true capacity of wells.

Table 5.2. Summary of well yields by rock type.

Lithology	Basalt	Metamorphic (foliated)	Metamorphic (non-foliated)	Granite	Alluvium
No. Wells	50	30	20	30	16
Yield (L/min)					
Min	6.00	12.00	2.00	12.00	17
Max	1200.00	422.00	240.00	600.00	480
Mean(log)	105.00	81.50	32.00	70.00	75.0
St.Dev.	3.25	2.73	2.92	2.61	3.2
Depth (m)					
Min	4	6	8	4	5
Max	80	70	70	60	60
Mean	43.67	37.32	35.27	36.00	38.2
St.Dev.	16.75	16.21	17.60	14.00	12.10
Static Water Level Depth (m)					
Min	1.0	1.0	1.0	1.0	1
Max	35.0	12.0	10.0	26.0	14
Mean(log)	5.7	4.1	3.8	5.6	6.9
St.Dev.	2.4	1.6	2.1	2.2	1.87
Elevation in meters above sea level					
Min	1735	1748	1544	1517	1609
Max	2326	2518	2526	2364	2084
Mean	2005	2150	2139	1990	1903
St.Dev.	130	235	289	220	155

Lineament and Yield

Lineament interpretations of the study area were correlated with existing boreholes. The correlation studies took advantage of the high positional accuracy of around 85 GPS-positioned or surveyed boreholes in the study area. The analysis is carried out for the two test sites together to have more data. Figure 5.25 shows a comparison between distance to lineaments and logarithmic mean yield for the same boreholes, with and without repositioning with GPS. Inverse relationships between yield of GPS-positioned boreholes and proximity to satellite image lineaments is shown.

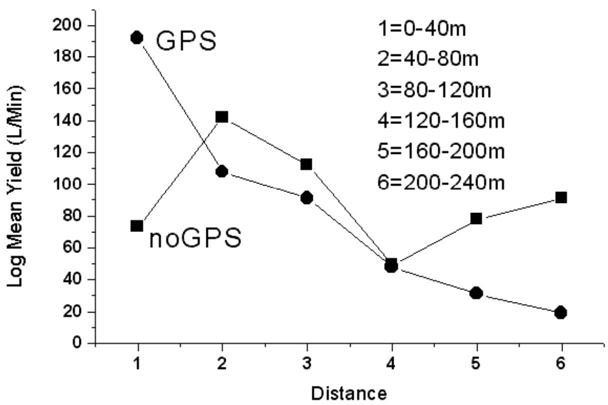

Figure 5.25. Correlation between borehole log mean yield (Litres per minute) and distance to lineaments, before and after repositioning with GPS.

The yield-proximity relationship for the same boreholes from previous investigations without GPS-positioning or surveying is more ambiguous (fig. 5.25). Although based on a small borehole population, this study clearly demonstrates the need for accurate coordinates when comparing various spatial data in a GIS. Proximity to lineaments does not necessarily imply, however, that the borehole yield is high. Low yielding boreholes sited on satellite lineaments could occasionally be connected to poorly transmissive dykes or clay gouge in fracture zones (Sander 1996).

Topography and Yield

The relationship of local topography to well yield is presented in figure 5.26. The positive values indicate topographic highs and the negative values topographic lows. Figure 5.26 shows that although there are low yielding boreholes over all topographic features, that is, the topographic highs, depressions and plains, most of the high yielding boreholes generally lie in flat to slightly lower topography. It appears also that the yield increases from the depression towards the flat topography. The presence of low yielding boreholes on higher grounds is presumed due to poor well site selection during drilling. It is important to note that there are wide ranges of yield values on the low to flat topography, which is attributed to variations in lithology and the underlying structures. Variation of well yield with local topography using the SRTM digital elevation model data shows no clear relationship.

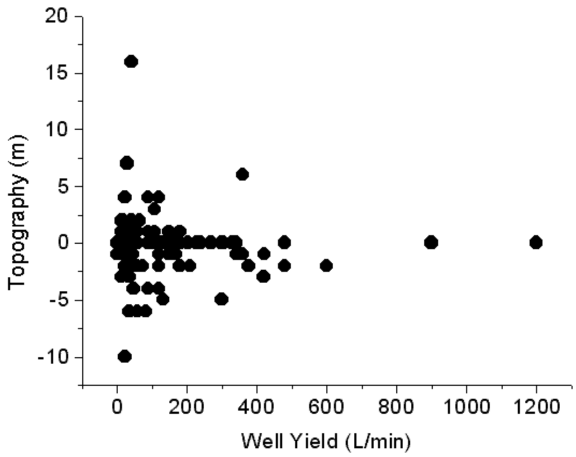

Figure 5.26. Relationship of topography and well yield.

Geomorphology and Yield

The measured yield in each landform is given in Table 5.3. The channels show good to very good groundwater potential possibly due to structural control. Moreover valley fill deposits of unconsolidated materials in the drainage channels provide groundwater storage. Where the drainage channels exert structural control they can together with the valley fill deposits form an integrated aquifer system. The plains and terraces have good to very good groundwater-potential with high well yields. In the basaltic rocks (site-1), the planes represent different lava flow layers of gentle to flat slopes with individual flow layers forming terraces. In the crystalline rock areas the planes represent either peneplains or alluvial plains. The hydrogeology of the peneplains and alluvial deposits are discussed in detail in relation to field investigations in Section 5.4.2. Pediments over basalts show measured yield values (site-1, Table 5.3) as high as 480 L/min and can be classified as moderate to good groundwater potential zones. Scarps and ridges have very low measured yields and are thus poor to very poor groundwater potential zones. The presence of some wells in such landforms further indicates poor well site selection. Peaks have no groundwater potential.

Table 5.3. Output of geomorphology vs. yield from GIS analysis.

Landforms	Measured Yields (L/min)		Groundwater Potential
	Site-1	Site-2	
Channels	48-330	6-240	Good to very good
Plains	26-270	17-600	Good to very good
Terraces	30-1200	-	Good to very good
Pediment	21-480	2-120	Moderate to good
Scarps	0-13	0-36	Very poor
Ridges	0-30	34-45	Very poor
Peaks	-	-	Nil

5.4.2 Field Investigations

Alignment of vegetation along N-S, NW-SE and NE-SW directions are common in the field. Depth to groundwater level in dug-wells is often very shallow (0.5 to 1 m). At places, the water table reaches the ground surface. Most wells are usually sited close to a river on either side of its banks. However, the siting of certain wells appears to be guided by proximity to villages and access to drilling rig. This indicates that not always due considerations are given to the local structure and topography. A typical example is the one sited on the foot of a hill in the vicinity of Gergera village (Figure 5.27). This can possibly explain the prevalence of low yields in boreholes even close to major lineaments.

Figure 5.27. Example of a low yielding well sited on the foot of a hill close to the village Gergera in the nonfoliated metavolcanic rocks (see Fig. 5.3a for location).

Figures 5.6a and 5.6b show the location of boreholes with high yields together with groundwater outcrops in the form of springs and riverbed flows. It can be seen from fig. 5.6 that springs and wells lie on major lineaments of different orientations. For instance, the spring (S1 in Fig. 5.6a) at Debarwa is flowing on the upstream side of a NW-SE oriented river intersected by a NNE-SSW trending dyke. High yielding boreholes (480 L/min, borehole 1 in Table 5.4) are also sited within 100 m distance of the same dyke. Also at Alla (Fig. 5.6b) a dugwell sunk over NNW-SSE trending dyke yield sustained flow while close by dugwells sunk on alluvium and weathered granite remain dry. Furthermore boreholes sunk in granitic rocks that intersect dykes at depth exhibit high yield when compared with adjacent boreholes. A typical example is given in Table 5.4 (Borehole 8). The high yield could be due to increased permeability owing to adjacent dyke parallel joints.

All these observations indicate the hydrogeological significance of the lineaments (structures). Fractures associated with dykes are extensional fractures and can be considered as 'open' fractures, which are potential sites of groundwater storage and circulation. Likewise, normal faults are potential groundwater bearing fractures since they are formed under lateral extension, and therefore, can be considered as ’open’ fractures. From the hydrogeological point of view, the shear fractures associated with the strike slip-faults may serve as potential zones for groundwater movement and storage. The shear fractures appear to be reactivated along extension fractures. Broken and crushed rocks due to the strike-slip motion along these extensional fractures may keep them open, and enhance the permeability of the crystalline rocks. Moreover lack of mineral infilling, close spacing and the good interconnections in a three dimensional network from the steeply dipping joint sets will contribute to increased groundwater storage. From the hydrogeological point of view, the subhorizontal to gently dipping joint systems are considered less promising for groundwater storage because of low porosity and permeability attributed to mineral infilling.

Well logs

The borehole geology as obtained from drilling operations are exemplified in the cross-sections A-A’ and B-B’ (Figures 5.28a and 5.28b) in the basaltic and granitic rocks, respectively. The stratigraphy established from the lithological log show different basaltic flow layers (Fig. 5.28a). Boundaries between successive layers are marked by highly weathered and lateritized basalts and/or basement rocks. The top layer consists of cotton soil derived from in situ weathering of the parent material with a depth between 3 to 10 m, on average 5 m thick. The thickness of the weathered basalt varies from sequence to sequence and from site to site and ranges from 7 to 30 m with an average of 20 m. The thickness of the fresh basalt layer varies from 5 to 25 m with average of 15 m. The thickness of the lateritized basement varies from 25 to 40 m.

In the igneous intrusive rock areas (Fig. 5.28b) the top alluvial cover of unconsolidated sand to gravel ranges in thickness from 6 to 21 m. The underlying weathered granite varies in thickness from 16 to 36 m. In Borehole 8, 2-4m thick mafic dykes/sills occur within this layer at depths of 25 m and 41 m. The bottom

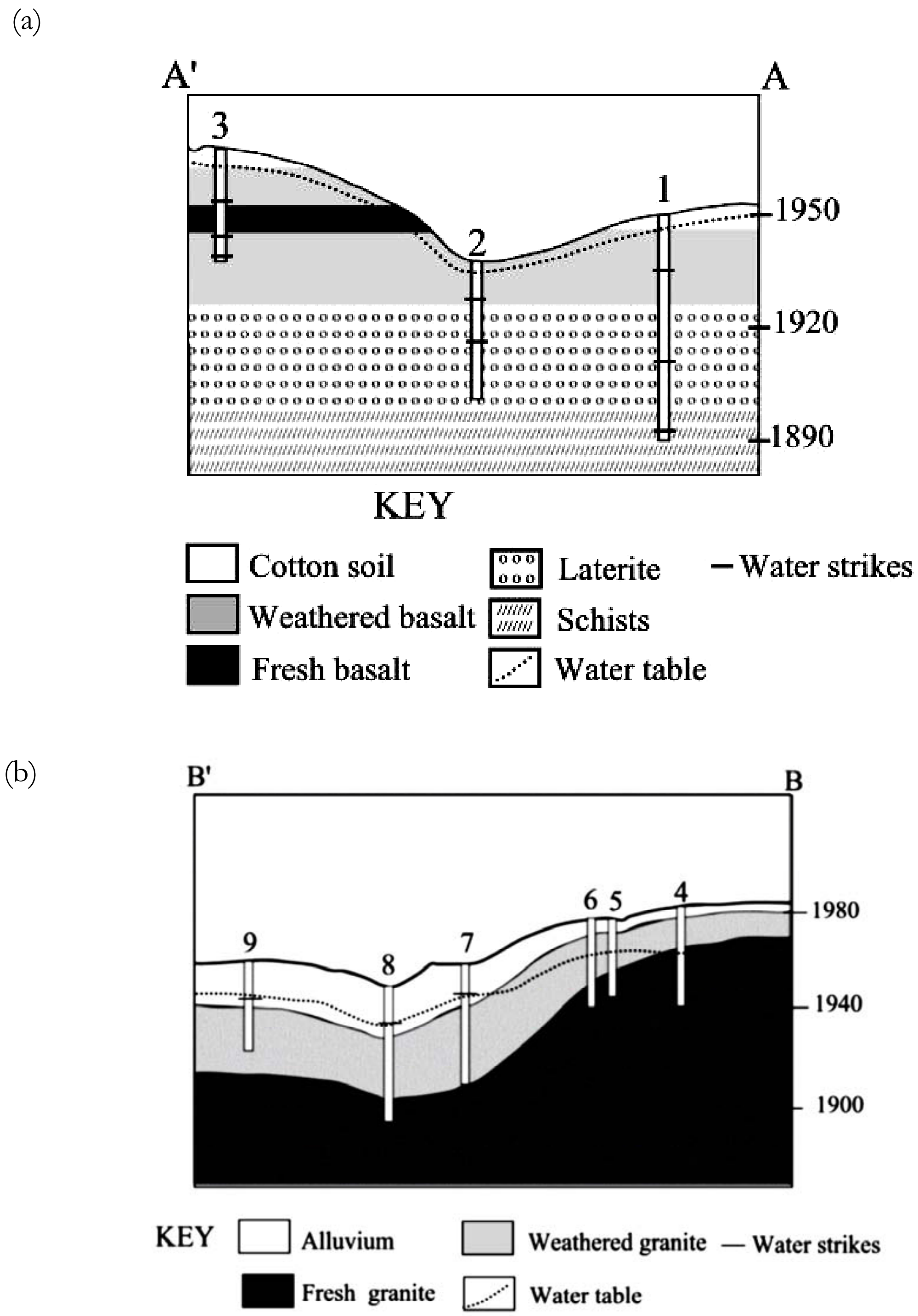

Figure 5.28. Lithological cross-section along (a) A-A' in the basaltic rock aquifers, location fig. 5.3a, and (b) B-B' in the granitic rock aquifers, location fig. 5.3b.

lithologic unit is the fresh massive bedrock granite and is encountered at varying depths.

Table 5.4 shows the borehole information used to construct the cross-sections in the basaltic and granitic rocks (Fig 5.28). In the basaltic aquifers, the water strike depths mostly correspond to weathered zones at varying depths (Table 5.4). In certain cases the water strikes occur at greater depths in other lithologic horizons such as the lateritized and fresh crystalline basement rocks (borehole 1) and also at the boundary between weathered and fresh basalts of vesicular nature (borehole 3). Although complete data on the yields at different water strike depths are lacking, in borehole 1 generally the yield increases as the depth to water strike increases. The measured yield at the first water strike depth in borehole 1 in the weathered basalt is 60 L/min. The yield increases to 120 L/min at the second water strike depth that lies in the deeply weathered crystalline rocks (laterites). The third water strike depth exists below the contact of deeply weathered schists and fresh schists with a yield of 480 L/min. At the base of the weathered zone rounded, sand to gravel sized particles of lateritic origin are observed during drilling. The high yield is presumed to be attribute to the increased permeability. In weathered crystalline mantles, aquifers tend to occur at the base of the mantle where less aggressive weathering is associated with saturated conditions and where coarse, partly weathered sand-sized clasts predominate (Eswaran and Bin 1978; McFarlane 1992; Taylar and Howard 1999a). Moreover fractures within the bedrock can form an aquifer. The static water levels in the basaltic aquifers occur at shallower depth (about 5 m) than the depth at which water was first encountered during drilling. Enhanced weathering in the unsaturated zones as well as saturated zones produces a clay-rich material of lower permeability and is responsible for apparent semi-confined to confined conditions in both weathered-basalt and -crystalline aquifers.

Table 5.4. Borehole information used to construct the cross-sections in Figure 5.28.

Boreholes	Total Depth (m)	Depth to SWL (m)	Pumping Rate (L/min)	Water Strike Depths (m)	Remark
Basaltic aquifers					
1 Debarwa	60	5.3	480	1st 16m 2nd 38m 3rd 55m	W. basalt Laterite Schists
2 Adi Watot	37	4	120	1st 12m 2nd 21m	W. basalt Laterite
3 Tera Emni	29	5.8	480	1st 15m 2nd 24m 3rd 28m	W. basalt W. Basalt W. basalt
Granitic and Alluvial aquifers					
4 Dekemhare	44	20	90	-	-
5 Dekemhare	35	13	83.4	-	-
6 Amhur	43	14	168.6	-	-
7 Dekemhare	53	8.7	146.4	1st 8.5m	Alluvium
8 Dekemhare	60	13	330	1st 13m	Alluvium
9 Mai Edaga	38	13	156	1st 14 m	Alluvium

In the granitic aquifers, the water strike depths lies in the top alluvial cover and varies from 8.5 to 14 m at an average borehole yield of about 120 L/min (Table 5.4). The water strike depths are not recorded in both weathered and fresh granite. The static water levels (about 13 m) occur at the same depth where water was first encountered during drilling suggesting unconfined aquifer conditions. The estimated yield in the granitic and alluvial aquifers range from 83.4 to 330 L/min. It is important to note that the yield values mentioned in this discussion is made in reference to Table 5.4. Low yields are usually associated with wells sited on the upstream part of the drainage network where the catchment area is small and the alluvial cover is relatively thin. The high yielding wells are generally located at the downstream part of the drainage network with large catchment areas and relatively thick alluvial cover. In these areas high recharge rates are expected owing to the accumulation of surface water flow draining from the upstream catchments. Moreover due to high permeability and thick alluvial cover good groundwater storage is likely to occur.

The highest yield in the granitic rocks is obtained in borehole (8) at Dekemhare where the borehole depth is 60 m and the borehole intersects a dyke/sill at a depth of 41-45m. Moreover this borehole is sited at the intersection of two major lineaments with N-S and NW-SE trends (fig. 5.6b) and a local depression with relative thick alluvial cover and weathered horizon. This highlights the significance of local topography, structures and weathering when selecting a well site.

Pumping tests
The pumping test data are used to get some knowledge about the hard rock aquifers. A log-log plot of drawdown vs. time for the pumping test is given in Figure 5.29. In the basaltic aquifers the plot for borehole 1 at Debarwa (Fig. 5.29a) shows a straight line suggesting linear flow. Although water strikes are recorded at three lithological units (Table 5.4), the pumping test indicates flow from fractures or fracture zones. This borehole is sited close to a dyke, which parallels the foliation. Dyke parallel adjacent joints are also common. The most likely source of the groundwater is thus from fractures associated with the dykes. The overlying weathered horizon provides storage for the fractured bedrock aquifer, and thus the two units form an integrated aquifer system. For borehole 3 (Tera Emini) the curve can be fitted to a Theis type curve suggesting a radial flow pattern. In this borehole all the water strike depths correspond to the weathered zones (Table 5.4) indicating the source from a homogeneous aquifer as reflected

in the pumping test data. In the basaltic aquifers the occurrence of groundwater is controlled both by lithologic and structural factors.

The response of pumping in the granitic rock aquifers is presented in Figure 5.29b. The plots in the two boreholes show consistently an early time-drawdown curve that fits the Theis type (radial flow) followed by late time-drawdown curves of linear pattern with very gentle slopes. Depth to static water level in the vicinity of the two boreholes is about 13.5 m and average drawdown is about 4.5 m. The sum of these two (18 m) lies within the weathered horizon.

(a)

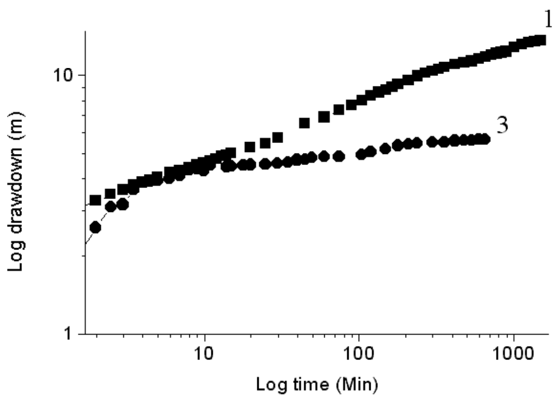

(b)

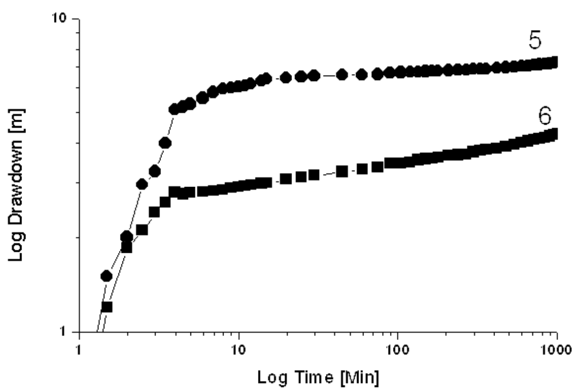

Figure 5.29. Pumping test results (a) basaltic aquifers wells 1 and 3 (b) granitic aquifers wells 5 and 6, see fig. 5.6a and 5.6b for locations.

Thus the pumping test results are interpreted as the first segment being due to pumping of water from storage in the weathered zone. The second segment shows more or less constant drawdown due to a contribution from storage in bedrock fractures. Low slopes imply that the fractured bedrock aquifers have very low transmissivity. The drawdown in borehole 6 is lower than that of borehole 5 despite of its higher pumping rate (Table 5.4). This is probably related to variations in transmissivity of the bedrock fractures. Boreholes tapping less transmissive bedrock owe greater drawdown within the fractured bedrock aquifer and induce increased drawdown in the weathered mantle (Taylor and Howard 2000). Furthermore existences of dry wells sunk in the weathered horizons are reported in the study area. This suggests the fractured bedrock that is hydraulically connected to the alluvium and/or weathered zones controls the occurrence of groundwater in the granitic aquifers. A combination of alluvial cover and weathered horizon together with the fractured bedrock are thus hydrogeologically significant.

5.4.3 GIS Modelling

The delineation of groundwater potential zones was made by grouping the raster composite layer, into different potential zones*; Very Good, Good, Moderate, Low and Poor*. The classification of the groundwater units into different categories was made by professional judgment considering the appropriate geological conditions in order to arrive at distinct groundwater potential zones. As a consequence a class interval of 40 is considered as cutoff value for classifying the groundwater prospect zones. The different categories are given in Table 5.5. By utilizing this model a map showing different groundwater potential zones were prepared (figure 5.30). The validity of the model developed was tested against the borehole yield data, which reflects the actual groundwater potential. Although very low yielding wells exist in all groundwater potential zones, the highest yields lie in the *very good* and *good* groundwater prospect zones (Figure 5.31).

Table 5.5. Groundwater prospect zones.

Zone	Class Interval	Groundwater Prospects
1	281-320	*Very Good*
2	241-280	*Good*
3	201-240	*Moderate*
4	161-200	*Low*
5	<=160	*Poor*

The groundwater potential zones prepared through this model (Fig. 5.30) show that the *very good* potential zones have average yield of 201 L/min. *Good* groundwater prospect zones have average well yields of 102 L/min. The moderate, low and poor groundwater potential zones have average yields of 85, 56 and 25 (L/min), respectively. All well yields in each category represent average logarithmic values. It is important to point out that the model generated will help as a guideline for designing a suitable groundwater exploration plan in the future. The spatial distributions of the various groundwater potential zones obtained from the model generally show regional patterns of lineaments, drainage, landform and lithology. Spatially the *very good* and *good* categories are distributed along major lineaments and drainage channels with and without structural control. This highlights the importance of lineaments and hydrogeomorphological units for groundwater investigations. Areas with *moderate* groundwater prospects are attributed to contributions from combinations of the lithology, slope and landform. The low to poor categories of groundwater potential zones are spatially distributed mainly along ridges and pediments and to some extent along lineaments with low to poor slope classes. The basalts that lie west in site-1 (fig. 5.30a) are classified as *moderate* to *verygood* groundwater potential zones. With densely fractured basaltic rocks showing *good to verygood* groundwater prospects. The alluvium that lie northwest and southwest in site-2 (fig. 5.30b) have *moderate* to *verygood* groundwater potential. The most promising targets in the alluvium constitute areas with dense lineaments.

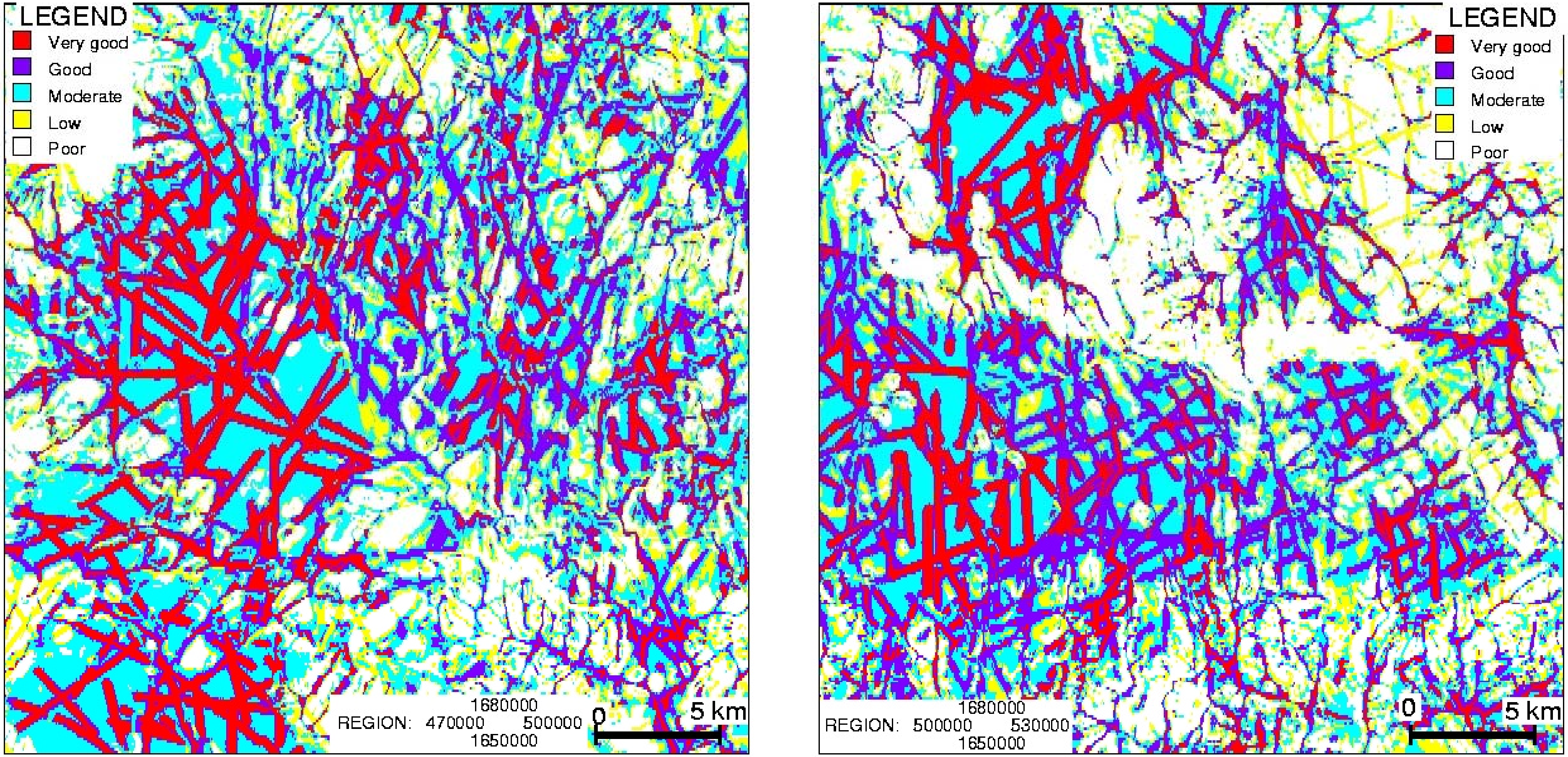

(a) (b)

Figure 5.30. Groundwater potential zone maps (a) site-1 and (b) site-2.

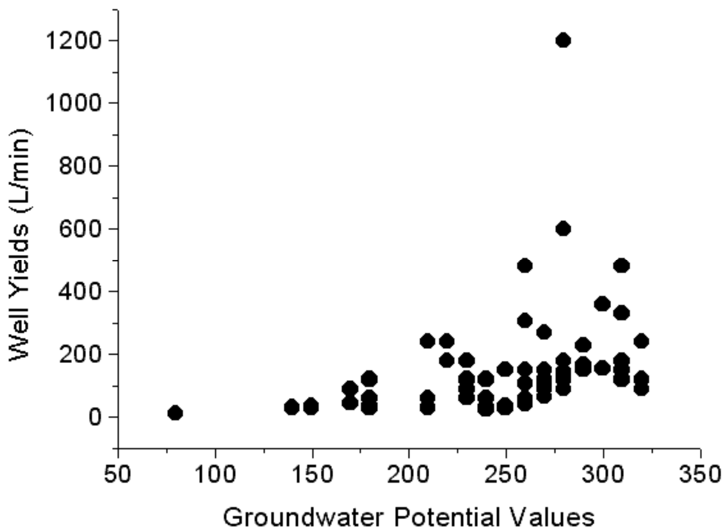

Figure 5.31. Model validation results, scatter plot of well yield vs. groundwater potential values.

The peneplains in the crystalline rocks generally have *moderate* groundwater potential (e.g. south of the escarpment in figure 5.30b). Most of the zones with *low to poor* groundwater potential lie in the crystalline rocks due to the rugged nature of the landform.

Vegetation types and patterns are usually good indicators of shallow groundwater in arid and semi-arid areas. Dry season green vegetation is often used as an indicator of moisture in the near surface zone. It is important to note that in the models derived through the integration of the various thematic maps in the GIS, the presence of natural vegetation cover was not considered. The main reason is that SPOT (acquired in April) and Landsat (acquired in September) data were taken immediately after the short and long rainy seasons, respectively. They thus would represent wet season vegetation cover. A dry season image such as the ASTER data allows to generate an improved model with appropriate considerations given to natural vegetation cover.

5.4.4 Groundwater Recharge Estimation

Water-table Fluctuation Method

Table 5.5 summarizes the estimated groundwater recharge in different rock units. Values of representative effective porosity were taken from Singhal and Gupta (1999). Seasonal water table fluctuation varies from 1.5 to 3.0 m in open dug-wells. The rise of water levels observed in open dug-wells in the crystalline rocks, basalts and alluvium are 1.5, 2.5 and 3.0 m, respectively. One third of the observed values in each aquifer type were used in the calculation of the groundwater recharge (Table 5.6). The rationale for considering one third of the observed groundwater level rise is that the volume of water withdrawn from a well divided by the area of influence of the drawdown should be approximately equivalent to the average fluctuation in water table over the zone of drawdown. The following relationship was used:

$$\text{Average rise in water level} = \frac{\text{Volume of drawdown } (\pi r^2 h/3)}{\text{Area of drawdown } (\pi r^2)}$$

In considering the volume of water withdrawn from the well, the drawdown was approximated to a straight line and volume of an ideal cone of depression calculated. The average rise in water level will be approximately one-third of the observed rise in water level (h) in open dug-wells. It should be pointed out that the volume of the cone of depression is overestimated when using a straight line instead of the curved line, but this can provide a good approximation of water table fluctuation around the well.

Assuming the average of the effective porosity values as representative for the respective rock units, the estimated groundwater recharges are 43 mm for the basaltic rocks, about 9 mm for the crystalline (igneous intrusive and metamorphic) rocks and 225 mm for the alluvium. With an average rainfall in the region of 550 mm per annum the groundwater recharge is about 8% of annual rainfall in basalts, 1.6% in crystalline rocks and 41% in alluvium. The results of the current study are close to previous studies carried out by FAO (1994) and UNESCO (1975) in particular in the basaltic rocks. For alluvial aquifers the current study overestimates the values relative to the study by Euroconsultant group that assumes about 40 mm. The estimated groundwater recharge in the crystalline rock aquifers appears to be slightly higher than estimates made in other parts of the world (e.g. Australia) but is in good agreement with recharge rate estimates recorded in continental parts of Africa. Field investigations show groundwater discharge in the form of riverbed flows during dry spells in catchments draining alluvium and crystalline rocks suggesting occurrence of consistent recharge. The high recharge rates in the alluvium can be attributed to the accumulation of surface flow draining from the upstream parts of catchments (indirect recharge) dominated by crystalline rocks. The relative low slopes in the alluvium coupled with high permeability provide good groundwater recharge conditions.

Table 5.6 Estimated groundwater recharge in different rock units and values of representative effective porosity (Singhal and Gupta 1999).

Rock type	Effective Porosity Ranges (%)	Average Fluctuation (m)	Estimated Groundwater Recharge (mm)
Basalt	2 – 10	0.8	16 – 80
Crystalline Rocks	0.5 – 3	0.5	2.5 – 15
Alluvium	15 – 30	1.0	150 – 300

Chloride Mass-Balance Method

The average chloride concentration in groundwater (Cl_{gw}) in the area studied is 25.7 mg/l. This value is based on 18 chemical analysis of groundwater and was calculated by excluding zones of anomalously high concentrations of chloride in certain boreholes (JICA, 1997). The precipitation weighted average chloride (Cl_{wap}) concentration for samples of wet and dry precipitation during 1999 in the area studied is 2.30 mg/l. This value is based upon two samples collected during the 1999 wet season. Precipitation is variable in space as well as time but a reasonable estimate based on historical data records for this region is approximately 550 mm/yr. Thus using the equation in Section 4.4.4, the average recharge flux for the study area is approximately 49 mm/yr. This result could be subjected to great errors because of the various assumptions involved. Determination of chloride content in rainwater is based on two samples only and this can affect the reliability of the value. Also there is a strong requirement of evaluating the rate of evaporation, because there has been reports that in (semi-) arid regions there are occasions where all the water which entered the soil was eventually returned to the atmosphere via evaporation, without any net downward movement of deep drainage (Bromley et al, 1997). However, recharge rates of 38.5 mm/yr have been calculated using the same method for the aquifers in the central highlands of Eritrea (personal communication Haile, 2002).

5.4.5 Hydrogeological Implication of ASTER Data

Analysis of image data from the ASTER sensor revealed the capability of mapping regional variations in the degree of chemical weathering in rocks. This information could not be recognized in Landsat TM data. Also the improved spatial resolution from the VNIR wavelength region allowed to identify lineaments such as dykes that are hardly recognizable from SPOT and Landsat TM image data. Moreover the nadir and backward looking near-infrared bands provide stereo-coverage and can facilitate detailed lineament mapping. The regional variations in the degree of weathering in rocks as well as the dykes and lineaments that can be detected from the ASTER data due the improved resolution and its stereo-coverage capability have hydrogeological significance in the area studied. On the plateau south of the escarpment groundwater occurrence depends on the depth of weathered zone and presence of lineaments. In contrast down the escarpment in the low lands due to less weathered cover groundwater occurrence should rely on the presence of alluvial cover and/or existence of lineaments. Groundwater resources in the alluvium north of the escarpment (Alla Valley) are reported to be under critical conditions due to overexploitation of the aquifer. However, field investigations in this area show that hand dug-wells sunk on dykes yield sustained flow while nearby hand dug-wells sunk on the alluvium and weathered granite remain dry. This observation supports that lineaments should be given high priorities for groundwater development.

A three dimensional view of part of the study area in site-2 is given in Figure 5.32. In the dominantly green NE corner with layers of light blue are the various types of metamorphic rocks continuing towards SE. Alluvium appears in white to yellow color and lies in the NW corner and partly towards SE. Also down the escarpment in red to brown color are syn-tectonic granites. Up the escarpment to the south cyan and light blue represent post-tectonic granite (west), dominantly blue color granite gneiss (center) and east of the granite gneiss the post-tectonic granite in light cyan color. Vegetation cover appears in dark blue color. The variations in color on rocks down and up the escarpment, which have been discussed earlier is also clearly visible in this figure. The diagram summarizes the geology, topography, weathering and their hyrogeological significance. It further demonstrates the importance of the ASTER and SRTM data for hyrogeological studies.

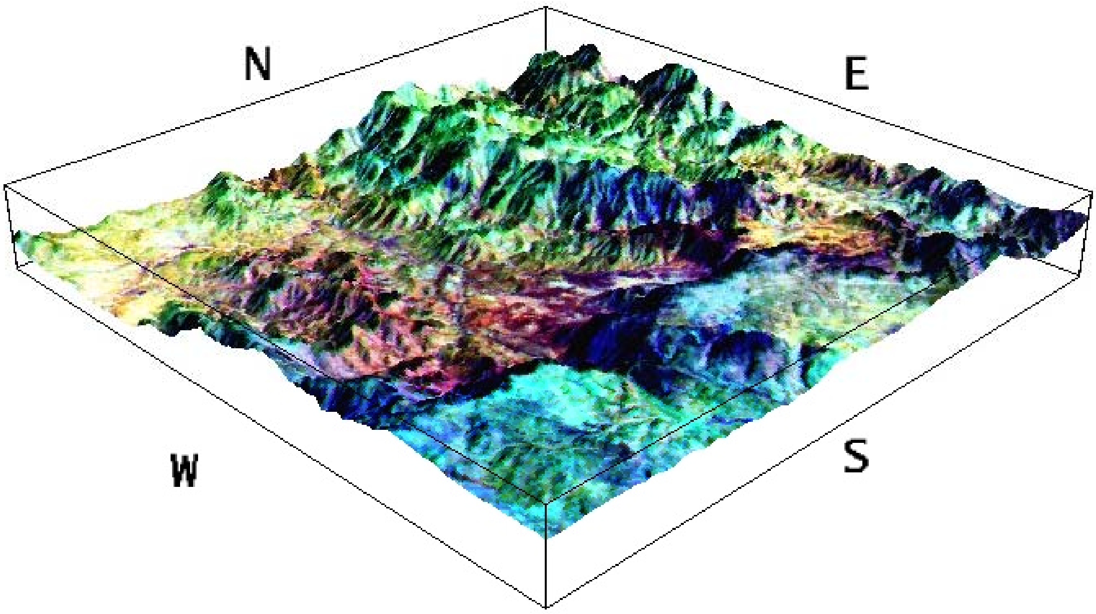

Figure 5.32. Three dimensional view of part of the study area in site-2 created by draping ASTER bands 13, 5 and 3 in RGB order over the SRTM DEM data.

6 CONCLUSIONS AND RECOMMENDATIONS

6.1 Remote Sensing

Landsat Thematic Mapper data were used in parts of the central highlands of Eritrea for geological mapping. In areas with high mineralogical contrast, standard color composites proved useful for lithological mapping. Principal component analysis was helpful in discriminating subtle differences in lithologies in localities where mineralogical contrast is low but difficulties in interpreting the colors remain. Intensity-Hue-Saturation enhancement gives good results for image interpretation due to saturation of hues in addition to its relatively straightforward nature. Decorrelation stretch is generally superior to other techniques because it allowed easy lithological discrimination as consequence of color accentuation in most cases.

Lineament mapping was carried out using Landsat TM, SPOT and digital elevation models and applying various image processing techniques. Most of the lineaments can be identified in black and white and digitally processed color composite images, but finer details are enhanced in directionally filtered images. Certain lineaments are more conspicuous in black and white as well as color composites than in filtered images possibly due to lithological variation.

Directional filtering along N-S direction provides an effective way to detect most lineaments. The image data on which the directional filter is applied is important and not only the filter direction. Since the study area is characterized by rough terrain, image groups that preserve the topographic features such as PC1 image offer better results from directional filtering than other images. Major linear features of prominent trends and of regional scale appear more conspicuous in the DEM output than in the Landsat TM and SPOT images, because topographic features are contained in the former. On the other hand, minor lineaments are clearly discernible in the TM and SPOT images and are not conspicuous in the DEM data. Density and number of lineaments is higher in the remote sensing data than in the DEM due to the spatial resolution. Lineament analysis showed that in the areas studied the direction N-S (NNW-SSE), NW-SE, NE-SW, ENE-WSW and WNW-ESE dominate. Results demonstrate that remote sensing data can be used to prepare lithological and lineament maps. Moreover digital elevation model data proved to be useful for lineament mapping.

One of the common problems in using multi-spectral image data is to select the most informative bands for image analysis. Determinant and principal component analyses are very useful in this regard. Principal component analysis of 14 bands of ASTER data helped to show regional lithological variations due to chemical weathering of rocks, vegetation cover and landform types. Higher order principal component color composite images highlight local variations due to lithologic and mineralogical differences in areas with less altered rocks, bare soil and little vegetation covers. PC images from Landsat TM proved to be less useful to identify subtle mineralogical differences. Moreover the improved ground resolution in the VNIR bands of ASTER data proved very useful to distinguish lineaments of great hydrogeological significance. Such lineaments could not be detected easily in the SPOT and Landsat TM data. The improved spectral and spatial resolutions from ASTER data compared to other satellite data such as Landsat TM and SPOT, is a significant advantage in preparing detailed lithological and lineament maps of excellent quality that have hydrogeological importance with considerable savings in time.

6.2 Structures

Comparison of rose diagrams of total joints, dykes and regional lineaments show a good agreement in the orientations of the major structures in the study area. High correlation exist between spacing of joints and lineaments. In general, high correlation in orientation of all structural features with dense joint spacing suggests that most of the mapped lineaments correspond to fractures or fracture zones. The fractures are either tensile or shear or both. Some of the fracture sets are filled with magma to form dykes. Most of the encountered structural features occur regionally and fit well into the current tectonic setup of the region. The N-S, NW-SE and WNW-ESE oriented fractures are considered to be part of structures related to the Red Sea. NE-SW and ENE-WSW oriented fractures are postulated to be the youngest, possibly as extension of transform faults identified in the Red Sea.

Relating structures observed in the field with lineaments mapped from remote sensing data it can be concluded that most lineaments correspond to one of three distinct categories or their associated fractures:

(i) Dykes (extensional fractures)
(ii) Normal faults (extensional fractures) and
(iii) Strike-slip faults (shear fractures)

Linear features associated with dykes can be separated from other types of lineaments using remote sensing data as shown in this study. But differentiation of other fracture types, for instance normal faults from strike-slip faults is more difficult. Field studies of structures are needed to discern the nature of structures and correlate lineament interpretation with geological structures. This integrated approach provided good results and allowed to characterize the lineaments better. Since most of the structures are controlled by pre-existing older structures, all mapped lineaments may not necessarily belong strictly to the categories outlined above. Some lineaments may reflect Precambrian structures, however, it can only be verified from field studies.

6.3 Geomorphology

Landform types must be understood to assess groundwater potential. Topographic parameters derived from digital elevation models can provide valuable information on the characteristics of a land surface. The classification of a landscape into geomorphological units is commonly performed through conventional field surveys or by interpreting remote sensing data. This method is both time-consuming and subjective. The numerical description or parameterisation of a surface coupled with local knowledge of the topography allows a more accurate delineation of landforms. Classification of multivariate data by means of statistical cluster analysis is common practice in GIS and remote sensing. To classify topographic regions into landform types an iterative cluster analysis was used using DEM derived parameters as input. It demonstrated that DEM's allow to create a detailed description of landforms that is useful for groundwater potential assessment. By parameterisation of surface forms it was possible to examine and quantify spatial variation systematically. Parameterisation of a DEM allowed to generate more useful information for geomorphological mapping and identification of landform potential for groundwater development.

Comparison between digital elevation models demonstrates that models derived from SRTM data are better for detection of drainage systems and linear features than those derived from contours. This superiority is mainly due to more details in the SRTM data as a result of improved resolution and continuous data. Availability of digital elevation data with dense data points such as SRTM data is an advantage to prepare detailed geomorphological and lineament maps.

6.4 Hydrogeology

The occurrence of groundwater is controlled by rock type, structures and landforms as revealed from GIS analyses and field investigations. In basaltic rocks intensely weathered lava flow layers largely control groundwater storage and availability. High yields are due to primary and secondary porosities. Flat topography with dense lineaments characterizes high groundwater potential. Basaltic layers overlaying lateritized crystalline rocks form multiple aquifer systems.

In metamorphic rocks foliation serves as weak planes and facilitates flow and storage of groundwater. Due to rugged landforms, groundwater occurs mainly in drainage channels with valley fill deposits. Fractures along drainage channels together with valley fill deposits form an integrated aquifer system and have high groundwater potential. In granitic rocks groundwater availability is largely controlled by bedrock fractures. Alluvial materials and weathered bedrock in hydraulic connection with bedrock fractures constitute promising sites for groundwater exploration. Dense lineaments on alluvial flood plains have high groundwater prospects. High yields are often related to thick alluvial cover and thick weathered horizons.

Coordinate reliability is critical when analysing borehole data in relation to interpreted lineaments and GPS technology can improve coordinate accuracy significantly. Borehole yield shows a high negative correlation with distance to lineaments interpreted from satellite images. High yielding wells and springs are often related to large lineaments, lineament intersections and corresponding structural features with dense fracture spacing. Dykes often show high yields due to enhanced permeability owing to adjacent dyke parallel joints. They are potential targets for groundwater exploration and are thus hydrogeologically significant. Low yielding boreholes close to major lineaments are due to both poor site selection and inhomogeneous nature of hard rock aquifers.

GIS are very time- and cost-effective once the database is created and have many advantages over traditional approaches. To fully understand the hydrogeological nature of hard rock aquifers, traditional techniques are also crucial. Integration of different data layers in a GIS environment followed by spatial and statistical analysis of the data allowed to understand the correlation between different parameters and to unravel the nature of hard rock aquifers. This shows the strength of a GIS, its ability to perform spatial and statistical analysis combining various data types. The groundwater potential model derived through integration of various thematic maps demonstrates the hydrogeological significance of rock types, structures and landform types. This integrated approach will help to design suitable groundwater exploration plans in the future. The overall results demonstrate that the integration of remote sensing, GIS, traditional fieldwork and models provide a powerful tool for the assessment of groundwater resources.

Recharge estimation is very important for the assessment of groundwater resources. Groundwater recharge estimations using the chloride-mass balance method result in higher rates in the region as compared with estimates from parts of Africa with similar climatic conditions as Eritrea. Values obtained with the water-table fluctuation method are in good agreements with estimates recorded elsewhere and thus are considered representative for the areas studied. Recharge rates of 10 - 50 mm can be assumed safely for this region with the lower bound for crystalline rock aquifers and the upper bound for basaltic as well as alluvial aquifers.

6.5 Recommendations

Several approaches were applied to understand the hydrogeological conditions of the hard rock aquifers in parts of the central highlands in Eritrea. Because of the inhomogeneous nature of hard rock aquifers, it is crucial to use investigation techniques that maximize the information from various sources. An attempt was made to optimize the available data using methods that have proved to be successful in hydrogeological studies in other parts of the world. The following recommendations are given.

Remote Sensing

Remote sensing data are powerful tools to improve our understanding of groundwater systems. While not directly measuring hydrogeological properties, they provide continuous detailed terrain information and allow the mapping of features significant to groundwater development. Various satellite data with different spectral and spatial resolutions coupled with digital image processing techniques help to accurately produce detailed maps. Ground verification is crucial to increase the accuracy of the interpretation results. Principal component analysis in combinations with decorrelation stretch are useful for lithologic mapping and their use is highly recommended. Directional filtering of principal component 1, intensity images and digital elevation models improves lineament mapping. Improved digital elevation model data from SRTM and high resolution data from the visible and near-infrared bands of ASTER are of great help in lineament extraction. Nadir and backward looking near-infrared bands provide stereo-coverage and facilitate detailed lineament mapping. ASTER data are highly recommended for future groundwater prospection because of their improved spatial and spectral resolution as well as their stereo-coverage.

Field Studies

Structures are assessed at the outcrop scale to decipher the nature of lineaments interpreted from remote sensing data. Field investigations of well sites in relation to location, topography and structures as well as subsurface information such as pumping test and lithological log data are most valuable to improve our understanding of the hydrogeological conditions. High priority should be given to the compilation of such data also in other areas. To understand the various aquifer systems better controlled pumping tests should be made to determine:

- Safe yield of wells
- Hydraulic parameters of aquifers such as transmissivity and storativity.

Artificial fracturing is recommended to improve transmissivity and storage capacity of wells in hard rock aquifers and thus increase sustained yield. Well locations and other sites should be surveyed with GPS to facilitate data integration in a geographic information system.

Geomorphology

Geomorphologic investigations are important to delineate and map landform and drainage characteristics that have a direct control on occurrence and flow of groundwater. Digital elevation model data are efficient to delineate landforms and SRTM data are highly recommended.

Hydrogeology

Geographic Information Systems are very time- and cost-effective once the database is created and provide many advantages over traditional approaches. Integration of different data layers such as remote sensing, geomorphology and field data in a GIS environment provide means to unravel the nature of hard rock aquifers. Spatial and statistical analysis allows to understand the correlation between different parameters. This integrated approach of groundwater potential assessment in a GIS is highly recommended.

The model derived through integration of various thematic maps demonstrates the hydrogeological significance of rock types, structures and different landform types. The integrated approach adopted provides a basis for designing suitable groundwater exploration plans. Alluvium and basalts have high groundwater potential due to high primary porosity and permeability. In both aquifers, areas with high lineament density are the most favourable sites and should be given high priority for groundwater exploration. Groundwater exploration in basaltic rock aquifers should include the underlying deeply weathered crystalline rocks (laterites) because they form multiple aquifer systems often with high yields. In metamorphic and igneous intrusive rock aquifers groundwater exploration should focus on lineaments, which coincide with drainage channels with valley fill deposits. Lineament intersections and dyke swarms should be considered as targets for future groundwater development. Combinations of parameters such as local depressions, lineament intersections, dyke swarms, thick alluvial cover and deeply weathered horizons are best sites for high yields.

Routine monitoring of groundwater levels, water quality and the amount of water abstracted should be made at wells. This provides an early warning system for over-abstraction and water quality deterioration and essential background data for efficient groundwater management. It is highly recommended to study and quantify groundwater recharge in the region as a crucial parameter for groundwater management.

REFERENCES

Abrams, M.J., Hook, S.J. and Ramachandra, B. 2002. ASTER User Handbook version 2. Jet Propulsion Laboratory, NASA, 135pp.

Abrams, M.J. 1984. Landat-4 Thematic Mapper and Thematic Mapper simulator data for a porphyry copper deposit. Photogrammetric Engineering & Remote Sensing, 50, pp.1171-1173.

Abrams, M.J. and Hook, S.J. 1994. Simulated Aster Data for Geologic Studies. IEEE Transactions on Geoscience and Remote Sensing, 33, 3, pp.692-699.

Allison, G.B and Hughes, M.W., 1978. The use of environmental chloride and tritium to estimate total recharge to an unconfined aquifer. Aust. J. Soil Res., 16: 181-195.

Amos, B.J., and Greenbaum, D., 1989. Alteration detection using TM imagery: The effects of supergene weathering in arid climate. Int. J. Remote Sensing, 10, pp. 515-527.

Andrews D. M.E., 2003. Facies discrimination in laterites, using Landsat TM and ASTER data. International Journal of Remote Sensing.

Asgedom, A. 1998. Groundwater Assessment in the South Highlands of Eritrea using TM Images. M.Sc. thesis, University of New South Wales, Australia, 128 pp.

Berhe, S.M. 1986. Geologic and geochronologic constraints in the evolution of the Red Sea, Gulf of Aden and Afar Depression, Journal of African Earth Sciences, 5, pp.101-117.

Berhe, S.M. 1991. Tectonic Evolution of the Pan-African Mozambique Belt in NE and E Africa: Extended Abstract International Field Geotraverse /Workshop through The Mozambique Belt. Tanzania, July 23-August 6, 1991.

Brabyn, L. 1996. Landscape Classification using GIS and National Digital Database. The University of Canterbury, New Zealand. Ph.D dissertation.

Bromley, J., Edmunds, W.M., Fellman, E., Brouwer, J. Gaze, S.R., Sudlow, J. and Taupin, J-D. 1997. Estimation of rainfall input and direct recharge to the deep unsaturated zone of southern Niger using the chloride profile method. Journal of Hydrology, 188-189, pp139-155.

Burrough, P.A., 1986. Principles of Geographic Information Systems for Land Resource Assessment. OUP, Oxford, UK.

Bäcker, H., Lange, K. and Richter, H. 1975. Morphology of the Red Sea central graben between Subai Islands and Abul Kizan. Geologisches Jahrbuch, D13, pp.79-123.

Chavez, P.S., Jr., and Kwarteng, A. Y., 1989. Extracting spectral contrast in Landsat Thematic Mapper data using selective Principal Component Analysis. Photogrammetric Engineering & Remote Sensing, 55, pp. 339-348.

Cross, A.M. 1988. Detection of circular geologic features using the Hough Transform. Int. J. Remote Sensing, 9, pp. 1519-1528.

Cross, A. and Wadge, G. 1988. Geological lineament detection using the Hough Transform. Proc. Of the GRASS'88 Symposium, Edinburgh, Scotland, 13-16 Sept., ESA, pp. 1779-1782.

Davis, P.A. and Berlin, G.L. 1989. Rock discrimination in the complex geological environment of Jabal Salma, Saudi Arabia using Landsat Thematic Mapper data. Photogrammetric Engineering & Remote Sensing, 7,pp.1147-1160.

Dixon, T.H., Stern, R.J. and Hussein, I.M. 1987. Control of the Red Sea rift geometry by Precambrian structures. Tectonics, 6, pp.51-57.

Drury, S.A., 1987. Image Interpretation in Geology. (London: Allen & Unwin), 243pp.

Drury, S.A., Berhe, S.M., Kibreab, A. and Mesfin, A., 1991. Thematic Mapper Data and Geological Reconnaissance of Pan-African terrane in Eritrea NE Africa. The Context for Hydrothermal Mineralization, 8th Conference on Geological Remote Sensing, Denver, Colorado, USA.

Drury, S.A., and Berhe, S.M., 1993. Accretion tectonics in northern Eritrea revealed by remotely sensed imagery. Geol. Mag., 130 (2), pp.170-190.

Drury, S.A., Kelley, S.P., Berhe, S.M., Collier, R.E. and Abraham, M. 1994. Structures Related to Red Sea evolution in northern Eritrea. Tectonics, 13, pp. 1371-1380.

Drury, S.A., Peart, R.J., Deller, M.E.A. 2001. Hydrogeological potential of major fractures in Eritrea. Journal of African Earth Sciences, 32, 2, pp. 163-177.

Eriksson, E. and Khunakasem, V., 1969. Chloride concentration in groundwater, recharge rate and rate of deposition of chloride in the Israel Coastal Plain. Jour. of Hydrol., 7, pp.178-179.

Eswaran, H. and Bin, W.C. 1978. A study of a deep weathering profile on granite in peninsular Malaysia: I. Physico-chemical and micromorphological properties. Journal of Soil Science Society of America, 42, pp.144-149.

Euroconsult, 1998. Sector Study on National Water Resources and Irrigation Potential. Stage I Draft Report, Groudwater Resources, Volume 1. Water Resources Department. Asmara, Eritrea.

Euroconsult, 1998. Sector Study on National Water Resources and Irrigation Potential.Stage I Draft Report, Groundwater Resources, Volume 2. Water Resources Department. Asmara, Eritrea.

Evans, I.S., 1972. General Geomorphometry, derivatives of altitude, and descriptive statistics: in Chorley, R.J. ed. Spatial Analysis in Geomorphology, Methuen, London, pp. 17-90.

Evans, I.S., 1979. An integrated system of terrain analysis and slope mapping. Final report on grant DA-ERO-591-73-G0040, University of Durham, England.

Evans, I.S., 1980. An integrated system of terrain analysis and slope mapping. Zeitschrift fur Geomorphologie, Suppl-Bd 36, pp.274-295.

Evans, I.S., 1984. Correlation structures and factor analysis in the investigation of data dimensionality: statistical properties of the Wessex land surface, England, International Symposium on Spatial Data Handling, Zurich, 1, pp.98-116.

Fairhead, J.D. and Girdler, R.W. 1970. The seismisity of the Red Sea, Gulf of Aden and Afar triangle. Philosophical Transactions of the Royal Society of London, Series A, 267, pp.49-74.

FAO Investment Center 1994. Eritrea: Investigation of water resources development options in high potential areas in Seraye Province. Annex 1, Water Resources Department. Asmara, Eritrea.

GEOZAVOD-Belgrade (Institute for Investigation of Mineral Resources), 1982. Program and Project of Geological Investigation in Metallogenic Zone of Asmara (N. Ethiopia). Unpub. Minst. Mines & Energy, Addis Ababa.

Ghebreab, W., 1996. An outline of major Pan-African lithologic assemblages and shear zones in Eritrea: implications for mineral exploration. African Geoscience Review, 3, 3/4, pp. 355-366.

Ghebreab, W., 1998. Tectonics of the Red Sea region reassessed. Earth Science Reviews, 45, pp. 1-45.

Ghebreab, W., 1998. Geological Map of Massawa Sheet (1:250,000). Asmara, Eritrea.

Gillespie, A.R., Kahle, A.B. and Walker, R.E., 1986. Color enhancement of highly correlated images. Decorrelation and HSI contrast stretches. Remote Sensing of Environment, 20, pp.209-235.

Gillespie, A.R., Kahle, A.B. and Walker, R.E. 1987. Color enhancement of highly correlated images, II. Channel ratio and "chromaticity" transformation techniques. Remote Sensing of Environment, 22, pp.343-365.

Goetz, A.F., Rock, B.N., and Rowan, L.C. 1983. Remote Sensing for Exploration: an overview. Economic Geology, 78, pp.573-590.

Grasso, D.N., 1993. Application of the IHS color transformation for 1:24,000-scale geological mapping: A low cost SPOT alternative. Photogrammetry Eng. & Remote Sensing, 59, pp. 73-80.

Greenbaum, D. 1987. Lineament Studies in Masvingo Province, Zimbabwe, British Geological Survey Report WC/87/7.

Greenbaum, D. 1992. Structural influences on the occurrence of groundwater in SE Zimbabwe. In: Wright, E. P. & Burgess, W. G. (eds) 1992, Hydrogeology of Crystalline Basement Aquifers in Africa, Geological Society Special Publication No 66, pp. 77-85.

Haile, E. 2002. Department of Land and Water Resources Engineering, Royal Institute of Technology, Stockholm, Sweden.

Hamrla, H. 1978. The massive sulphides and magnetite deposits of northern Ethiopia. Geologia, 21, pp.255-310.

Hodgson, G. 1999. Application of HARSD landscape classification and groundwater surface mapping techniques to study catchment at Ucarro, Western Australia. Task Report GAH99_2, pp. 15.

Holmes, A. 1951. The sequence of Precambrian Orogenic belts in South and Central Africa. 18th Int. Geol.Congr., London, 1948, 4, pp. 254-269.

Hord, M.R., 1982. Digital Image Processing of Remotely Sensed Data. (New York: Academic Press).
Hunt, G.R. 1977. Spectral signatures of particulate minerals in the visible and near-infrared. Geophysics, 42, pp.501-513.

Hunt, G.R. 1979. Near-infrared (1.3-2.4 μm) spectra of alteration minerals – potential for use in remote sensing. Geophysics, 44, pp.1974-1986.

Hunt, G.R. and Salisbury, J.W. 1970. Visible and near-infrared spectra of minerals and rocks: I Silicate minerals. Modern Geology, 1, pp.283-300.

Hunt, G.R. and Ashley, R.P. 1979. Spectra of altered rocks in the visible and near-infrared. Economic Geology, 74, pp.1612-1629.

Jensen, J.R., 1986. Introductory Digital Image Processing: A Remote Sensing Perspective (Englewood Cliffs, New Jersey: Prentice-Hall).

Jet Propulsion Laboratory (JPL) website (http://www.jpl.nasa.gov).

JICA 1997/98. Study on groundwater development and water supply fro seven towns in southern region of Eritrea. Water Resources Department. Asmara, Eritrea.

Kahle, A.H. and Goetz, A.F.H. 1983. Mineralogical information from a new airborne thermal infrared multispectral scanner. Science 222, pp.24-27.

Kamaraju, M., Bhattacharya, A., Reddy, G., Rao, G. Murthy, G. and Rao, T. 1996. Ground-Water Potential Evaluation of West Godavari District, Andrha Pradesh State, India: A GIS Approach. Ground Water, 34, 2, pp.318-325.

Kar, A. 1994. Lineament control on channel behaviour during the 1990 flood in the southeastern Thar Desert. Int. Jour. of Remote Sensing, 15, pp.2521-2530.

Karnieli, A., Meiseis, A., Fisher, L. and Arkin, Y. 1996. Automatic extraction and evaluation of geological linear features from digital remote sensing data using the Hough Transform. Photogrammetric Engineering & Remote Sensing, 62, pp. 525-531.

Kauffman, H., 1988. Mineral exploration along the Aquaba-Levant structure by use of TM – data: Concepts, processing and results. Int. J. Remote Sensing, 9, pp. 1639-1658.

Kenea, N.H., 1997. Improved geological mapping using Landsat TM data, Southern Red Sea Hills, Sudan: PC and IHS -decorrelation stretching. Int. J. Remote Sensing, 18, pp. 1233-1245.

Koch, A. 2002. Analysis of SRTM DTM – Methodology and practical results. Paper presented in X-SAR/SRTM PI Workshop, Germany, 17-18 Oct. 2002.

Koch, M., and Mather, P.M., 1997. Lineament mapping for groundwater Resource assessment: a comparison of digital Synthetic Aperture (SAR) imagery and stereoscopic Large Format Camera (LFC) photographs in the Red Sea Hills, Sudan. Int. J. Remote Sensing, 18, pp. 1465-1482.

Koopmans, B.N. 1986. A comparative study of lineament analysis from different remote sensing imagery over areas in the Benue Valley and Jos Plateau Nigeria. Int. Jour. of Remote Sensing, 7, pp.1763-1771.

Krishnamurthy, J., Manavalan, P., and Saivasan, V., 1992. Application of digital enhancement techniques for groundwater exploration in a hard-rock terrain. Int. J. Remote Sensing, 13, pp. 2925-2942.

Krishnamurthy, J., Kumar, N.V., Jayaraman, V., and Manivel, M., 1996. An approach to demarcate groundwater potential zones through remote sensing and a geographic information system. Int. J. Remote Sensing, 17, pp. 1867-1885.

Lattman, L.H. 1958. Technique of mapping Geologic Fracture Traces and Lineaments on Aerial Photographs, Photogrammetric Engineering, 19, 4, pp.568-576

Lattman, L.H. and Parizek, R.R. 1964. Relationship between fracture traces and the occurrence of groundwater in carbonate rocks. Jour. Of Hydrology, 2, pp. 73-91.

Lillesand, T.M., and Kiefer, R.W., 1994. Remote Sensing and Image Interpretation (New York: Wiley), 750pp.

Lloyd, J.W. 1999. Water resources of hard rock aquifers in arid and semi-arid zones. Studies and reports in hydrology, UNESCO publ., 58, 284pp.

Mabee, S.B., Hardcastle, K.C., and Wise, D.W. 1994. A Method of Collecting and Analyzing Lineaments for Regional-Scale Fractured Bedrock Aquifer Studies, Ground Water, 32, 6, pp.884-894.

Mather, P.M., 1987. Computer Processing of Remotely Sensed Images: An Introduction (New York: Wiley), 352pp.

McFarlane, M.J. 1992. Groundwater movement and water chemistry associated with weathering profiles of the African surface in Malawi. In: Wright, E.P. and Burgess, W.G. (eds) Hydrogeology of crystalline basement aquifers in Africa. Geological Society, London, Spec. Publ. 66, pp.131-154.

Ministry of Mines and Energy, 1998. Geological Map of Eritrea (1:2,500,000). Unpub. Asmara, Eritrea.

Ministry of Mines and Energy, 1977. Geological Map of Adi Grat Sheet (1:250,000). Addis Ababa, Ethiopia.

Minor, T.B., Carter, J.A., Chesley, M.M., Knowles, R.B. and Gustafsson, P. 1994. The use of GIS and remote sensing in groundwater exploration for developing countries. Proc. 10th Thematic Conference on Geological Remote Sensing, San Antonio, TX, USA, 1994, part I, pp. 168-179.

Mohr, P. 1970. The Geology of Ethiopia. Addis Ababa press, Addis Ababa, 268 pp.

Mohr, P. 1979. Lithology and structure of the Precambrian rocks of Eritrea. Bulletin of the Institute of Applied Geology, Jeddah, 2, pp.7-15.

Mohr, P. 2001. The Asmara dyke swarms, Eritrean plateau: physical parameters of an off-rift olivine dolerite injection zone. Unpul. manuscript, University of Asmara, Eritrea.

Nalbant, S.S., and Alptekin, O., 1995. The use of Landsat Thematic Mapper imagery for Analysing lithology and structure of Korucu-Dugla area in western Turkey. Int. J. Remote Sensing, 16, pp. 2357-2375.

Nkotagu, H. 1996. Application of Environmental isotopes to groundwater Recharge Studies In a semi-arid fractured crystalline basement area of Dodoma, Tanzania. Journal of African Earth Sciences, 22(4), pp443-457.

Olofsson, B., Jacks, G., Knutsson, G. and Thunvik, R. 2001. Groundwater in hard rock – a literature review. Excerpt from: Nuclear waste state-of-the art reports 2001 in Swedish Government Official Reports SOU 2001-35, 77pp.

Philip, G. 1996. Landsat Thematic Mapper data analysis for Quaternary tectonics in parts of the Doon Valley, NW Himalaya, India. Int. Jour. of Remote Sensing, 17, pp.143-153.

Pike, R.J. 1988. The geometric signature: Quantifying landslide terrain types from digital elevation models. Mathematical Geology, 20 (5), pp.491-511.

Pike, R.J. 1993. A bibliography of geomorphometry. USGS Open-File Report 93-262-A, pp. 132, Menlo Park, CA.

Pontual, A. 1988. Investigations of the Colorado Pluton, northern Chile using Landsat Thematic Mapper images. Proceedings of IGRASS'88 Symposium, Edinburgh, Scotland, 13-16 Sept. 1988, ESA SP-284, pp.1049-1052.

Rothery, D.A., and Hunt, G.A., 1990. Technical note: A simple way to perform decorrelation stretching and related techniques on menu-driven image processing systems. Int. J. Remote Sensing, 11, pp. 133-137.

Sabins, F. F., 1987. Remote Sensing Principles and Interpretation. (San Francisco, Calif.: W.H. Freeman), 449pp.

Sander, P. 1996. Remote Sensing and GIS For Groundwater Assessment in Hard Rocks: Applications to Water Well Siting in Ghana and Botswana. PhD dissertation, Chalmers University of Technology, Sweden, Publ. A 80.

Sander, P., Chesley, M.M. and Minor, T.B. 1996. Groundwater Assessment Using Remote Sensing And GIS In A Rural Groundwater Project in Ghana: Lessons Learned. Hydrogeology Jour., 4, 3, pp. 40-49.

Sander, P., Minor, T.B. and Chesley, M.M. 1997. Ground-Water Exploration Based on Lineament Analysis and Reproducibility Tests. Ground Water, 35, 5, pp. 888-894.

Saraf, A.K. and Choudhury, P.R. 1998. Integrated remote sensing and GIS for groundwater exploration and identification of artificial recharge sites. Int. Jour. of Remote Sensing, 19, 10, pp.1825-1841.

Schowengerdt, R.A., 1983. Techniques for Image Processing and Classification in Remote Sensing (London: Academic Press).

Sheffield. C. 1985. Selecting Band Combinations from Multispectral Data. Photogrammetric Engineering and Remote Sensing. 51. 6. pp. 681-687.

Siegal, B.S., and Gillespie, A.R., 1980. Remote Sensing in Geology (New York: Academic Press), 702pp.
Simmers, I (ed) 1988. Estimation of Natural Groundwater Recharge. NATO ASI Series C222. Reidel, Dordrecht, 510pp.

Singhal, B.B.S. and Gupta, R.P., 1999. Applied Hydrogeology of Fractured Rocks. Kluwer Academic Publishers, Dordrecht, pp 400.

Suzen, M.L. and Toprak, V. 1998. Filtering of satellite images in geological lineament analysis: application to a fault zone in Central Turkey. Int. J. Remote Sensing, 19, pp. 1101-1114.

Swati, G. 2002. Landscape Proposes, DEM Discloses. GIS@development, Asia's first GIS/GPS/RS monthly magazine, May 2002.

Talbot, C.J. and Ghebreab, W. 1997. Red Sea detachment and basement core complexes in Eritrea. Geology, 25, 7, pp.655-658.

Taud, H. and Parrot, J.F. 1992. Detection of circular structures on satellite images. Int. J. Remote Sensing, 13, pp. 319-335.

Taylor, R. and Howard, K. 2000. A tectono-geomorphic model of the hydrogeology of deeply weathered crystalline rock: Evidence from Uganda. Hydrogeology Journal, 8, pp.279-294.

Taylor, R. and Howard, K. 1999a. Lithological evidence for the evolution of weathered mantles in Uganda by tectonically controlled cycles of deep weathering and stripping. Catena, 1, pp.65-94.

Teklay, M. 1997. Petrology, Geochemistry and Geochronology of Neoproterozoic Magmatic Arc Rocks form Eritrea: Implications for Crustal Evolution in the Southern Nubian Shield. Ph.D. dissertation, Department of Mines, Memoir No.1, Eritrea.

UNESCO, 1975. Analytical and investigational techniques for fissured and fractured rocks, In Groundwater Studies (eds R.H. Brown, et al.) Studies and Reports in Hydrology (Chapter 14), Supplement 2, UNESCO, Paris.

Vail, J.R., 1987. Late Proterozoic terrains in the Arabian-Nubian Shield and their characteristic mineralization. Geol. Jour., 22, pp. 161-175.

Viswanatham, K.S. 2002. Water Resources Development – Management of Critical Areas in Eritrea. Journal of Applied Hydrology, XV, 4, pp.21-25.

Waters, P., 1990. Methodology of lineament analysis for hydrogeological investigations. In Satellite Remote Sensing for Hydrology and Water Management edited by E.C. Barret, C.H. Power, and A. Micallef (New York: Gordon & Breach), pp.1-23.

Weibel, R. and Heller, M. 1990. A framework for digital terrain modeling, 4th International Symposium on Spatial Data Handling, Zurich, pp. 219-229.

Weibel, R. and Heller, M. 1991. Digital Terrain Modelling, in: Maguire, D.J., Goodchild, M.F., and Rhind, D.W. (eds.) Geographic Information Systems: Principles and Applications, Longman, London, pp. 269-297.

Wester, K. 1992. Spectral Signature Measurements and Image Processing for Geological Remote Sensing. PhD Dissertation, Stockholm University, Sweden, Nr A 273.

Wood, J. 1996. The Geomorphological Characterization of Digital Elevation Models. Ph.D. dissertation, Department of Geography, University of Leicester, UK.

Younis, M.T., Gilabert, M.A., Melia, J. and Bastida, J. 1997. Weathering process effects on spectral reflectance of rocks in a semi-arid environment. Int. J. Remote Sensing, 18, 16, pp.3361-3377.

Zerai, H. 1996. Groundwater and geothermal resources of Eritrea with emphasis on their chemical quality. Jour. of African Earth Sciences, 22, 4, pp. 415-421.

Zerai, T. 2001. Universal Water Resources Consultant, Asmara, Eritrea.

Zhang, M.C., Campbell, J.B. and Haralick, R.M. 1990. Automatic delineation of drainage basins within digital elevation data using the topographic primal sketch. Mathematical Geology, 22, 2, pp. 189-209.

APPENDICES

Appendix i. Terrain Parameters and Definitions

Evans (1979) considers five terrain parameters that can be defined for any two dimensional continuous surface. These are elevation, slope, aspect, profile convexity and plan convexity. These correspond to groups of 0 (elevation), 1st (slope and aspect) and 2nd (profile and plan convexities) order differentials, where the 1st and 2nd order functions have components in the XY and orthogonal planes. Evans approximates the surface using a bivariate quadratic function of the form:

$$Z = ax^2 + by^2 + cxy + dx + ey + f$$

For the purpose of general geomorphometry, these five terrain parameters can be defined considering the partial differential equations of the general quadratic form. The detailed mathematical derivation of these terrain parameters is given in Wood (1996).

Slope is defined as the magnitude of rate of change of elevation in both x and y directions and *Aspect* as direction of maximum gradient. Surface curvatures are further defined as follows.

Profile convexity represents intersection with the plane of Z-axis and aspect direction. It is the measure of the rate of change of slope along the profile.

Plan convexity represents intersection with the XY plane. It is the measure of the rate of change of aspect along the plan.

Longitudinal curvature represents intersecting with the plane of the slope normal and aspect direction.

Cross-sectional curvature represents intersecting with the plane of the slope normal and perpendicular aspect direction. *Maximum, Minimum and Mean curvatures* are defined in any plane.

The most appropriate form of curvature will depend partly on the nature of the surface patch being modeled (Wood 1996). For geomorphological analysis, it would be useful to know curvature along, for example, channel cross-sections and longitudinal profiles (Figure i). The down-slope curvature value is referred to as longitudinal curvature and curvature in the orthogonal direction referred to as cross-sectional curvature.

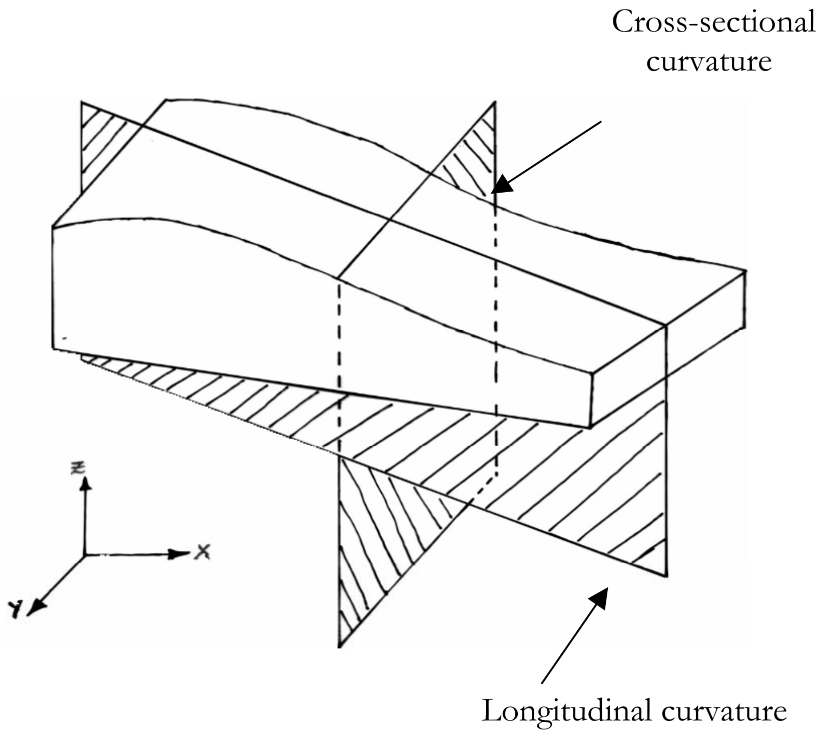

Figure i. Schematic diagram showing cross-sectional and longitudinal curvatures in relation to the XYZ coordinates.

Appendix ii. Determinant Analysis results for Landsat Thematic Mapper data.

Table ii. Ranked Results for 3 bands from Site-1 (Basalts and Crystalline rocks) and Site-2 (Crystalline rocks).

Rank	Determinant (Site-1)	Band Combinations	Determinant (Site-2)	Band Combinations
1	155,555,466	1 4 5	2,336,522	1 4 5
2	79,5689,81	1 4 7	2,292,984	3 4 5
3	59,055,575	3 4 5	1,205,116	4 5 7
4	55,737,330	1 3 5	1,156,663	1 4 7
5	52,859,820	1 5 7	1,034,214	3 4 7
6	29,491,189	1 3 4	812,316	2 4 5
7	28,078,151	2 4 5	798,247	1 5 7
8	26,253,344	3 4 7	733,644	3 5 7
9	21,589,091	4 5 7	528,794	1 3 5
10	19,458,913	1 3 7	381,769	2 4 7
11	13,987,332	3 5 7	324,273	1 3 4
12	13,158,397	2 4 7	291,975	2 5 7
13	10,202,701	1 2 5	202,899	1 3 7
14	9,312,189	2 5 7	104,504	1 2 5
15	4,665,818	2 3 5	90,807	2 3 5
16	4,034,821	1 2 4	50,313	2 3 4
17	4,002,145	1 2 7	44,340	1 2 7
18	2,146,292	2 3 4	41,564	1 2 4
19	1,650,785	2 3 7	33,018	2 3 7
20	564,276	1 2 3	5,660	1 2 3

Appendix iii. Stereographic plots by rock type poles on the lower-hemisphere equal area projection.

a) Foliated metavolcanics

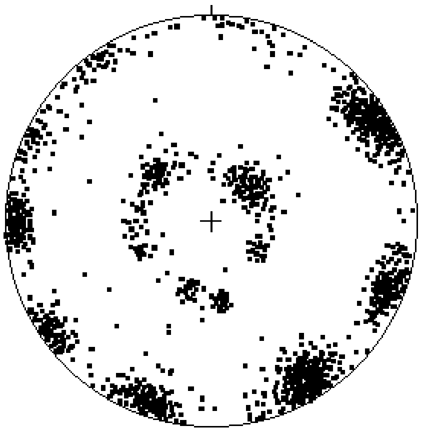

n=1376

b) Non-foliated metavolcanics

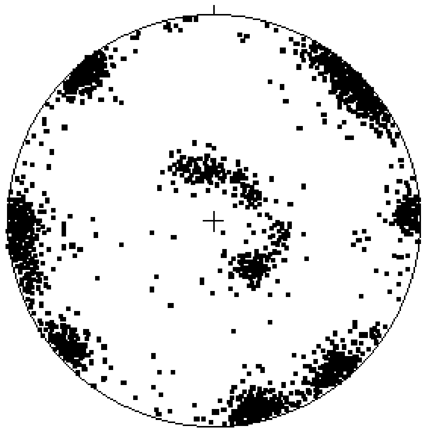

n=1635

c) Syn-tectonic granites

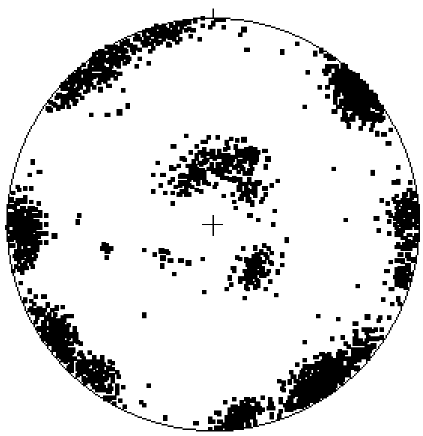

n=2087

d) Post-tectonic granites

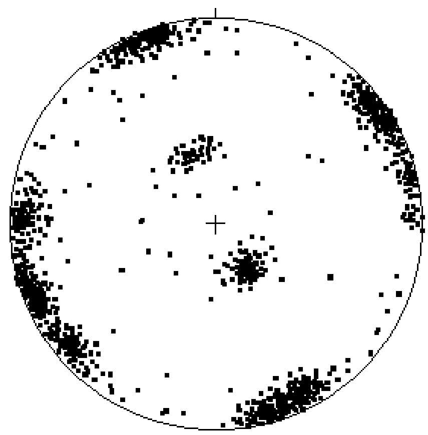

n= 976